Application des signaux CPM pour la collecte de données à grande échelle provenant d'émetteurs faible cout

Malek Messai

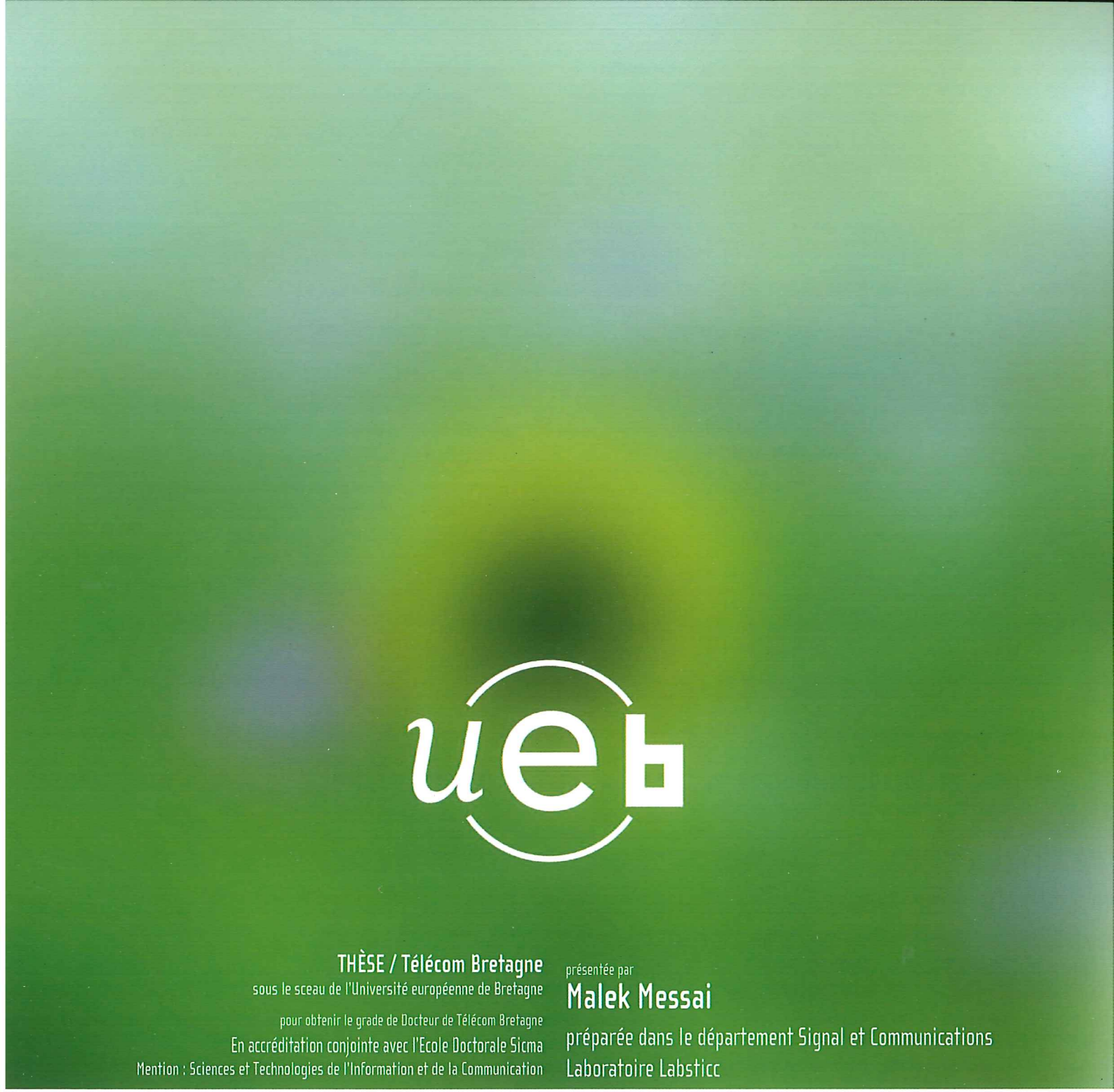

THÈSE / Télécom Bretagne
sous le sceau de l'Université européenne de Bretagne

pour obtenir le grade de Docteur de Télécom Bretagne
En accréditation conjointe avec l'Ecole Doctorale Sicma
Mention : Sciences et Technologies de l'Information et de la Communication

présentée par
Malek Messai
préparée dans le département Signal et Communications
Laboratoire Labsticc

Application des signaux CPM pour la collecte de données à grande échelle provenant d'émetteurs faible coût

Thèse soutenue le 20 novembre 2015
Devant le jury composé de :

Gilles Burel
Professeur, Université de Bretagne Occidentale / président

Mérouane Debbah
Professeur, CentraleSupélec – Gif Sur Yvette / rapporteur

Philippe Ciblat
Professeur, Télécom Paris Tech / rapporteur

Giulio Colavolpe
Docteur, Università degli Studi di Parma (Italie)/ examinateur

Jérôme Lebrun
Chercheur CNRS, Université de Nice Sophia Antipolis/ examinateur

Frédéric Guilloud
Maître de conférences, Télécom Bretagne / examinateur

Karine Amis
Maître de conférences (HDR), Télécom Bretagne / directrice de thèse

Alain Dominique Thomas
R&D senior engineer, Zodiac data Systems SAS – Les Ulis / invité

N ° d'ordre: 2015telb0367

Sous le sceau de l'Université Européenne de Bretagne

Télécom Bretagne

En accréditation conjointe avec l'Ecole Doctorale Sicma

Application des signaux CPM pour la collecte de données à grande échelle provenant d'émetteurs faible coût

---

Thèse de Doctorat

Mention: Sciences et Technologies de l'information et de la Communication (STIC)

Présentée par: Malek MESSAI

Département: Signal et Communications

Laboratoire: LabSTICC Pôle CACS/COM

Directrice de thèse: Karine AMIS

Soutenue le 20 Novembre 2015

Jury :

Rapporteurs:	Mérouane Debbah	-	Centrale-Supélec/ HUAWEI
	Philippe Ciblat	-	Telecom Paris Tech
Examinateurs:	Giulio Colavolpe	-	Università degli Studi di Parma (Italy)
	Gilles Burel	-	Université de Bretagne Occidentale
	Jérôme Lebrun	-	CNRS/ Université de Nice Sophia Antipolis
Encadrants:	Karine Amis	-	Telecom Bretagne
	Frédéric Guilloud	-	Telecom Bretagne
Invité:	Alain Dominique Thomas	-	Zodiac Aerospace

Acknowledgments

I would like to express my sincerest thanks and appreciation to all the members of the Signal and Communications department for welcoming me in your laboratory. I have met many people inside and outside the work sphere that made the Ph.D an enjoyable adventure.

I am deeply grateful to my supervisors, Dr. Karine AMIS and Dr. Frédéric GUILLOUD, for their invaluable advice, kindness, encouragements, patience and support during these three years. Their profound scientific knowledge, invaluable insight and experience have had a great impact on the success of the thesis. There is no doubt in my mind that without their comments, criticisms and guidance, my Phd will not be accomplished. I am also indebted to them for giving me the opportunity to improve my research background and experience. I am very lucky to have had the opportunity to work with them. It was always a pleasure to share unforgettable moments rich with new results.

A special thanks to Prof. Giulio COLAVOLPE at University of Parma for his great hospitality and supervision of a part of my PhD in Italy. It was a pleasure to work with such a brilliant, insightful, knowledgeable and kind supervisor.

Furthermore, I also wish to thank the committee members, Prof MÃ©rouane Debbah, Prof Philippe Ciblat, Prof Giulio Colavolpe, Jérôme Lebbrun, Prof Gilles Burel and Dr. Alain Dominique Thomas for reviewing my thesis and enhancing me with their valuable comments.

I thank all my colleagues and friends who have accompanied me throughout my thesis, they made my life more enjoyable and less difficult in Brest. I warmly thank Souhaila and Hakim for the precious advice and all the fruitful discussions, for the organizations of the sweet events (IEEE day, laser game, bowling, paintball, cinema,...) that will remain a beautiful memories. Thanks to my wonderful office-mates: Ihsen, Omid, Kien, Thomas, Budhi for the nice company and the good times. I think Ihsen for his several invitations to his house and offering us the delicious Iranian foods. Fethi, I think that I am now an expert in the cooking of the "Algerian burek" thank to your menus in Ramadan. Thank to Yesser, Rabbie, Ghada, Sileye, Carole, Redouane, Marja, Nhan. Vincent: You have already learnt many words in Arabic. To Said and Jia thanks for the sweet smile that gave me the energy every time I enter to your office. Thanks to Safa every time I get hungry, I went directly to her office where I found the chocolates and cakes. Big Thanks to my friend Brahim for the nice companion since our internship.

Last but not least, the whole acknowledgement is dedicated to my parents for their unlimited support, guidance and help. I am unable to count their graces and without them and their unselfish love, and kindness, and tenderness, and affection, I have not been come thus far and achieved my thesis. I would like to thank my two sisters and dear brother for their encouragement and love.

Résumé des Travaux de thèse

Introduction

De la 2G à 4G d'aujourd'hui, les communications mobiles ont considérablement évolué de manière à assurer la connectivité des utilisateurs avec des débits toujours plus élevés. La course au débit reste présente dans la conception des futurs systèmes de cinquième génération (5G). Elle est cependant accompagnée de la prise en compte de l'augmentation de la diversité des cas d'usages, avec notamment le concept de communications entre machines (noté M2M, pour *Machine-to-machine communication*). Ce type de communications peut être illustré par exemple dans des applications de surveillance ou de contrôle à distance dans divers domaines tels que l'environnement (anticiper les éruptions volcaniques par exemple), la santé (pour le suivi d'un patient) ou de l'industrie (réseaux de capteurs, compteurs intelligents pour le gaz, l'eau ou l'électricité). Les communications M2M se caractérisent par la présence d'un très grand nombre de machines connectées, souvent autonomes en énergie (batterie, panneaux solaires, ...), possédant une complexité de traitement limitée. Par conséquent, les enjeux posés par ce type de communications sont essentiellement la réduction de la consommation énergétique et l'optimisation de l'efficacité spectrale. Les communications M2M sont aussi souvent asymétriques, c'est à dire que les informations sont toutes transmises à un concentrateur (ou au centre de fusion) ayant une capacité de traitement plus élevée.

Cette thèse est donc inscrite dans ce contexte des communications avec un très grand nombre de machines (*Massive Machine Communications* ou *Massive M2M*): notre objectif est de déterminer un système de communication multi-utilisateur adapté à la limitation matérielle des machines et aux spécificités des applications de collecte d'informations à grande échelle.

Les modulations à enveloppe constante permettent d'utiliser des amplificateurs non linéaires qui possèdent une très bonne efficacité énergétique. Parmi les modulations à enveloppe constante, les modulations à phase continue (CPM pour *continuous phase modulation*) possèdent une meilleure efficacité spectrale. En outre, la nature récursive du modulateur CPM les rend intéressantes dans des schémas de concaténation en série d'un codeur et d'un modulateur. Les avantages des CPM (enveloppe constante, efficacité énergétique et efficacité spectrale) permettent aux CPM d'être largement utilisées dans les applications à faible coût et à faible consommation énergétique. La continuité de phase des signaux CPM est obtenue par filtrage des symboles de modulation, introduisant ainsi un effet mémoire (appelé interférence entre symboles). Le récepteur optimal maximisant la vraisemblance (MLSD pour *Maximum Likelihood Sequence Detector*) peut être implémenté avec l'algorithme de Viterbi (VA) exécuté sur un treillis. La complexité du récepteur MLSD dépend du nombre d'états de ce treillis.

Pour réduire le coût de l'émetteur, une implémentation analogique du modulateur CPM peut être simplement obtenue avec un composant de type oscillateur commandé en tension (VCO, pour *Voltage Controlled Oscillator*). Cependant, ce type d'implémentation ne permet pas de garantir une valeur précise des paramètres de la modulation, comme par exemple l'indice de modulation qui correspond au gain du VCO et qui est noté h. Or le récepteur MLSD ne fonctionne plus lorsque les paramètres de la CPM s'écartent de leur valeur nominale. Le treillis permettant d'implémenter le récepteur MLSD est défini si et seulement si l'indice de modulation nominal h est rationnel.

Les contributions de cette thèse sont les suivantes :

- Tout d'abord, nous avons proposé un schéma de pré-codage appliqué à une CPM ternaire pour augmenter l'efficacité spectrale des CPM binaires.
- Deuxièmement, nous avons développé un démodulateur CPM d'une complexité réduite basé sur la technique *per survivor processing* (PSP).
- Troisièmement, nous avons traité la robustesse au décalage de l'indice de modulation par rapport à sa valeur nominale, ainsi que la robustesse au bruit de phase en travaillant soit du côté émetteur, soit du côté récepteur. Côté émetteur, nous avons d'abord défini des systèmes CPM ternaires pré-codés où le pré-codeur est conçu de manière à borner l'évolution de la phase. Du côté récepteur, nous avons appliqué l'algorithme somme-produit (SPA) sur un graphe pour tenir compte de la distribution de l'erreur faite sur l'indice de modulation.
- Quatrièmement, nous avons étendu le problème de robustesse au cas multi-utilisateurs. Nous avons proposé tout d'abord une technique d'accès multiple basée sur un pré-codage des signaux CPM ternaires avec un pré-codeur de type *Alternate Mark Inversion* suivi d'une séparation de phase avec une détection multi-utilisateurs effectuée en réception. Nous avons également implémenté un schéma de multiplexage fréquentiel des modulations CPM et nous avons développé au récepteur une détection conjointe multi-utilisateurs basée sur l'algorithme somme-produit pour la rendre robuste aux incertitudes sur l'indice de modulation et au bruit de phase.

Augmentation de l'efficacité spectrale des modulations CPM binaires par précodage et modulation ternaire

Dans cette partie nous nous concentrons sur l'efficacité spectrale (SE) d'une modulation CPM binaire. Nous souhaitons proposer un schéma de transmission qui permet d'augmenter le débit *information rate* (IR) transmis sur le canal sans augmenter l'occupation spectrale. Ce schéma est basé sur la concaténation d'un pré-codeur à entrée binaire et sortie ternaire avec une modulation CPM ternaire. Nous commençons cette partie en définissant le pré-codeur proposé et puis nous décrivons le détecteur correspondant. Le pré-codeur adopté ne change pas la nature récursive

du schéma CPM. Donc, il est toujours adapté à la concaténation série, via un entrelaceur pseudo-aléatoire, avec un code correcteur d'erreur externe et la convergence du schéma itératif est analysée par la technique des diagrammes EXIT.

Définition du pré-codeur

Le pré-codeur reçoit en entrée les bits $\{b_n\}$ appartenant à l'alphabet $\{0, 1\}$ et fournit à sa sortie les symboles ternaires $\{a_n\}$ appartenant à l'alphabet $\{0, \pm 2\}$. Le débit peut être augmenté en élevant l'ordre de modulation, mais ceci conduit à un élargissement de la densité spectrale de puissance. Cependant, pour le même ordre de modulation, le débit maximum atteignable dépend du taux d'erreur qui est une fonction décroissante de la distance minimale. Ainsi, pour améliorer IR, il est plus approprié d'augmenter la distance minimale.

En ce qui concerne l'occupation spectrale d'un signal CPM, la largeur du principal lobe spectral est liée aux accroissements de phase. Elle augmente avec l'élévation de l'ordre de modulation M ou de l'indice de modulation h, c'est pourquoi l'utilisation sans précaution de symboles ternaires au lieu de symboles binaires conduit à un élargissement de la bande à cause des transitions de 2 vers -2 et vice versa. Cependant un signal CPM ternaire sans transitions entre +2 et -2 ou vice versa possède quasiment la même occupation spectrale qu'un signal CPM binaire. L'absence de telles transitions peut être obtenue en utilisant un pré-codeur externe.

Notre finalité est de concevoir un pré-codeur de manière à augmenter le débit d'information, sans élargir l'occupation spectrale, c'est-à-dire, la conception d'un pré-codeur qui assure simultanément:

- une distance minimale élevée (débit d'information).
- l'absence de transitions de 2 à -2 et vice versa (occupation spectrale).

La stratégie adoptée est d'augmenter la distance minimale tout en gardant à peu près constante l'occupation spectrale. Notre pré-codeur proposé est ainsi défini par:

$$a_n = b_n a_{n-d}(-1)^{d+1}, \tag{1}$$

où a_{n-d} est le dernier symbole tel que $|a_{n-d}| = 2$.

Principe du détecteur

Pour le détecteur correspondant, considérons une séquence binaire de longueur N. Elle peut prendre 2^N valeurs. Cependant, selon l'initialisation, le précodeur a 2^{N+1} sorties possibles. Par exemple, pour $N = 3$, nous avons 16 séquences possibles pré-codées : $\{000, 020, 200, 220, 002, 0-20, -200, -2-20, 00-2, 022, 20-2, 222, 000, 0-2-2, -202, -2-2-2\}$. Étant donnée une transition de l'état $\sigma_i(n)$ à $\sigma_{i+1}(n)$, il existe deux codages différents du bit '1' en fonction de l'encodage précédent. Le nombre des états de phase est donc le double par rapport à une CPM binaire classique. On note $\overline{\theta}$ l'état complémentaire de θ qui satisfait $\overline{\theta} \equiv -\theta + 2\pi$.

Prenons une CPM à réponse complète ($L = 1$) avec un indice de modulation $h = 1/3$. Le diagramme d'état de phase est représenté sur la figure 1 et le treillis est représenté sur la figure 2. Il est important de mentionner que lorsque p est pair, $\theta_i(n)$ et $\overline{\theta_i(n)}$

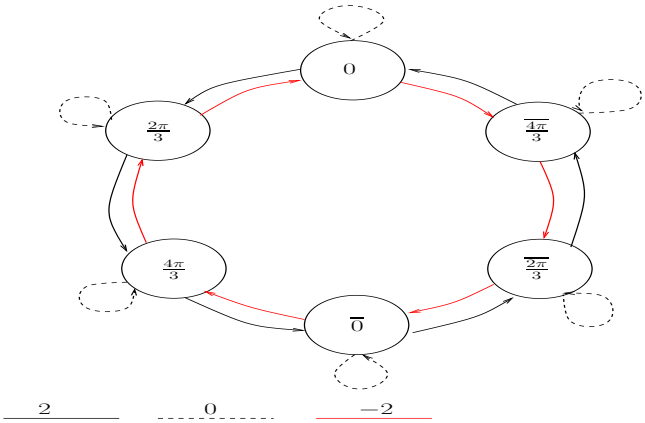

Figure 1: Diagramme d'état de phase d'une CPM ternaire pré-codée dans le cas $h = 1/3$ (indice de modulation dont le dénominateur est impair).

auront le même encodage du bit '1', et les métriques de branches qui sortent de ces deux états seront égales. Cela implique que les deux états $\theta_i(n)$ et $\overline{\theta_i(n)}$ peuvent être combinés en un seul état $\theta_i(n)$. Ainsi, le nombre d'états est $p([p]_2 + 1)2^{L-1}$ où $[.]_2$ désigne l'opérateur "modulo 2". Pour le même pré-codeur, la CPM ternaire pré-codée sera représentée par un treillis avec un nombre d'états égal au nombre d'états de la CPM binaire pour les valeurs paires de p, et double pour les valeurs impaires de p. Pour estimer l'efficacité spectrale, la largeur de bande choisie est celle qui contient 99% de la puissance totale. L'efficacité spectrale pour la modulation 1REC avec différents indices de modulation $h = \{1/7, 1/5, 1/4\}$ est illustrée sur la figure 3.

Récepteur de signaux CPM de complexité réduite

Dans cette partie, nous développons un démodulateur CPM d'une complexité réduite basé sur la technique per survivor processing (PSP). Ce démodulateur repose sur un treillis avec un nombre d'états réduit et défini à partir d'un indice de modulation rationnel éventuellement différent de l'indice de modulation d'émission et dénommé indice de modulation virtuel. L'indice de modulation virtuel doit être choisi de manière à obtenir un compromis entre les performances en taux d'erreurs et la réduction de la complexité. Le récepteur de complexité réduite repose sur la décomposition du h sous la forme $h = h_v + \Delta h$ tel que $h_v = \frac{l_v}{p_v}$ soit un nombre rationnel. L'idée principale est d'utiliser l'algorithme de Viterbi ou l'algorithme BCJR avec des métriques de branches et d'états modifiées sur un treillis conçu à partir de l'indice de modulation virtuel h_v. Le calcul des métriques tient compte de la différence de phase proportionnelle à Δh et calculée par la technique *per survivor processing* (PSP). Grâce à la décomposition de h sous la forme $h = h_v + \Delta_h$, la

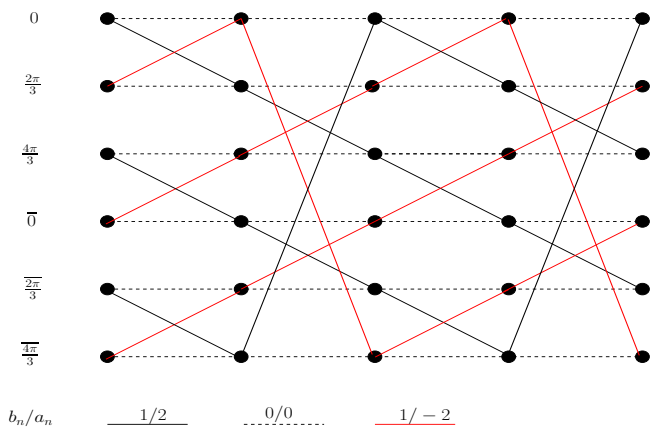

Figure 2: Treillis d'une modulation CPM ternaire pré-codée à réponse complète dans le cas $h = 1/3$ (indice de modulation dont le dénominateur est impair).

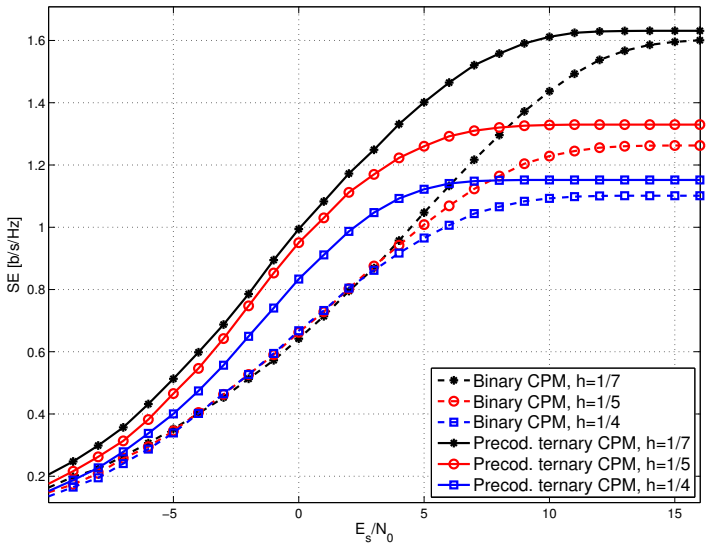

Figure 3: Efficacité spectrale pour la modulation 1REC avec différents indices de modulation.

phase du signal modulé peut être exprimée en fonction de h_v et Δ_h :

$$\begin{aligned}
\phi(t,h,\boldsymbol{a}) &= \pi h \sum_{i=0}^{n-L} a_i + 2\pi h \sum_{i=n-L+1}^{n} a_i q(t-iT), \\
&= \pi h_v \sum_{i=0}^{n-L} a_i + \pi \Delta_h \sum_{i=0}^{n-L} a_i + 2\pi h_v \sum_{i=n-L+1}^{n} a_i q(t-iT) \\
&\quad + 2\pi \Delta_h \sum_{i=n-L+1}^{n} a_i q(t-iT), \\
&= \underbrace{\phi_{h_v,n} + \phi_{h_v,n}(t)}_{\phi(t,h_v,\boldsymbol{a})} + \underbrace{\Delta\phi_n + 2\pi\Delta_h \sum_{i=n-L+1}^{n} a_i q(t-iT)}_{\phi(t,\Delta_h,\boldsymbol{a})}, \qquad (2)
\end{aligned}$$

avec $\Delta\phi_n = \pi\Delta_h \sum_{i=0}^{n-L} a_i$.
Les deux premiers termes de (2) sont estimés par l'algorithme de Viterbi et le troisième terme est la différence de phase qui s'accumule à chaque symbole. Cette accumulation est calculée en utilisant la technique PSP en associant à chaque état $i, i \in \{0, 1, ..., p_v - 1\}$ un paramètre supplémentaire $\Delta\phi_n^i$. Le dernier terme de (2) est calculé à la sortie du filtre adapté. Nous pouvons écrire la relation suivante:

$$\begin{aligned} \phi_h^i &= \Delta\phi_n^i + i\frac{l_v}{p_v}\pi, \qquad i = \{0, 1, 2, ..., p_v - 1\}, \\ &= \Delta\phi_n^i + \phi_{h_v}^i. \end{aligned} \tag{3}$$

La métrique de branche modifiée est égale au produit scalaire qui est calculé comme suit :

$$\Omega_{k,i}^{\text{modified}} = \Re\big(e^{-j\Delta\phi_n^k} \int_{nT}^{(n+1)T} r(t) e^{-j\phi_{k,i}(t,h_v)} . e^{-j\psi_{k,i}(t,\Delta_h)} dt\big). \tag{4}$$

où

$$\phi_{k,i}(t, h_v) = \phi_{h_v,n}^k + 2\pi h_v \sum_{\ell=n-L+1}^{n-1} a_\ell^k q(t - \ell T) + 2\pi h_v a_n^i q(t - nT) \tag{5}$$

$$\psi_{k,i}(t, \Delta_h) = 2\pi\Delta_h \sum_{\ell=n-L+1}^{n-1} a_\ell^k q(t - \ell T) + 2\pi\Delta_h a_n^i q(t - nT). \tag{6}$$

La seule tâche supplémentaire qui doit être effectuée sur l'algorithme de Viterbi est la mise à jour PSP de la différence de phase pour chaque état $\Delta\phi_n^i$. L'équation d'actualisation est donnée par:

$$\Delta\phi_{n+1}^i = \Delta\phi_n^{k^*} + a_{(k^*,i)}\pi\Delta_h, \tag{7}$$

où k^* est l'indice correspondant à la métrique cumulée maximale sélectionné parmi les M états précédents de $\boldsymbol{x}_{(n+1)}^i$ et $a_{(k^*,i)}$ est la dernière composante du vecteur d'état $\boldsymbol{x}_n^{k^*}$. Nous appliquons (4) pour calculer le produit scalaire entre le signal reçu et le signal correspondant à la transition $\boldsymbol{x}_n^k \to \boldsymbol{x}_{n+1}^i$ utilisée dans l'algorithme Viterbi modifié :

$$\left(\phi_{h_v}^k(\Delta\phi_n^k), a_{n-1}^k, a_{n-2}^k, ..., a_{n-L+1}^k\right) \xrightarrow{a_n} \left(\phi_{h_v}^i(\Delta\phi_{n+1}^i), a_n^i, a_{n-1}^i, , ..., a_{n-L+2}^i\right),$$

avec $a_n^i = a_n$, $a_{n-1}^i = a_{n-1}^k$, $\cdots$, $a_{n-L+2}^i = a_{n-L+2}^k$.

La détection de sortie *souple* cohérente optimale qui minimise la probabilité d'erreur symbole est atteinte par une détection selon le critère du maximum a posteriori (MAP) des symboles transmis a_n. Le détecteur MAP symbole sert à maximiser la *probabilité a posteriori* (APP) $p(a_n|r(t))$:

$$\hat{a}_n = \arg\max_{a \in \mathcal{M}} \; p(a_n = a|r(t)). \tag{8}$$

Dans l'algorithme BCJR modifié, nous calculons d'abord les probabilités *forward* α_n, où la métrique de branche entre les états $\boldsymbol{x}_n^k$ et $\boldsymbol{x}_{n+1}^i$ est modifiée comme suit :

$$\gamma_n(\boldsymbol{x}_n^k, \boldsymbol{x}_{n+1}^i) \propto \exp\left(\frac{\Omega_{k,i}^{\text{modified}}}{2N_0}\right) p(\boldsymbol{x}_n^k | \boldsymbol{x}_{n+1}^i), \tag{9}$$

où le terme $\Delta\phi_{n+1}^i$ est calculé récursivement selon (7), avec l'indice k^* défini par $k^* = \arg\max_k\{\alpha_n(\boldsymbol{x}_n^k)\gamma_n(\boldsymbol{x}_n^k, \boldsymbol{x}_{n+1}^i)\}$, et $a_{(k^*,i)}$ défini comme la dernière composante du vecteur d'état $\boldsymbol{x}_n^{k^*}$. Ici, il est important de mentionner la principale différence entre l'algorithme BCJR original pour lequel les métriques *forward* et *backward* sont calculées en parallèle. Dans le treillis à nombre d'états réduit, la métrique *backward* est calculée une fois que toutes les métriques *forward* ont été calculées. Il est donc nécessaire de garder une trace du chemin survivant associé à chaque transition et à chaque temps symbole lors du calcul des métriques *forward* $\alpha_n(\boldsymbol{x}_n^k)$. Ensuite, les chemins survivants sont utilisés dans le calcul des métriques *backward* $\beta_n(\boldsymbol{x}_n^k)$. Cela signifie que les valeurs de $\gamma_n(\boldsymbol{x}_n^k, \boldsymbol{x}_{n+1}^i)$ seront enregistrées au cours du calcul *forward* pour être utilisées dans le calcul *backward*. En fait, l'approche PSP est uniquement mise en oeuvre dans la récursion *forward* pour les deux raisons suivantes:

- d'abord, la phase accumulée $\Delta\phi_N$ associée à la dernière période symbole est inconnue, tandis que la phase accumulée $\Delta\phi_0$ est connue et est égale à zéro.

- ensuite, la métrique de branche dépend de l'état de la phase accumulée (calculée par le processus PSP). Si on appliquait le PSP dans les deux étapes *forward* et *backward*, cela produirait différentes métriques de branche pour une même transition, ce qui n'est pas admissible.

L'algorithme proposé est résumé ci-dessous :

Algorithme BCJR modifié à base de PSP

- Étape 1: Initialiser ($n = 0$)
  $\Delta\phi_0^k = 0$, pour tous les états $\boldsymbol{x}_0^k$,
  $\alpha_0(\boldsymbol{x}^0) = 1$, $\alpha_0(\boldsymbol{x}^k) = 0$, $k \neq 0$.

- Étape 2: *Forward* récursion $n : 0 \to N-1$
  Calculer pour toutes les transitions possibles $\boldsymbol{x}_n^k \to \boldsymbol{x}_{n+1}^i$ dans le treillis au nombre d'états réduit, les métriques de branche $\gamma_n(\boldsymbol{x}_n^k, \boldsymbol{x}_{n+1}^i)$ selon (9). Ensuite, pour chaque $\boldsymbol{x}_{n+1}^i$, mettre à jour $\Delta\phi_{n+1}^i$ selon (7).

- Étape 3 : *Backward* récursion $n : N \to 0$
  Initialiser $\beta_N(\boldsymbol{x}_N^k) = \frac{1}{N_s}\ \forall\ k$, où N_s désigne le nombre d'états.
  Actualiser la métrique *backward* cumulée β_n en utilisant les métriques de branche calculées dans l'étape 2.

Sur la figure 4, nous considérons une modulation CPM Quaternaire à réponse partielle ($L > 1$) avec une impulsion de fréquence en cosinus surélevé de longueur $L = 2$ avec deux indices de modulation de transmission possibles : $h = 1/4$ et $3/8$. Pour $h = \frac{1}{4}$, nous pouvons recevoir de façon optimale en utilisant l'un des indices de modulation virtuels $h_v \in \{1/2, 2/3, 2/5\}$. Notons que le treillis construit avec $h_v = \frac{2}{5}$ a 20 états, et le treillis construit avec $h_v = \frac{1}{2}$ a seulement 16 états, alors que le treillis construit avec $h_v = h = 1/4$ a 64 états. Le treillis ayant le moins d'états (12) est construit avec $h_v = 2/3$ mais on constate une dégradation d'environ 2 dB pour un TEB $= 10^{-3}$.

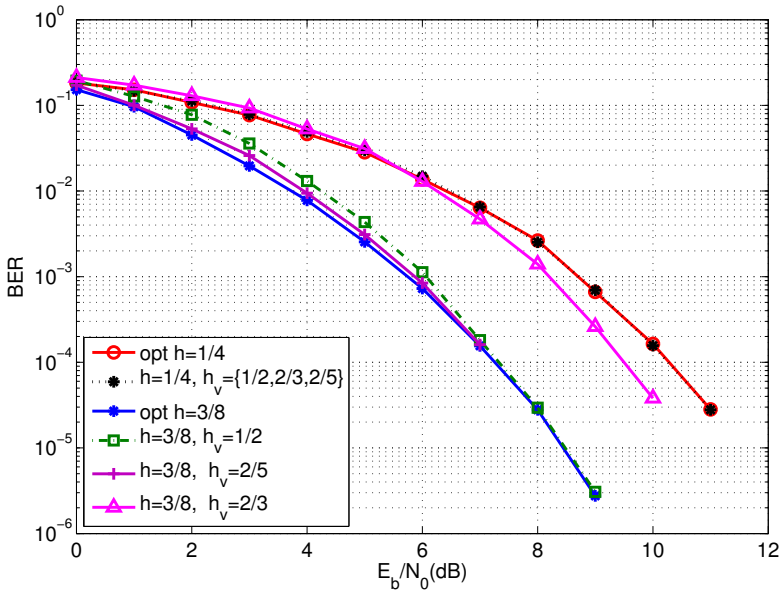

Figure 4: TEB d'une modulation 2RC Quaternaire avec $h = \frac{1}{4}$ et $\frac{3}{8}$ détectée en utilisant un récepteur à nombre *d'états réduit* basé sur les indices de modulation $h_v = \frac{2}{3}$, $\frac{1}{2}$ et $\frac{2}{5}$.

Robustesse au décalage d'indice de modulation et au bruit de phase pour une CPM binaire

Dans cette partie, nous traitons le problème de l'incertitude de la valeur de l'indice de modulation, soit en agissant du côté de l'émetteur, soit du côté du récepteur.

Solution côté émetteur

Nous proposons un nouveau schéma binaire basé sur la concaténation d'un précodeur à entrée binaire et sortie ternaire, combiné avec une modulation CPM ternaire, comme au premier chapitre dans lequel nous souhaitions améliorer l'efficacité

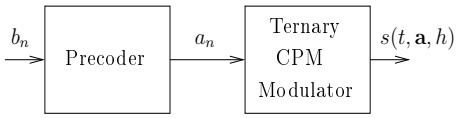

Figure 5: Schéma proposé.

spectrale. La conception du pré-codeur ici n'a pas les mêmes spécifications puisque nous visons à rendre la transmission robuste vis à vis d'un décalage d'indice de modulation et d'un bruit de phase. Le résultat est une famille de formats CPMs dont l'état de phase est contrainte de suivre une évolution spécifique. Deux pré-codeurs sont considérés, ils ne changent pas la nature récursive des schémas CPM et sont donc toujours compatibles avec une concaténation en série d'un code correcteur d'erreur externe, à travers un entrelacement pseudo-aléatoire.

Le but du pré-codeur est de contraindre l'évolution de l'état de phase des signaux CPM. Le premier pré-codeur n'a que deux états, indépendamment de l'indice de modulation adopté. Le second pré-codeur possède un nombre d'états qui dépend du dénominateur de l'indice de modulation nominal et sera introduit pour éviter la présence d'impulsions dans la densité spectrale de puissance du signal émis.

Pré-codeur *AMI*

Le pré-codeur classique de type *Alternate Mark Inversion* (AMI) représenté sur la figure 5 encode le bit $b_n = 0$ en $a_n = 0$ et code le bit $b_n = 1$ alternativement en $a_n = 2$ ou $a_n = -2$. A part pour les valeurs de $h = 1/2, 3/2, ...$, la densité spectrale de puissance du signal résultant du système basé sur le pré-codeur AMI comporte des raies spectrales à des fréquence multiples de la cadence de signalisation $1/T$. Ces raies peuvent être utilisées par des algorithmes de synchronisation temporelle et fréquentielle. Dans le cas où elles ne sont pas désirables, un autre pré-codeur est proposé ci-après.

Pré-codeur sans raie spectrale

Nous proposons de définir un pré-codeur de telle sorte que tous les états de phase se produisent avec la même probabilité. Ce pré-codeur est basé sur cette règle simple: le bit $b_n = 0$ est à nouveau codé comme $a_n = 0$, tandis que le bit $b_n = 1$ est codé comme $a_n = 2$ ou $a_n = -2$. Cette fois cependant, le pré-codeur fournit en sortie un bloc de p symboles de 2 suivi d'un bloc de p symboles de -2, l'un après l'autre. L'état de phase pour ce schéma est non seulement lié à la CPM, mais aussi au signe des symboles en cours de transmission. Le diagramme d'états du système global est illustré sur la figure 6 pour $p = 4$ ou $p = 5$. les résultats de simulations sont donnés sur la figure 7 où nous considérons le cas des modulations CPM à réponse complète avec les formes d'ondes REC et RC. Dans ce cas, les indices de modulation h employés à l'émetteur et ceux utilisés pour concevoir le récepteur h sont explicitement signalés dans la légende de la figure. Les résultats

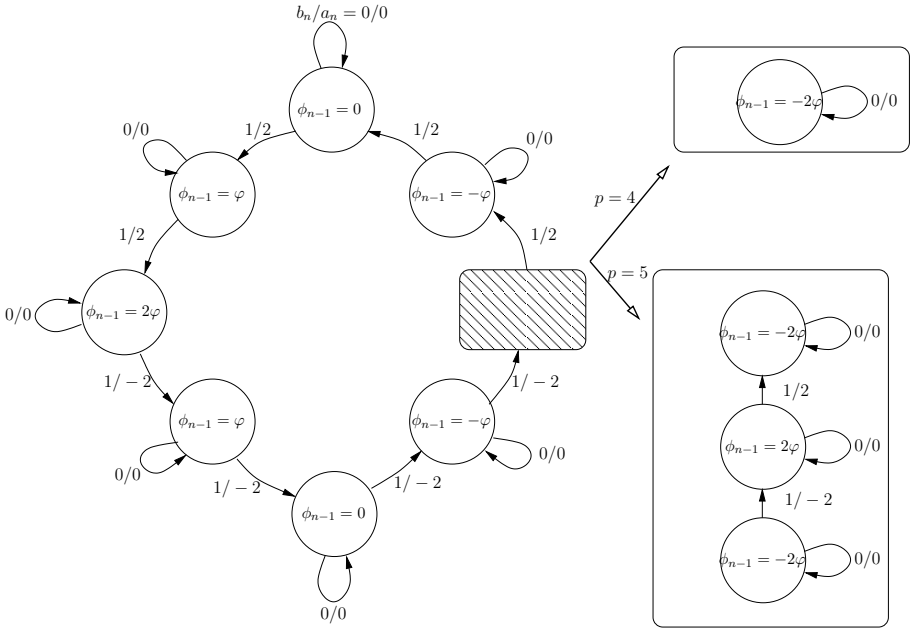

Figure 6: Diagramme d'état de phase dans le cas du pré-codeur proposé pour $p = 4$ ou $p = 5$.

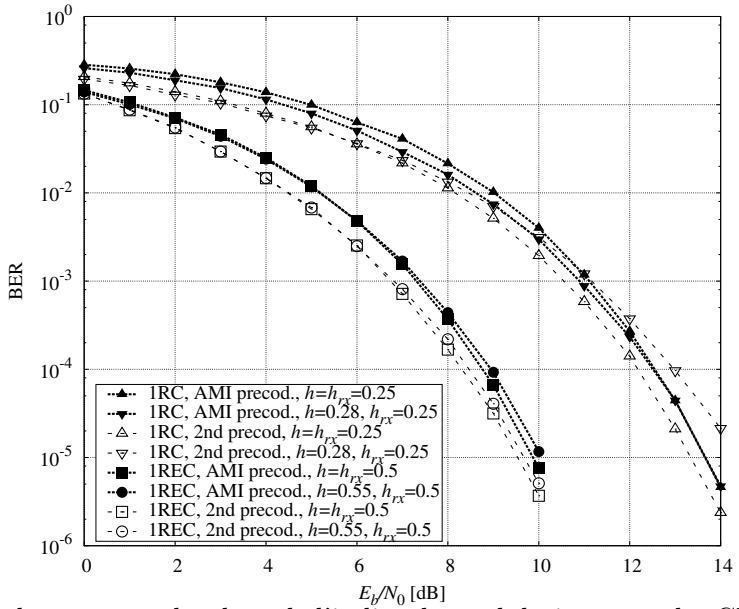

Figure 7: Robustesse au décalage de l'indice de modulation pour des CPM à réponse complète, en fonction des pré-codeurs mis en oeuvre.

confirment notre intuition sur la robustesse des schémas proposés pour lesquels la perte de performance observée est négligeable, même lorsque le décalage de l'indice de modulation est grand.

Solution côté récepteur

Nous considérons ici le problème de la détection à entrée et sortie souple (SISO) d'un signal CPM binaire caractérisé par une incertitude significative de l'indice de modulation et transmis sur un canal affecté par un bruit de phase. Nous adoptons une représentation simplifiée du signal CPM binaire en ne gardant de sa décomposition de Laurent que sa composante principale, et en décrivant le calcul de la probabilité conjointe a posteriori des symboles transmis, la phase de canal, et la variation de l'indice de modulation par un graphe factoriel (FG, pour *factor graph*). L'algorithme somme-produit (SPA) est alors mis en oeuvre pour calculer les probabilités a posteriori des symboles transmis.

Cette technique ne nécessite pas une estimation explicite de l'indice de modulation, ni de la phase du canal. De plus, ce détecteur est très robuste aux grandes incertitudes sur l'indice de modulation. Le détecteur à sortie souple peut être utilisé pour la détection et le décodage itératif de bits codés entrelacés d'un système CPM codé. Nous considérons d'abord une transmission binaire non codée (figure 8) en utilisant le format GFSK de la norme Bluetooth en mode BR (*Basic Rate*). Dans ce cas, l'indice de modulation peut prendre sa valeur dans l'intervalle $[0.28, 0.35]$. Nous supposons qu'il est fixé à $h = 0.28$. Au niveau du récepteur, pour le détecteur proposé nous avons considéré les deux cas de $h_{rx} = 0.3$ et $h_{rx} = 1/3$. On considère

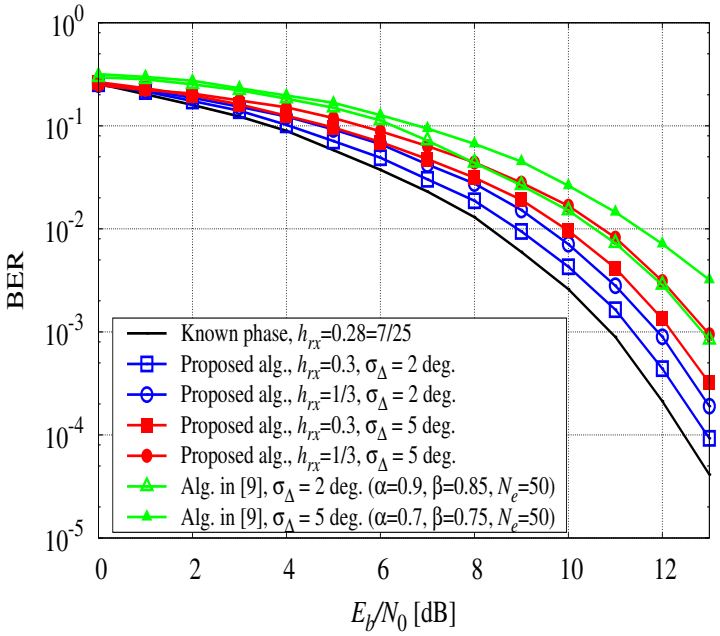

Figure 8: Détection Bluetooth en présence de bruit de phase avec un écart-type égal à 2 et 5 degrés, $h = 0.28$.

maintenant une concaténation en série, à travers un entrelaceur pseudo-aléatoire de longueur 2048 bits, d'un codeur convolutif binaire avec des générateurs (7,5)

(notation octal) et une modulation CPFSK binaire avec un indice de modulation de transmission irrationnel $h = \frac{\pi}{5}$ (figure 9). Lorsque l'indice de modulation est irrationnel, une description du treillis n'est pas possible et nous n'avons donc pas de borne de performance optimale pouvant servir de référence. Pour cette raison, nous avons considéré la performance du détecteur optimal lorsque $h = h_{rx} = \frac{5}{8}$ (une valeur très proche de l'indice de modulation irrationnel considéré), avec une phase de canal parfaitement connue au niveau du récepteur. Pour tous les récepteurs considérés, 12 itérations maximum sont effectuées entre le détecteur CPM et le décodeur du code convolutif.

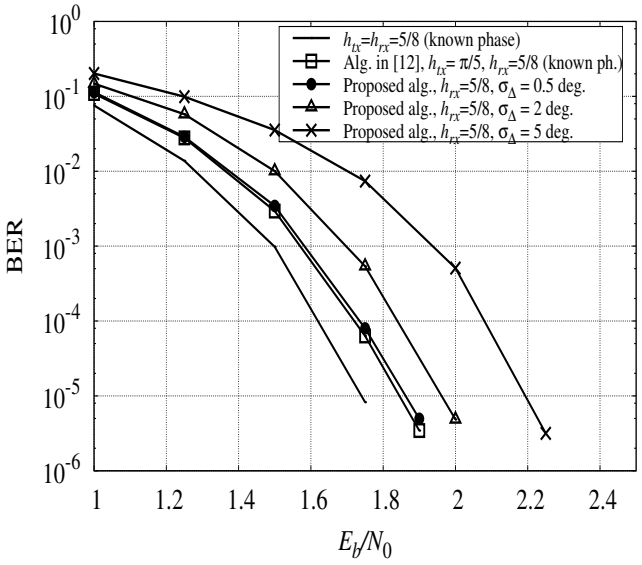

Figure 9: Performances en TEB d'une modulation CPFSK binaire concaténée en série avec un CC (7,5) à travers un entrelacement pseudo-aléatoire de longueur 2048, avec un indice de modulation irrationnel $\frac{\pi}{5}$ et en présence d'un bruit de phase avec une déviation standard σ_Δ.

Systèmes multi-utilisateurs basés sur la CPM robustes

Solution côté émetteur

Dans cette partie, nous abordons le problème de la robustesse dans un système multi-utilisateurs basé sur la modulation CPM. Chaque émetteur faible coût génère un signal CPM binaire avec une erreur sur l'indice de modulation. Nous nous concentrons ici sur des solutions côté émetteur où une nouvelle technique d'accès multiple pour la modulation CPM est proposée. Nous proposons un système de communication multi-utilisateur qui garde la même largeur de bande qu'un système mono-utilisateur et qui permet ainsi d'avoir une augmentation significative de l'efficacité spectrale. Le schéma multi-utilisateurs proposé (figure 10) recourt à la

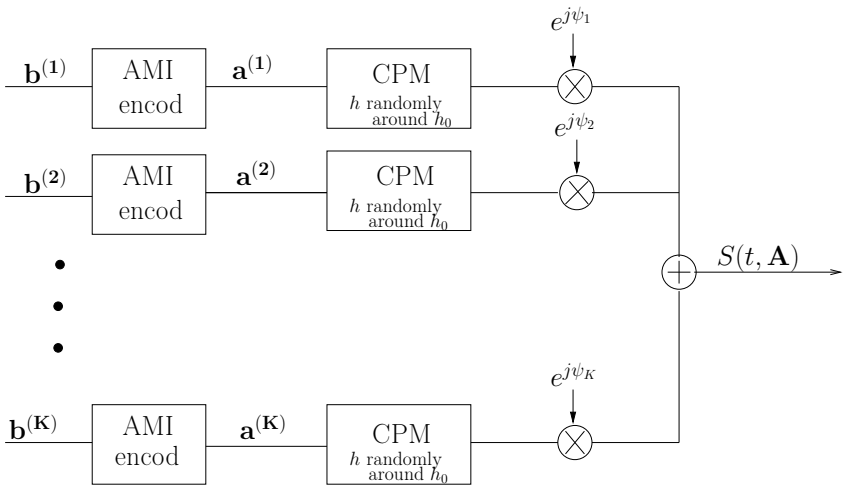

Figure 10: Modèle d'un système multi-utilisateur

concaténation en série d'un pré-codeur AMI avec un CPM ternaire suivi d'un dispositif de séparation entre utilisateurs basé sur une rotation de phase. Cela permet d'obtenir un système robuste pour des utilisateurs synchrones.

Les performances en TEB du cas non codé sont représentées sur la figure 11 pour 1 à 5 utilisateurs ; tous les utilisateurs ont le même format de modulation qui est 1RC avec l'indice de modulation nominal $h_0 = 3/8$. L'indice de modulation d'un utilisateur k noté $h^{(k)}$ est choisi selon une distribution uniforme dans l'intervalle $[h_0 - 0.05, h_0 + 0.05]$. Le critère de performance est la moyenne du TEB de tous les utilisateurs. Les phases séparant les utilisateurs ψ_k sont choisies d'une manière équidistante, c'est-à-dire $\psi_k = k\frac{\frac{3\pi}{4}}{K}$. L'optimisation théorique de ces phases pourra être faite ultérieurement : notre objectif est ici de montrer la faisabilité de la séparation des utilisateurs. La dégradation des performances de 1 à 2 utilisateurs est négligeable. Pour les deux utilisateurs, la quasi-orthogonalité entre les signaux est due principalement à la phase accumulée par le décalage causé par l'indice de modulation. Nous pouvons également noter que la perte de performance entre k et $k+1$ utilisateurs n'est pas constante. Par exemple, pour un TEB $= 10^{-4}$, la dégradation entre 2 et 3 utilisateurs est d'environ 3 dB alors entre 3 et 4 utilisateurs, il est d'environ 2 dB. On peut noter également qu'il n'y a pas de plancher d'erreur quand le nombre d'utilisateurs augmente.

Solution côté récepteur

Nous abordons maintenant la question de la robustesse du côté récepteur, dans un contexte multi-utilisateurs. Les détecteurs multi-utilisateurs optimaux ont une complexité qui augmente de façon exponentielle avec le nombre d'utilisateurs, donc des schémas de détection sous-optimales sont nécessaires. Récemment, un algorithme multi-utilisateurs de complexité réduite pour une transmission sur un canal AWGN a été proposé et utilise le *factor graph* et l'algorithme *sum-product* (SPA). Dans notre

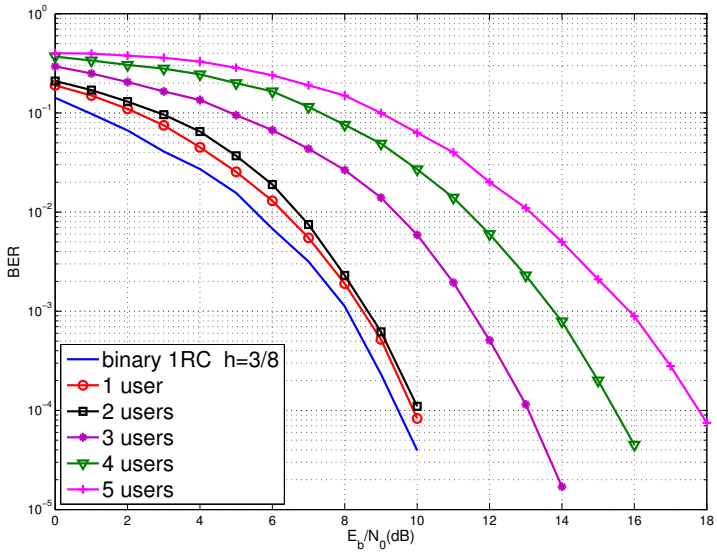

Figure 11: Performances en TEB dans le cas non codé, tous les utilisateurs ont la même modulation $1RC$ et le même indice de modulation nominal $h_0 = 3/8$

cas, l'outil constitué du *Factor Graph* et de l'algorithme *Sum product* est utilisé dans un double sens : en plus de son utilisation pour la réception multi-utilisateurs avec une complexité réduite, il est aussi utilisé pour effectuer une détection en présence d'une incertitude de l'indice de modulation et d'un bruit de phase, comme étudié au chapitre 3. Le détecteur multi-utilisateur robuste résultant est dénommé "*robust* FG-MUD".

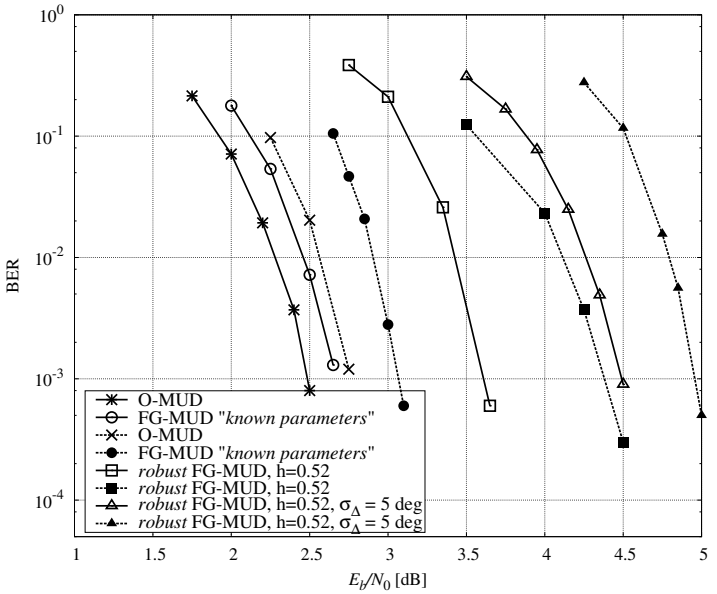

Figure 12: Performances multi-utilisateurs - solution côté récepteur:

List of Figures

List of Tables

Acronyms

5G fifth generation

M2M machine to machine

CPM continuous phase modulation

MMC massive M2M (machine-to-machine) communication

URC ultra-reliable communication

MTD machine type devices

FG factor graph

SPA sum product algorithm

PN phase noise

BER bit error rate

CE constant envelope

CSI channel state information

SNR signal-to-noise ratio

CDF cumulative distribution function

PDF probability distribution function

MGF moment generating function

AWGN additive white Gaussian noise

VA Viterbi algorithm

VCO voltage-controlled oscillator

PSP per survivor processing

AMI alternate Mark inversion

PSD power spectral density

METIS mobile and wireless communications enables for the twenty-twenty information society

MLSE maximum likelihood sequence detection

RC raised cosine

GFSK Gaussian frequency shift keying

GMSK Gaussian minimum shift keying

MAP maximum a posteriori

BCJR Bahl, Cocke, Jelinek and Raviv

SCCPM serial concatenation CPM

APP a posteriori probability

PSD power spectral density

TDMA time division multiple access

FDMA frequency division multiple access

CDMA code division multiple access

DVB-S digital video broadcasting by satellite

UEP uniform error property

AM amplitude modulation

FM frequency modulation

BPSK binary phase shift keying

PSK phase shift keying

QAM quadrature amplitude modulation

SISO soft input soft output

SE spectral efficiency

IR information rate

EXIT extrinsic information transfer

MF matched filter

PAM pulses amplitude modulation

CPFSK continuous phase frequency shift keying

MM memoryless mapper

BICM bit interleaved coded modulation

LLR log likelihood ratio

MDD multiple differential detection

SOQPSK shaped-offset quadrature phase shift keying

PMF probability mass function

MUD multi-user detection

Notations

Symbol	Description
h	transmission modulation index
h_v	virtual modulation index
h_e	modulation index error
Δ_h	modulation index mismatch
$s(t)$	transmitted signal
$S(f)$	PSD of the transmitted signal
T	symbol duration
E	average symbol energy
E_b	energy per information bit
p	denominator of the modulation index
P_b	probability of bit error
M	modulation order
$\phi(t)$	transmitted signal phase
$q(t)$	phase response
$g(t)$	frequency response
$\boldsymbol{a}$	information symbol sequence
$\boldsymbol{b}$	information bit sequence
L	frequency response length
$r(t)$	received signal
N_0	power spectral density

N_s	oversampling factor
$\hat{\boldsymbol{a}}$	estimated symbol sequence
$\hat{\boldsymbol{b}}$	estimated bit sequence
Ω_n	branch metric
σ_n	trellis state
ϕ_n	phase state
$\Delta\phi_n$	accumulated phase state
θ_n	phase noise
α_n	forward recursion
β_n	backward recursion
d_{min}	normalized minimum Euclidean distance
d_B	upper bound on the minimum distance
I	information rate
η	spectral efficiency
I_A	a priori information
I_E	extrinsic information

List of Publications

Journal Papers

Published

- M. Messai, G. Colavolpe, K. Amis, and F. Guilloud, "Robust Detection of Binary CPMs with unknown modulation index" *IEEE Commun. Letters*, vol. 19, no.3, pp. 3339-342, March 2015. (Second part of Chap.4)
- M. Messai, G. Colavolpe, K. Amis, a nd F. Guilloud, "Binary Continuous Phase Modulations Robust to a Modulation index Mismatch" *IEEE Trans. Commun.* (First part of Chap.4)
- M. Messai, K. Amis, and F. Guilloud, "On the optimization of a PSP-based CPM detection" *IEEE Trans. Wireless Commun.* (Chap.3)
- M. Messai, A. Piemontese, G. Colavolpe, K. Amis and F. Guilloud, "Binary CPMs with Improved Spectral Efficiency" *IEEE Commun. Letters.* (Chap.2).

To be Submitted

- M.Messai, G.Colavolpe, F. Guilloud, and K. Amis, "A new multiple access technique for synchronous binary CPM system" *to be submitted at IEEE Transactions.* (Second part of Chap.5).

Conference Papers

Published

M. Messai, F. Guilloud, and K. Amis, "A low complexity coherent CPM receiver with modulation index estimation," *in Proc. European Signal Processing Conf., 2014.*. (Third part of Chap.3)

M. Messai, K. Amis, and F. Guilloud, "A Low Complexity Iterative Soft Detection for Bit Interleaved Coded CPM," *Turbo Codes and Iterative Information Processing (ISTC), 2014 8th International Symposium on.* (Fourth part of Chap.3)

M. Messai, F. Guilloud, K. Amis, and G.Colavolpe, "Robust Multiuser Binary CPM Detection with Unkown modulation index," *Proc. European Signal Processing Conf., 2015.*. (Fourth part of Chap.5)

M. Messai, F. Guilloud et K. Amis, "Détection Multi-utilisateurs Robuste pour un système Bluetooth" *"La 25ème édition du colloque Gretsi 2015.* (Fourth part of Chap.5)

French Patent

Brevet francais n^{o} 13/54723 "Procédé de démodulation et démodulateur d'un signal modulé à phase continue, et programme d'ordinateur correspondant" Karine AMIS, Frédéric GUILLOUD et Malek MESSAI. (Third part of Chap.3)

Contents

Chapter 1

Introduction

Contents

1.1 Machine-to-machine communications

From 2G to today's 4G, wireless systems have evolved considerably so as to ensure user connectivity at higher data rates. This evolution is expected to progress in the fifth generation (5G) wireless system. Many strong indications [1], [2] show that 5G will not only be "4G, but faster" but will also include at least two new operating modes which are *Ultra-Reliable Communication (URC)* and *Massive M2M (Machine-to-Machine) Communication (MMC)*. Machine-to-machine (M2M) communication is recognized as a new kind of communication that enables pervasive connectivity between one or more autonomous machine type devices (MTD) [3], [4]. A massive increase in the number of connected devices is expected: the number of machines connected to the cloud will reach 50 billion by 2020 and all will need to access and share data, wherever and whenever [5], [6]. Up to 2020, the future mobile and wireless communication systems challenge have to respond to these societal needs by improving the efficiency in cost, energy and spectral efficiency, by ensuring at once better scalability to deal with the large number of connected devices. This latter was the goal of the METIS (Mobile and wireless communications Enables for the Twenty-twenty Information Society) project [7]. However, M2M communication represents the key technology to facilitate the new paradigm of applications, such as smart city, intelligent transportation, building automation, eHealth, security and surveillance.

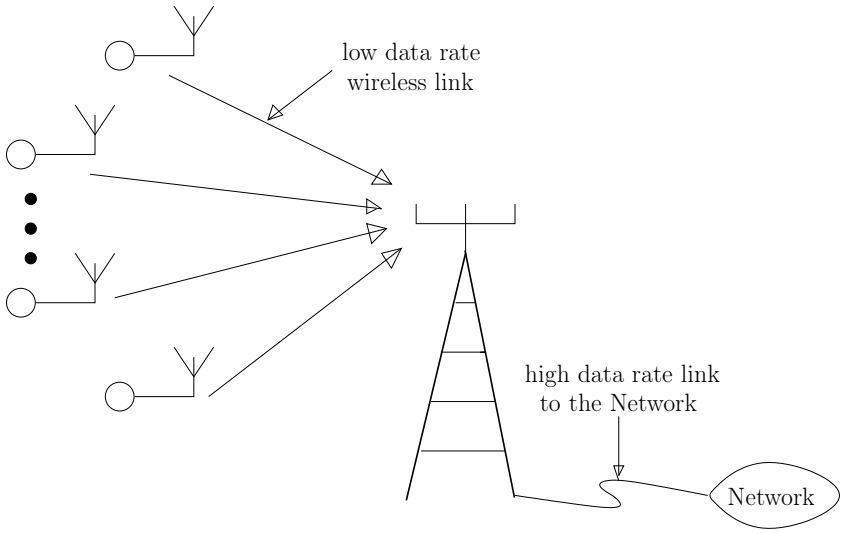

Figure 1.1: Massive deployment of machine type communication devices (MTD)

1.2 Scope of the Thesis

The analysis of communication evolution predicts an increase in the number of connected machines [8]. This is related especially to the regular emergence of surveillance applications/remote control in various fields such as the environment (to anticipate the volcanic eruptions for example), health (for tracking a patient at home from the surgery) or industry (sensor networks, smart meters). Machine-to-machine communication (M2M) is a future challenge [9]. The mentioned applications involve the deployment of a huge number of connected machines which are stand-alone devices into energy (battery, solar panels,...) and with a limited processing complexity. Information is transmitted to a concentrator (or fusion center) having a higher processing capability. The foundation of this thesis are laid in this framework: we aim to determine a multi-user communication system adapted to the material limitation of the machines and applications constraints. Power and cost efficient digital modulation is required for both economical and environmental reasons, the power consumption in the link should be as low as possible. Constant envelope modulation offers the possibility to use non-linear cost-effective and power-efficient amplifiers. Continuous phase modulation exhibits constant envelope and the continuous phase makes the power frequency spectrum be well confined with the possibility to achieve small spectral sidelobes. Continuous phase modulation (CPM) [10] is characterized by two interesting properties for the considered applications. The first is the constant envelope that allows the use of nonlinear amplifiers with lower quality-power and thus a low-cost transmitter. The transmitted base band signal amplitude doesn't vary which makes the CPM robust to amplitude distortion and well-adapted to satellite communications. The second property is the phase continuity that yields a spectrum with a narrower main lobe and lower sidelobes allowing an efficient bandwidth [11]. Spectral efficiency is today a crucial factor given the

scarcity of the spectrum resources. Moreover, the recursive nature of the CPM modulator [12] makes it attractive in serially concatenated schemes. These advantages: constant envelope, power efficiency and spectral efficiency enable CPM to be widely used in low-cost and low power consumption transmitter standards. The memory of CPM signals introduced by the phase continuity [12] requires reliable reception using the maximum likelihood sequence detection (MLSD) approach, which can be implemented using the Viterbi algorithm (VA) [13]. The complexity of MLSD demodulator highly depends on the number of matched filters and the number of states in the VA. Furthermore, the analog implementation of the CPM modulator enables to further reduce the transmitter cost, at the expense of possible variation of CPM waveform parameters around their nominal values yielding parameter mismatches between the receiver and the transmitter side. Therefore, the advantages of CPM are balanced with the primary disadvantages, which are *the complexity at the receiver side* and *the sensitivity to the parameters mismatch* around their nominal values. One of the most important parameters that define a CPM signal is the modulation index. For analog implementation of the transmitters, it depends on the gain of the voltage-controlled oscillator (VCO). The nominal modulation index, usually used at the receiver side denoted by h, is rational, which makes possible the trellis representation of the CPM. The optimum receiver for the signal with rational h is the trellis-based maximum likelihood sequence detector (MLSD). However, in analog implementation, since the gain of the VCO may not be well calibrated, the transmission modulation index h can vary with an error shift denoted by h_e with respect to its nominal value.
The PhD contributions are the following:

- First, we addressed the spectral efficiency improvement of binary CPM and we proposed a precoded ternary scheme for that purpose.

- Second, we considered the problem of demodulation complexity and designed a reduced-state per survivor processing-based CPM detector that strikes a balance between error-rate performance and computation cost.

- Third, we dealt with the robustness to modulation index mismatch and phase noise by tackling the issue from the transmitter and the receiver sides. We first defined precoded ternary CPM schemes where the precoder is designed so as to manage the phase evolution. We then applied the sum-product algorithm working on a proper factor graph to obtain a robust receiver.

- Fourth, we extended the robustness problem to the multi-user case. We first proposed a multiple access technique based on AMI-precoded ternary CPM user signals separated thanks to phase shifts. We then study the frequency division multiplexing-CPM scheme with optimized adjacent overlapping bandwidths and adapted the multi-user joint detection based on the sum-product algorithm working on an appropriate factor graph to make it robust to modulation index uncertainties and time-varying phase noise.

1.3 Continuous Phase Modulation

1.3.1 CPM Signal Model

The complex baseband CPM signal is defined as [10]:

$$s(t,h,\boldsymbol{a}) = \sqrt{\frac{E}{T}} e^{j\phi(t,h,\boldsymbol{a})}, \tag{1.1}$$

where E is the average symbol energy, T is the symbol duration and $\phi(t,h,\boldsymbol{a})$ is the information-carrying phase given by:

$$\phi(t,h,\boldsymbol{a}) = 2\pi h \sum_{i=0}^{\infty} a_i q(t-iT). \tag{1.2}$$

$\boldsymbol{a} = \{a_i\}$ denotes the information sequence. The information symbols a_i are assumed to be independent and identically distributed and to take on values in the M-ary alphabet $\mathcal{M} = \{\pm 1, \pm 3, ..., \pm(M-1)\}$. $q(t)$ is the phase response and it is expressed as the integral of the normalized frequency pulse $g(t)$ as follows:

$$q(t) = \int_{-\infty}^{t} g(\tau) d\tau, \tag{1.3}$$

where $g(t)$ is defined for $t \in [0,\ LT]$ and satisfies the two following conditions:

$$\begin{aligned} g(t) &= g(LT-t), \\ \int_0^t g(\tau)d\tau &= q(LT) = \frac{1}{2}, \quad t \geq LT. \end{aligned} \tag{1.4}$$

Below we give the definitions of some popular analytically defined frequency pulses together with their phase pulses. They will be used in our study. We denote also by LCPM the CPM frequency pulses with length L.

Rectangle referred to as: LREC

$$g(t) = \begin{cases} \dfrac{1}{2LT} & 0 \leq t \leq LT \\ 0 & \text{otherwise} \end{cases} \tag{1.5}$$

The popular MSK signal uses the REC pulse with $L = 1$.

Raised Cosine referred to as: LRC

$$g(t) = \begin{cases} \dfrac{1}{2LT}\left(1 - \cos\left(\dfrac{2\pi t}{LT}\right)\right) & 0 \leq t \leq LT \\ 0 & \text{otherwise} \end{cases} \tag{1.6}$$

Gaussian Frequency Shift Keying referred to as: LGFSK

$$g(t) = \begin{cases} \dfrac{1}{2T}\left(Q\left(\gamma.B\left(t-\dfrac{T}{2}\right)\right) - Q\left(\gamma.B\left(t+\dfrac{T}{2}\right)\right)\right), & 0 \leq t \leq LT \\ 0 & \text{otherwise} \end{cases} \tag{1.7}$$

with $\gamma = 2\pi/\sqrt{\log(2)}$, BT is the 3-dB bandwidth time product, and $Q(x) = \frac{1}{\sqrt{2\pi}} \int_x^{+\infty} \exp(-\frac{\tau^2}{2}) d\tau$.

Figure 1.2 shows the frequency pulse $g(t)$ and the corresponding phase pulse $q(t)$ for different waveforms. Using the properties of $q(t)$ and $g(t)$ given in (1.3) and (1.4),

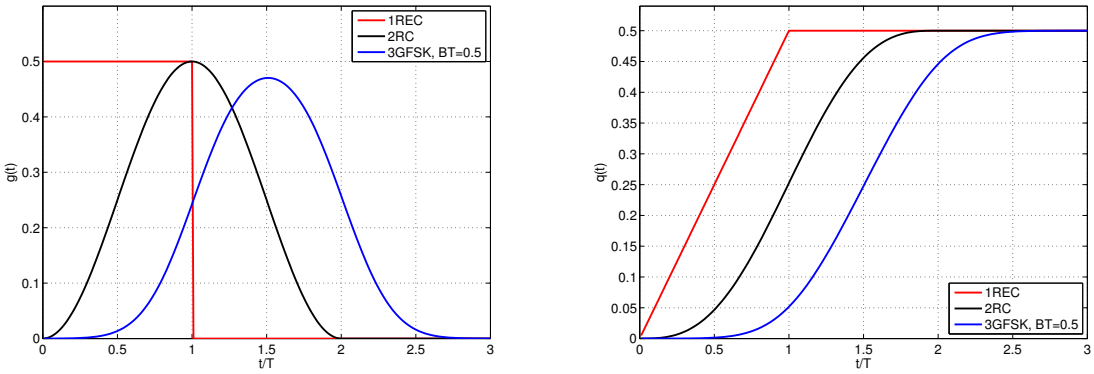

(a) Frequency pulses.

(b) Phase pulses.

Figure 1.2: Some frequency pulses and their corresponding phase pulses

the information-carrying phase during the n-th time interval, $t \in [nT,\ (n+1)T]$, $n \in \mathbb{N}$, can be written as:

$$\begin{aligned} \phi(t, h, \boldsymbol{a}) &= 2\pi h \sum_{i=0}^{\infty} a_i q(t - iT), \\ &= \pi h \sum_{i=0}^{n-L} a_i + 2\pi h \sum_{i=n-L+1}^{n} a_i q(t - iT), \\ &= \phi_{h,n} + \phi_{h,n}(t). \end{aligned} \tag{1.8}$$

From (1.8) we observe that the modulated signal over the n-th time interval depends both on the phase state denoted by $\phi_{h,n}$ and on the $L-1$ most recent symbols, i.e $\omega_n = (a_{n-1}, ..., a_{n-L+1})$. For a rational modulation index $h = \frac{r}{p}$ (r and p are relatively prime integers), the phase state $\phi_{h,n}$ modulo 2π can take only p different values. Therefore, the phase evolution can be described by a finite-state machine, where each state is represented by an L-dimensional vector $\sigma_n = (\phi_{h,n}, \omega_n)$ and where the number of such states is pM^{L-1} or $2pM^{L-1}$ respectively for r even or odd. The different possible phase trajectories constitute a phase tree. This tree is formed by all phase trajectories $\phi(t, h, \boldsymbol{a})$ having a common starting phase equal to zero at time $t = 0$. Figure 1.3 shows a phase tree for a 2RC scheme over the interval $[0, 5T]$. As mentioned before, $2RC$ means a CPM modulation with raised cosine waveforms of length $L = 2$.

1.3.2 Coherent Detection of the CPM Signal

Although the bandwidth of the CPM signal in (1.1) is infinite, strictly speaking, we assume hereafter that it can be limited to $N_s/2T$, N_s being a positive integer chosen such that the approximation is fair. Thus, a sampling rate yielding N_s samples per symbol produces an approximated set of sufficient statistics [14] provided that the received signal has been pre-filtered through an analog low-pass filter having a vestigal symmetry around $N_s/2T$. An oversampling factor $N_s = 10$ is considered in the whole document.

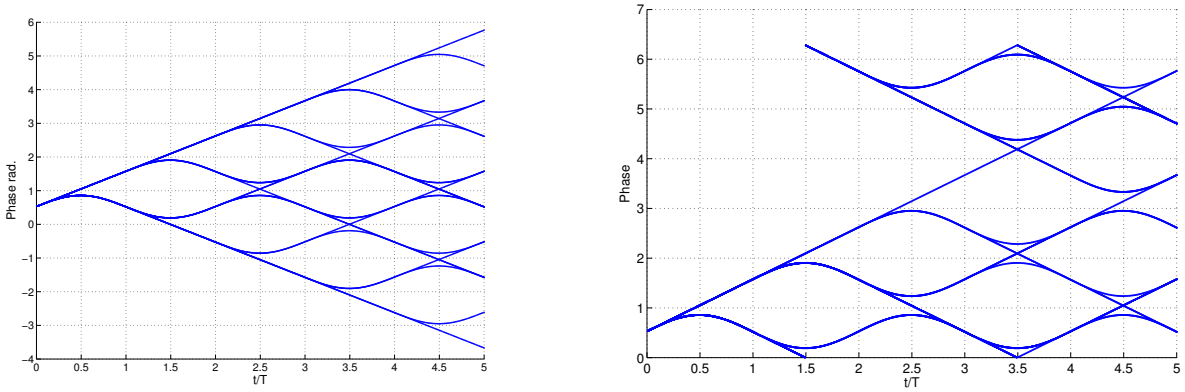

(a) Different phase trajectories for binary 2RC modulation with $h = 1/3$.

(b) Different phase trajectories (modulo 2π) for binary 2RC modulation with $h = 1/3$.

Figure 1.3: A phase tree for 2RC modulation

1.3.2.1 Optimal Maximum Likelihood Sequence Estimation (MLSE) Detector for CPM

We assume that the signal is transmitted over a Gaussian channel. The equivalent baseband received signal, denoted by $r(t)$, reads as:

$$r(t) = s(t, h, \boldsymbol{a}) + n(t), \tag{1.9}$$

where $n(t)$ is a realization of a zero-mean wide sense stationary complex circularly symmetric Gaussian noise, independent of the signal, and with double-sided power spectral density $2N_0$ over the bandwidth of $s(t, h, \boldsymbol{a})$. The MLSE-detector aims to find the sequence $\hat{\boldsymbol{a}}$ minimizing the Euclidean distance between $s(t, h, \hat{\boldsymbol{a}})$ and the received signal $r(t)$ defined by

$$\hat{\boldsymbol{a}} = \arg\min_{\tilde{\boldsymbol{a}}} \parallel r(t) - s(t, h, \tilde{\boldsymbol{a}}) \parallel^2, \tag{1.10}$$

Since $s(t,h,\tilde{\boldsymbol{a}})$ has a constant envelope, minimizing (1.10) is equivalent to maximizing the correlation

$$\hat{\boldsymbol{a}} = \arg\max_{\tilde{\boldsymbol{a}}} \underbrace{\mathrm{Re}\{\int r(t)s^*(t,h,\tilde{\boldsymbol{a}})dt\}}_{\Omega(\tilde{\boldsymbol{a}})}, \tag{1.11}$$

where $(.)^*$ is the complex conjugate. The correlation between $s(t,h,\tilde{\boldsymbol{a}})$ and $r(t)$ is called *path metric* of the sequence $\tilde{\boldsymbol{a}}$. The number of possible sequences $\tilde{\boldsymbol{a}}$ increases exponentially with the sequence length. Unfortunately due to their number, it is not possible to calculate all the path metrics. This structure is not feasible in practice even with reasonably short data burst. So, we define

$$\Omega_n(\tilde{\boldsymbol{a}}) = \mathrm{Re}\left\{\int_{-\infty}^{nT} r(t)s^*(t,h,\tilde{\boldsymbol{a}})dt\right\}. \tag{1.12}$$

Therefore, we can write

$$\Omega_n(\tilde{\boldsymbol{a}}) = \Omega_{n-1}(\tilde{\boldsymbol{a}}) + \Omega^{(n)}(\tilde{\boldsymbol{a}}), \tag{1.13}$$

where $\Omega^{(n)}(\tilde{\boldsymbol{a}})$ is the *branch metric* defined by

$$\Omega^{(n)}(\tilde{\boldsymbol{a}}) = \mathrm{Re}\left\{\int_{(n-1)T}^{nT} r(t)s^*(t,h,\tilde{\boldsymbol{a}})dt\right\} \tag{1.14}$$

By using the above formulas, we can recursively compute the function $\Omega(\tilde{\boldsymbol{a}})$ from (1.13). The Viterbi algorithm (VA) [13] is based on this principle and uses the trellis discussed earlier. The algorithm has to store the preceding path metric and the preceding path (corresponding to the *survivor path*) for all states in the trellis. The number of states and branch metrics in each symbol interval is respectively pM^{L-1} and pM^L. We introduce then, $\Omega_{i,k}^{(n)}$ the *branch metric* corresponding to the scalar product associated to the transition from state $\sigma_{n-1}^{(i)} = (\phi_{h,n-1}^{(i)}, a_{n-1}, a_{n-2}, ..., a_{n-L+1})$ to state $\sigma_n^{(k)} = (\phi_{h,n}^{(k)}, a_n, a_{n-1}, ..., a_{n-L+2})$, where a_n is the symbol related to the transition during the n-th time interval. The branch metric is calculated as follows:

$$\Omega_{i,k}^{(n)} = \mathrm{Re}\{\int_{(n-1)T}^{nT} r(t)e^{j(\phi_{h,n}^{(i)} + \phi_{h,n}^{(i)}(t))}dt\}, \tag{1.15}$$

The Viterbi algorithm is based on the recursive computation of the accumulated metric at state $\sigma_n^{(k)}$ and time instant nT denoted by $\Omega_n^{(k)}$ and defined as:
$\Omega_n^{(k)} = \max_i \left(\Omega_n^{(i)} + \Omega_{i,k}^{(n)}\right)$. At the end, the MLSE-based decision is given by the sequence $\tilde{\boldsymbol{a}}$ yielding the maximum of $\Omega_N^{(k)}$ over k.

1.3.2.2 MAP symbol coherent detection of CPM signals

While the Viterbi algorithm enables to estimate the most probable sequence, the *maximum a posteriori* (MAP) symbol detection provides the most likely symbol. It

aims to maximize the *a posteriori* probability (APP) $p(a_n|\boldsymbol{r})$ [15]:

$$\hat{a}_n = \arg\max_{a\in\mathcal{M}} p(a_n = a|\boldsymbol{r}) \tag{1.16}$$

The BCJR algorithm [16] performs a symbol by symbol MAP detection and uses the trellis representation of the CPM. Using the definition of σ_n given in (1.3.1), we can express the conditional probability of (1.16) as

$$p(a_n = a|\boldsymbol{r}) = \sum_{\sigma_{n+1}|a_n=a} p(\sigma_{n+1}|\boldsymbol{r}) \tag{1.17}$$

The BCJR algorithm associates to each node in the trellis the corresponding APP $p(\sigma_n|\boldsymbol{r})$ and to each branch in the trellis the corresponding $p(\sigma_{n-1}, \sigma_n|\boldsymbol{r})$,

$$\begin{aligned}
\lambda_n(\sigma_n) &= p(\sigma_n|\boldsymbol{r}), \\
&\propto p(\sigma_n|\boldsymbol{r}_0^{n-1}).p(\boldsymbol{r}_n^N|\sigma_n, \boldsymbol{r}_0^{n-1}), \\
&\propto p(\sigma_n|\boldsymbol{r}_0^{n-1}).p(\boldsymbol{r}_n^N|\sigma_n), \\
&\propto \alpha_n(\sigma_n)\beta_n(\sigma_n),
\end{aligned} \tag{1.18}$$

where $\boldsymbol{r}_{n_1}^{n_2}$ is the received signal from the begining of the n_1-th time interval until the end of the n_2-th time interval. $\alpha_n(\sigma_n)$ and $\beta_n(\sigma_n)$ denote the forward-accumulated and backward-accumulated metrics, respectively and are recursively computed as

$$\alpha_n(\sigma_n) = \sum_{\sigma_{n-1}} \alpha_n(\sigma_{n-1})\gamma_n(\sigma_{n-1}, \sigma_n), \tag{1.19}$$

and

$$\beta(\sigma_n) = \sum_{\sigma_{n+1}} \beta_n(\sigma_{n+1})\gamma_n(\sigma_n, \sigma_{n+1}), \tag{1.20}$$

where the branch metric $\gamma_n(\sigma_n, \sigma_{n+1})$ is defined as:

$$\begin{aligned}
\gamma_n(\sigma_n, \sigma_{n+1}) &= p(\sigma_n, \boldsymbol{r}_n|\sigma_{n-1}) \\
&= p(\boldsymbol{r}_n|\sigma_n, \sigma_{n-1})p(\sigma_n|\sigma_{n-1}) \\
&= \frac{1}{2\pi N_0} e^{-\frac{1}{2N_0}\int_{(n-1)T}^{nT} |r(t)-s(t,h,\boldsymbol{\alpha})|^2 dt}.p(\sigma_n|\sigma_{n-1}) \\
&\propto e^{\frac{1}{N_0}\,\mathrm{Re}\int_{(n-1)T}^{nT} r(t)s^*(t,h,\boldsymbol{\alpha})dt}.p(\sigma_n|\sigma_{n-1}).
\end{aligned} \tag{1.21}$$

As α and β are calculated iteratively, we need just to initialize $\alpha(\sigma_0) = 1$ and $\beta(\sigma_N) = \frac{1}{pM^{L-1}}$.

1.3.3 Performance of the CPM Modulation

The performances of a waveform modulation format are often described by two criteria which are its spectral efficiency and its power-efficiency. The existence of a compromise between these two criteria often makes it difficult to choose a waveform rather than another. In order to select the proper CPM formats, it's necessary to make a detailed study of the effect of each CPM parameter (h,L,$g(t)$). In this study, other aspects such as complexity will be considered to satisfy technical specifications.

1.3.3.1 Power spectral density (PSD)

This paragraph deals with the spectral properties of CPM signals. Despite the fact that the constant envelope is an interesting property, it is often detrimental at the expense of the PSD.It induces an occupied bandwidth much higher than the bandwidth of signals with envelope fluctuation. In the case of CPM modulations, this handicap can be compensated thanks to the high correlation of partial response CPM signals. The adoption of a frequency response length higher than one ($L > 1$) introduces a correlation in the signal, and thus reduces the spectral occupancy of the CPM signals. The higher parameter L the higher the reduction is. The spectrum of CPM signals also strongly depends on the frequency response, the modulation order and the modulation index.

Some estimation techniques of the CPM spectra have been proposed in [10], [17]. These semi-analytical methods are based on the computation of the signal correlation and thus allow to deduce an estimate of the spectrum [18]. The advantage of these techniques is that they require little numerical resources compared to other conventional methods. We opted for the periodogram method to estimate the spectra of CPM signals. In this calculation, we consider the Fourier transform averaged over several observation windows of the signal. Let x be a sampled signal of length N_x.

$$x = (x_1, x_2, ..., x_{N_x-1}, x_{N_x}) \tag{1.22}$$

Let m be an integer of the form $m = N_x/l$, where l is an integer divisor of N_x. We define then the window w by:

$$w(i) = \begin{cases} 1 & 0 \leq i \leq m-1 \\ 0 & \text{otherwise} \end{cases} \tag{1.23}$$

m is often a power of 2 which will allow to use fast algorithms to perform the Fourier transform. A shifted version of d terms of w denoted by w_d is defined by $w_d(i) = w(i - md)$. The power spectral density of the signal x denoted by $S_x(f)$, can be estimated by:

$$\hat{S}_x(f) = \frac{1}{m} \sum_{d=0}^{l} (|FFT(x * w_d)|^2). \tag{1.24}$$

where the notation $*$ denote convolution product.

Numerical Results

For a better analysis of the effect of each modulation parameter, several estimates of the spectra of different CPM signals were performed. Figures 1.4 and 1.5 illustrate respectively the effect of the frequency response length and the modulation index on the spectrum of a binary CPM. Whatever the order and the frequency response, the occupied bandwidth decreases with the length of the frequency response. It's maximal in the case $L = 1$ (full response CPM). We also note that the higher L the more reduced the secondary lobes. These lobes are almost absent when $L = 6$.

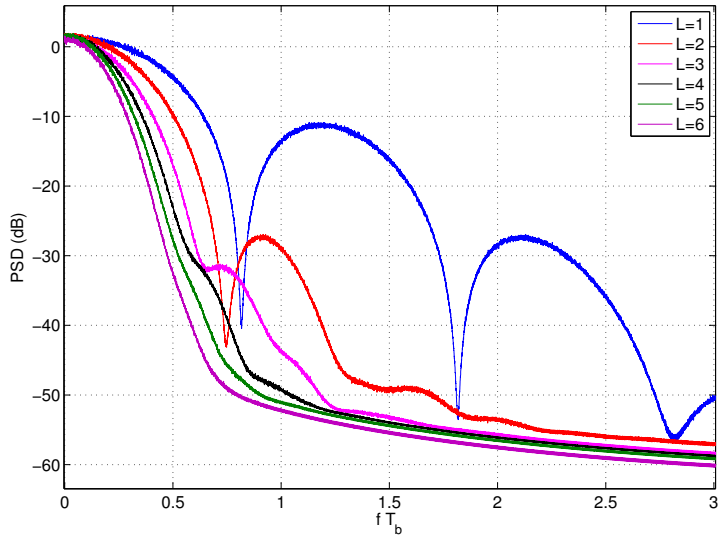

Figure 1.4: Spectrum of a binary CPM with a raised cosine frequency pulse for different frequency response length, $h = 1/2$

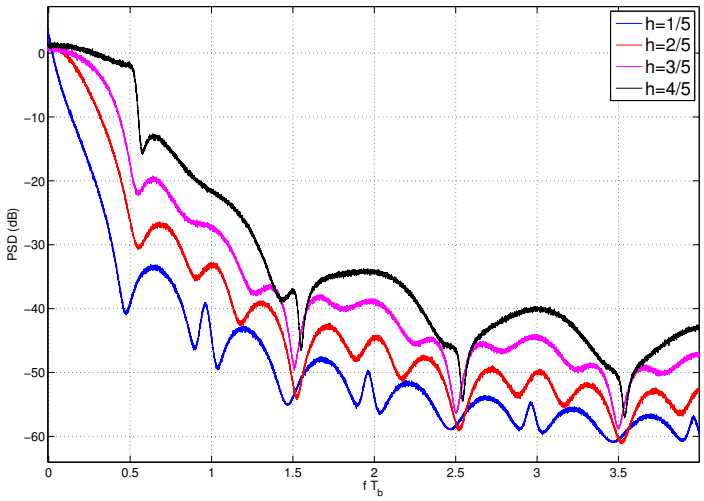

Figure 1.5: Spectrum of a binary 2REC with a rectangular frequency pulse for different modulation index

Given that the number of states in the trellis increases exponentially with L, and the bandwidth gain becomes less and less important with the increase of L, (Figure 1.4), it is more appropriate to choose a value of L less than 3. The modulation index h has also an impact on the spectral occupancy of the CPM signal, low values of h produce a narrower occupied bandwidth and vice versa. The frequency response

is also an element that affects the spectral properties of CPM signals. Figure 1.6 shows the shape of the spectra of some binary and quaternary CPM with different frequency responses.

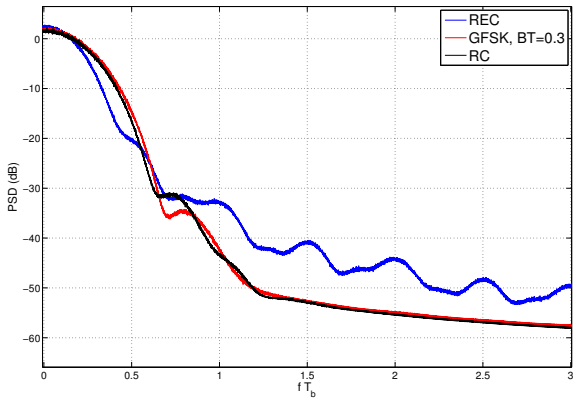

(a) Binary CPM

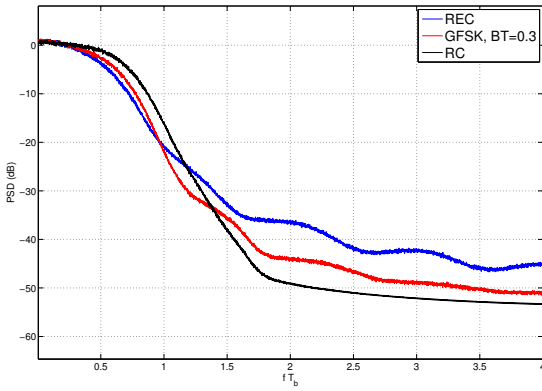

(b) Quaternary CPM

Figure 1.6: Spectrum of some binary (left) and quaternary (right) CPM for different frequency pulses, $L = 3$, $h = 1/2$

Compared with Gaussian and raised cosine frequency responses, the rectangular frequency response has a narrower main lobe, which provides better spectral efficiency (if we define the occupied bandwidth as the bandwidth that contains 99% of the overall signal power). On the other hand, the rectangular frequency response has an emitted outband power much higher than in the other two cases (Figure 1.6). This means that the adoption of a rectangular frequency response produces a relatively high level of interference. This point is important in a multi-user communication with a Multiple Frequency Time Division Multiple Access (MF-TDMA).

1.3.3.2 Bit Error Rate performance

In digital communications the bit error rate (BER) or symbol error rate (SER) is the measure criterion of the reliability of a transmission. In order to ensure the required quality of service, the BER should be less than a threshold value. This threshold value depends on the application. For example, it is of the order of 10^{-4} in the GSM mobile telephony service [19] and 10^{-3} in the Bluetooth standard [20]. For multimedia applications, the transmitted data are often highly compressed and very low BER is required. For example, in the case of the Digital Video Broadcasting by satellite (DVB-S) standard the bit error rate must be less than 10^{-10} [21]. For a Gaussian channel, the BER depends mainly on the minimum distance of the waveform denoted by d_{min}.

The theoretical calculation of the bit error rate is impossible in general, but for

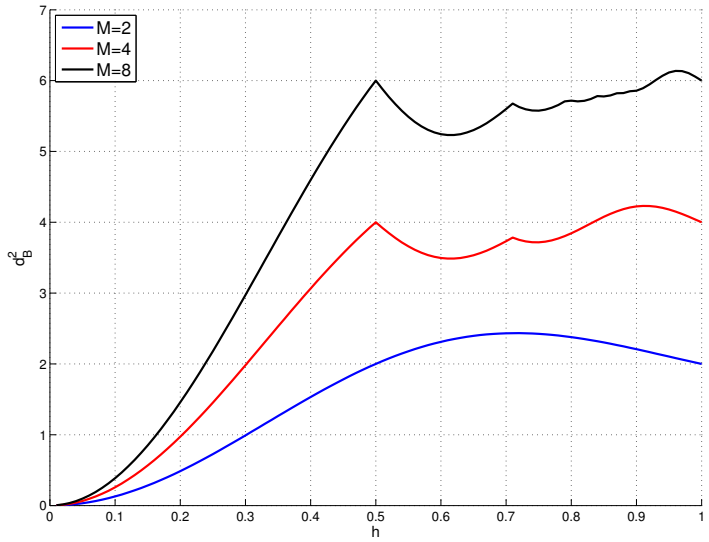

Figure 1.7: Upper bound on the minimum distance as a function of the modulation level M for 1REC modulation

relatively high SNR values the symbol error rate can be approximated by:

$$P_e \approx \mathrm{Q}\left(\sqrt{\frac{E_b}{N_0} d_{min}^2}\right). \tag{1.25}$$

where $\mathrm{Q}(*)$ is the error function defined by

$$\mathrm{Q}(x) = \int_x^{+\infty} \frac{1}{\sqrt{2\pi}} e^{-u^2/2} du \tag{1.26}$$

Error event

Unlike the *linear modulation*, errors of a CPM should satisfy particular conditions due to the CPM memory and its non-linearity. An error event starts when the estimated path through the trellis differs from the transmitted one. It ends when the two paths remerge into the same ending state. As CPM does not satisfy the Uniform Error Property (UEP) [22], the zero state cannot be assumed as a reference. Hence, a CPM error event has to be studied by considering all possible pairs of transmitted and detected paths. To this end, it is convenient to consider the so-called difference symbol sequence defined by $\boldsymbol{e} = \boldsymbol{a} - \hat{\boldsymbol{a}}$. Thus, reasoning in terms of the difference symbol sequence, an error event begins when a difference sequence leaves the all-zero path and ends when its path merges with the all-zero path for the first time.

Normalized squared Euclidean distance

The Normalized squared Euclidean distance between two $M-$ary CPM sequences $\boldsymbol{a}$ and $\hat{\boldsymbol{a}}$ of length N is:

$$\begin{aligned} d^2(\boldsymbol{a},\hat{\boldsymbol{a}}) &= \int_0^{NT} ||s(t,h,\boldsymbol{a}) - s(t,h,\hat{\boldsymbol{a}})||^2 dt \\ &= \frac{\log_2(M)}{T} \int_0^{NT} (1-\cos(\phi(t,h,\boldsymbol{e}))\, dt, \end{aligned} \tag{1.27}$$

The minimum normalized squared Euclidean distance $d^2_{\min}$ is defined as

$$d^2_{\min} = \min_{\substack{\boldsymbol{a},\hat{\boldsymbol{a}} \\ a_0 \neq \hat{a}_0}} \left(d^2(\boldsymbol{a},\hat{\boldsymbol{a}})\right) \tag{1.28}$$

The calculation of the minimum distance is practically impossible as it assumes that we consider sequences of infinite length. This minimum distance is approximated by an upper limit (upper bound) denoted d_B and estimated by using the error events of the first order. The pairs of sequences which interest us are those whose paths diverge at time 0 and coincide for the first time at $(L+m)T$ with $m \geq 1$. It's known [10], that the first merge occurs at time $(L+1)T$. In the simulations, we computed the upper bounds of the first, second, third and fourth orders and we considered the minimum of these curves to get an approximation of the minimum distance. The first results in Figure 1.7 illustrate the effect of the modulation index on the upper bound in the case of a binary 1REC with different modulation orders. Figure 1.8 shows the evolution of the upper bound for a partial response CPM for rectangular and raised cosine frequency pulses. It can be noticed that for a partial response CPM modulation, increasing the modulation order M enhances the power efficiency. The effect of the parameter L is illustrated in Figure 1.9 for binary CPM with a raised cosine frequency response. We observe that the modulation index interval can be divided into adjacent subintervals I_q such that $L = q$ enables to achieve the best minimum distance upper bound for $h \in I_q$ and thus a lower BER. For instance, $I_1 = [0, 0.5]$, $I_2 = [0.5, 0.6]$, $I_3 = [0.6, 0.75]$, $I_4 = [0.75, 1]$, $I_5 = [1, 1.2]$.

BER Simulations

In this section, we consider an uncoded CPM scheme. Both decoding algorithms, namely BCJR and Viterbi achieve exactly the same performance. The simulations focus mainly on the influence of the modulation index on the BER performance. Figure 1.10 shows the evolution of the BER according to the modulation index for binary 3GFSK modulation with $BT = 0.35$. It's clear that the higher h the lower the BER. For example, the passage from $h = 2/7$ to $h = 3/7$ is accompanied by a power gain of about 2.7 dB at BER $= 10^{-2}$.

Figure 1.11 shows the effect of the modulation index in the case of quaternary 2RC. A gain of 1 dB at BER$=10^{-5}$ is observed when passing from $h = 1/5$ to $h = 2/5$. Note that for both binary and quaternary CPM, the BER performance

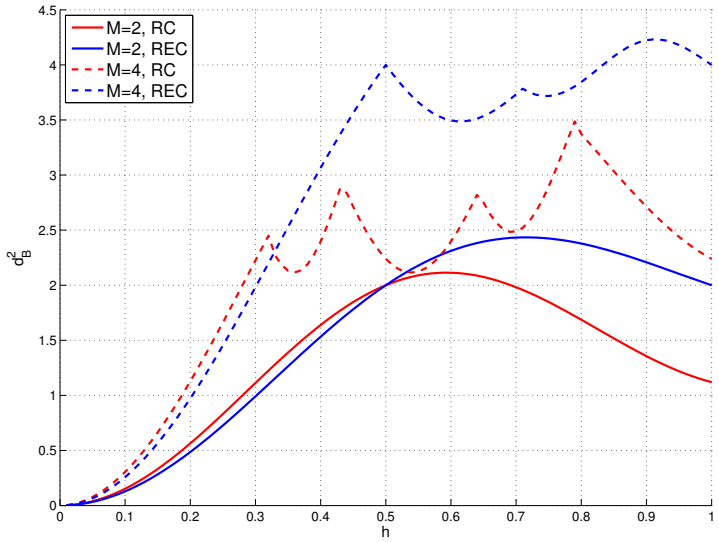

Figure 1.8: Upper bound on the minimum distance for different frequency pulses and different modulation orders

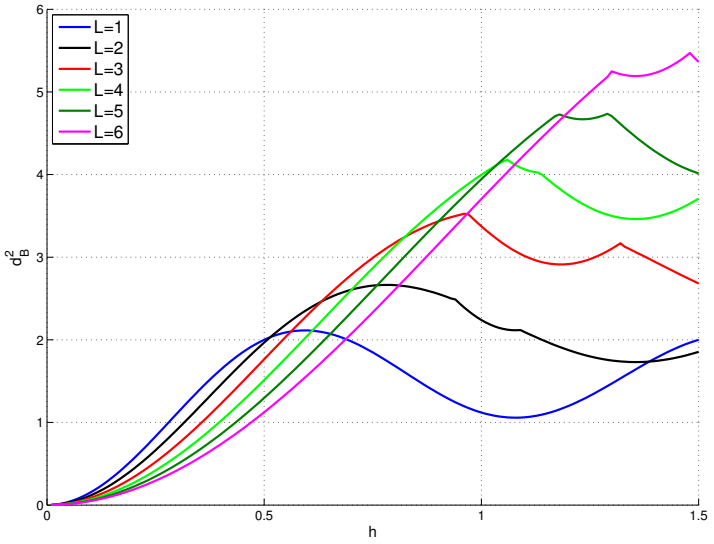

Figure 1.9: Upper bound on the minimum distance for raised cosine frequency pulses with different length L

is very sensitive to the modulation index value, especially when operating at low values of h.

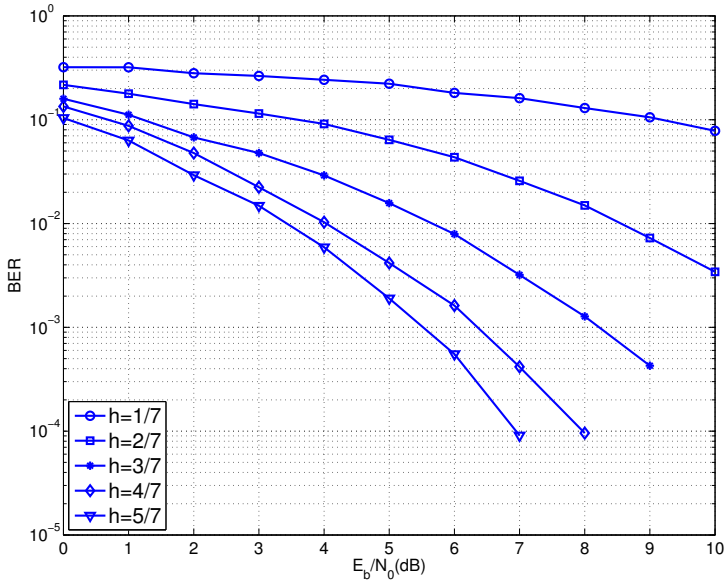

Figure 1.10: BER rate evolution for a binary 3GFSK with $BT = 0.35$ as a function of the modulation index

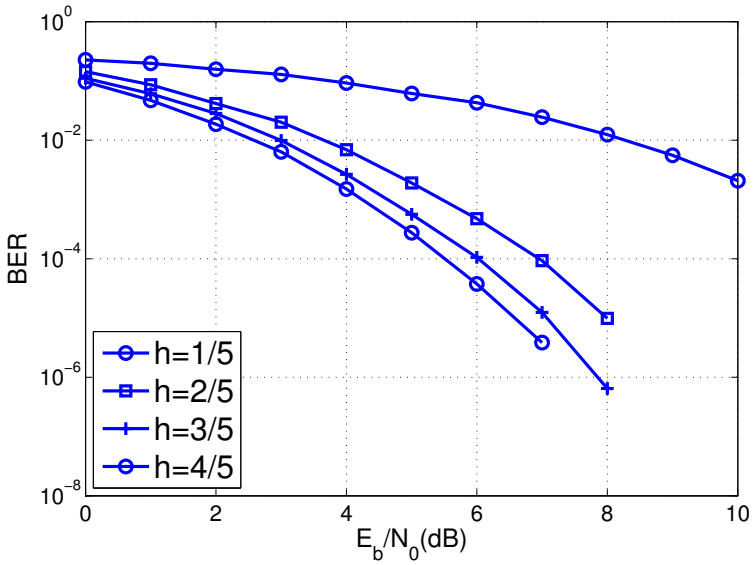

Figure 1.11: BER rate evolution for a quaternary 2RC as a function of the modulation index

1.3.4 Limitations of the CPM Modulation

Digital modulations can be classified into two main categories: amplitude or/and phase modulation, called also *linear modulation*, such as AM, BPSK, PSK, M-QAM,

APSK,..., and *non-linear modulation* also called *constant envelope modulation* like FM, CPM,... *Linear modulations* generally have better spectral properties than *non-linear modulations* [23],[24] since the constant envelope restricts the signal space and thus the minimum Euclidean distance at the receiver i.e the data partition is restricted to a unit circle. However, *linear modulations* map the information data into the amplitude and the phase of the transmitted signal. As a consequence, *linear modulations* are more susceptible to variations from interference and fading. Moreover, *linear modulation* techniques typically require linear amplifiers, which are more expensive and less power-efficient compared to the non-linear amplifiers which are used with the *non-linear modulation*. Therefore, the trade-off between *linear* versus *non-linear* modulation comes from the better spectral efficiency for the first one and the better power efficiency and robustness to channel impairments for the second one. The spectral efficiency is the first limitation of the CPM modulation. Optimal detection of *linear modulations* can be obtained through symbol-by-symbol demodulation methods where decisions are based on the observation of only one symbol period. Provided that the symbols are independent, the signal received on a given symbol period depends only on one symbol. The memory of CPM signals introduced by the phase continuity [12] requires detection of signals using the maximum likelihood sequence estimation (MLSE) approach. The complexity of MLSE demodulator highly depends on the number of states and on the matched filters in the VA. So, the second limitation of the CPM modulation is the detection complexity.

To perform optimally, the MLSE demodulation of a CPM signal requires the exact knowledge of the modulation index. Indeed whatever the signal to noise ratio, any imprecision on the modulation index can yield errors that accumulate over the whole observation interval. Hence, the third CPM constraint is the sensibility to phase offsets.

1.4 Outline of Thesis

The document is organized as follows:

Chapter 2 is dedicated to the increase of the spectral efficiency of CPM signals through the introduction of a precoder. We first focus on efficient design criteria and then we study the resulting demodulation structure. The performance in terms of theoretical BER and power spectrum density are also analysed.

In Chapter 3, we address the problem of low-complexity coherent detection of CPM signals. We exploit the per-survivor process (PSP) technique to build a reduced state trellis. Then, we give guidelines to choose the receiver parameters so as to ensure good error-rate performance.

In Chapter 4, we solve the problem of robustness either at the transmitter side or at the receiver side. Firstly, we consider the very general problem of soft-input soft-output (SISO) detection of a binary CPM signal with an unknown modulation index transmitted over a channel with phase noise. We adopt a simplified representation

of the CPM signal based on the principal component of its Laurent decomposition [25] and describe the joint a-posteriori probability of the transmitted symbols, the channel phase, and the modulation index through a factor graph (FG) [26]. The sum-product algorithm (SPA) is then advocated to compute the a-posteriori probabilities of the transmitted symbols [26]. Secondly, we resolve the problem of the unknown modulation index from the transmitter side. We design new binary schemes with a much larger robustness. They are based on the concatenation of a proper precoder with binary input and a ternary CPM format. The result is a family of CPMs formats whose phase state is constrained to follow a specific evolution.

Chapter 5 is devoted to the robustness problem in a multi-user system. Firstly, the Factor Graph and Sum Product algorithm framework will be used in a double way. It will serve to derive a robust multiuser binary CPM detector for FDM-CPM systems where the spectral efficiency (SE) of frequency-division-multiplexed (FDM) systems can be increased by reducing the spacing between adjacent users. Moreover, each user's binary CPM signal is generated through a low-cost transmitter, with the risk of a modulation index error, and transmitted over a channel affected by phase noise. The proposed algorithm is based on the Laurent representation of a CPM signal. The second scheme relies on the introduction of an AMI precoder per user so as to separate the users using their phase. It results in a robust multi-user CPM system for synchronous CPM users.

Finally chapter 6 concludes the document giving some perspectives and remarks on the main results.

Chapter 2

Precoded Ternary CPM with Improved Spectral Efficiency

Contents

2.1 Introduction

This chapter focuses on the *Spectral Efficiency* (SE) of binary CPM. We aim to find a transmission scheme that enables to increase the *Information Rate* (IR) without expanding the spectrum occupancy. The scheme is based on the concatenation of a binary input ternary output precoder and a ternary CPM. We start this chapter by defining the notion of *Information Rate* (IR) and *Spectral Efficiency* (SE). Then, we describe the designed precoder and its corresponding detector. The adopted precoder does not change the recursive nature of CPM schemes. So it is still suited for serial concatenation, through a pseudo-random interleaver, with an outer channel encoder. The performance of the interleaved coded CPM scheme resorts to an EXIT chart to analyse the convergence of the iterative receiver.

[0]This chapter is the subject of the publication: M. Messai, A. Piemontese, G. Colavolpe, K. Amis and F. Guilloud, "Binary CPMs with Improved Spectral Efficiency" *IEEE Commun. Letters.*

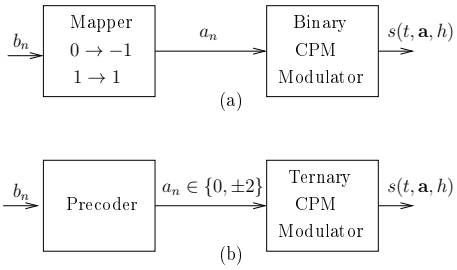

Figure 2.1: (a) Classical binary CPMs. (b) Proposed scheme.

2.2 Information rate and Spectral Efficiency

2.2.1 Information Rate

In [27] Arnold *et al.* proposed a simple simulation-based method to compute the information rates for channels with memory. For this purpose, let's consider a time-invariant discrete-time channel with memory where we denote respectively by $\boldsymbol{a} = (a_1, ..., a_J)$ and by $\boldsymbol{r} = (r_1, ..., r_J)$ the input and output sequences of the channel. We assume that the input symbols, belonging to a finite alphabet, are independent and identically distributed (i.i.d.) [1]. We define then the auxiliary state sequence $\sigma = (\sigma_1, ..., \sigma_{J+1})$, whose values vary according to a first-order Markov chain over a time-invariant finite-element set. Under these assumptions we can express

$$p(\boldsymbol{r}, \boldsymbol{\sigma}|\boldsymbol{a}) = P(\sigma_1) \prod_{i=1}^{J} p(r_i, \sigma_{i+1}|a_i, \sigma_i) \tag{2.1}$$

with $p(r_i, \sigma_{i+1}|a_i, \sigma_i)$ independent of i. To compute the IR between the input and output processes, we recall that if the number of transmitted information bits per channel use does not exceed the IR defined in [28], we can design a communication scheme with arbitrarily low error rate. For the considered channel, the IR $I(\boldsymbol{a}; \boldsymbol{r})$ reads

$$I(\boldsymbol{a}; \boldsymbol{r}) = \lim_{J \to +\infty} \frac{1}{J} \log_2 \left[\frac{p(\boldsymbol{r}|\boldsymbol{a})}{p(\boldsymbol{r})} \right], \tag{2.2}$$

The analytical computation of (2.2) is not possible in many cases of interest. So, we describe here some numerical methods [27] providing an accurate estimate of the IR. To use this simulation-based method, we need first to generate a very long sequence $\boldsymbol{a}$, according to the statistical properties of both the channel and the source (the length of the generated sequence is discussed in [27]). Then, $p(\boldsymbol{r}_1^i, \sigma_{i+1})$ can be efficiently calculated through the forward sum-product recursion of the BCJR algorithm [16]

$$p(\boldsymbol{r}_1^i, \sigma_{i+1}) = \alpha_{i+1}(\sigma_{i+1}) = \sum_{\sigma_i} \sum_{a_i} \alpha_i(\sigma_i) p(r_i, \sigma_{i+1}|\sigma_i, a_i) P(a_i) \tag{2.3}$$

[1] $\boldsymbol{a}$ is allowed to be Markovian [27].

and $p(\boldsymbol{r})$ is computed as

$$p(\boldsymbol{r}) = \sum_{\sigma_{J+1}} p(\boldsymbol{r}, \sigma_{J+1}) = \sum_{\sigma_{J+1}} \alpha_{J+1}(\sigma_{J+1}). \tag{2.4}$$

To compute $p(\boldsymbol{r}|\boldsymbol{a})$ we use a modified forward recursion defined in [27] as

$$\alpha'_{i+1}(\sigma_{i+1}) = \sum_{\sigma_i} \alpha'_i(\sigma_i) p(r_i, \sigma_{i+1}|\sigma_i, a_i) = p(\boldsymbol{r}_1^i, \sigma_{i+1}|\boldsymbol{a}_1^i). \tag{2.5}$$

Therefore, we obtain the estimate of (2.2) as

$$\hat{I}(\boldsymbol{a};\boldsymbol{r}) = \frac{1}{J}\left[\log_2\left(\frac{\sum_{\sigma_{J+1}} \alpha'_{J+1}(\sigma_{J+1})}{\sum_{\sigma_{J+1}} \alpha_{J+1}(\sigma_{J+1})}\right)\right] \quad \text{[bit/ch.use]}. \tag{2.6}$$

2.2.2 Spectral Efficiency

The spectral efficiency represents an important parameter for the evaluation of a modulation format quality, since it quantifies how many information bits per second can be loaded per unity of the available spectrum. To evaluate it, a suitable bandwidth definition is required. In fact, despite that almost the totality of power is located in a small portion of the spectrum [10], the PSD of a CPM signal has rigorously an infinite support. The most commonly used bandwidth definition is that based on the power concentration, which assumes that the CPM signal bandwidth is the portion which contains a given fraction ρ of the total power (this fraction is in general 99%,99.9%,...) [29, 30]. The total power of the transmitted CPM signal can be calculated as:

$$P_{tot} = \int_{-\infty}^{+\infty} |S(f)|^2 df \tag{2.7}$$

and the power in the bandwidth of interest associated to a defined fraction ρ:

$$P_{B_\rho} = \int_{-\frac{B_\rho}{2}}^{+\frac{B_\rho}{2}} |S(f)|^2 df \tag{2.8}$$

The SE is defined as the ratio between the information rate and the effective bandwidth. In the remainder of our study, we consider the bandwidth definition adopted in [10] ($\rho = 99\%$). The spectral efficiency η for the considered scheme can be computed as

$$\eta = \frac{\hat{I}(\boldsymbol{a};\boldsymbol{r})}{B_{99\%}T} \quad \text{[bit/s/Hz]} \tag{2.9}$$

2.3 Precoder Design

Our aim is to improve the SE of classical binary CPM modulators which is represented as depicted in Figure 2.1(a). Information bits $\{b_n\}$, belonging to the alphabet $\{0, 1\}$ are first mapped into symbols $\{a_n\}$ belonging to the alphabet $\{\pm 1\}$, before

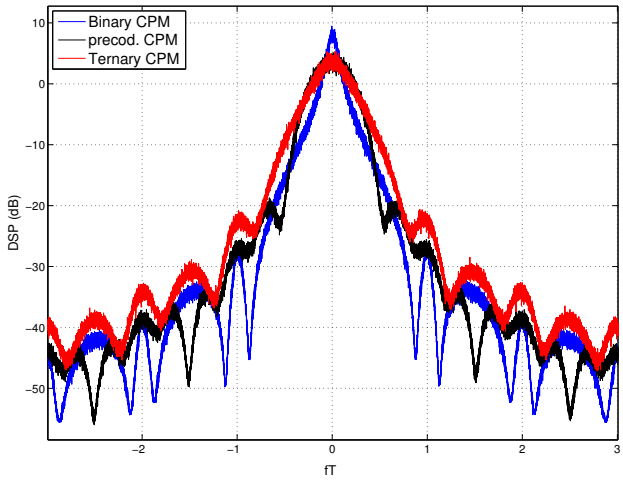

Figure 2.2: Power spectral densities comparisons for binary 1REC with $h = 1/4$

entering a binary CPM modulator. The schemes proposed in this chapter are based on the serial concatenation of an outer precoder and an inner ternary CPM. The outer precoder receives at its input bits $\{b_n\}$ belonging to the alphabet $\{0, 1\}$ and provides at its output ternary symbols $\{a_n\}$ belonging to the alphabet $\{0, \pm 2\}$. This concatenation is shown in Figure 2.1(b). It is reminiscent of the alternate mark inversion (AMI) precoder where the bit $b_n = 0$ is encoded as $a_n = 0$, whereas $b_n = 1$ is encoded alternately as $a_n = 2$ or $a_n = -2$ and of uncoded shaped-offset quadrature phase-shift keying (SOQPSK) [31] although the precoder is designed to reach a different goal and the ternary CPM scheme is generic here. The information rate can be increased by increasing the modulation order, but this results in an expansion of the spectrum occupancy. However, for the same modulation order, the IR depends on the bit error rate which is a decreasing function of the minimum distance. Thus to improve the IR, it is more appropriate to increase the minimum distance. Concerning the spectral occupancy of a CPM signal, the width of the main spectral lobe is related to the phase hopping that becomes important with the increase of the modulation order M or the modulation index h [10]. This is why using ternary symbols instead of binary symbols without precaution yields a bandwidth expansion due to the transitions from +2 and -2 and vice versa. However a ternary CPM signal without transitions between +2 and -2 or vice versa has the same spectrum occupancy as a binary signal. This can be achieved by using an outer precoder. The AMI precoder proposed in [32] yields a high frequency of such transitions which translates into a bandwidth expansion as compared to the binary CPM.

Our purpose is to design a precoder so as to increase the information rate without widening the spectrum occupancy that is to say design a precoder that ensures simultaneously:

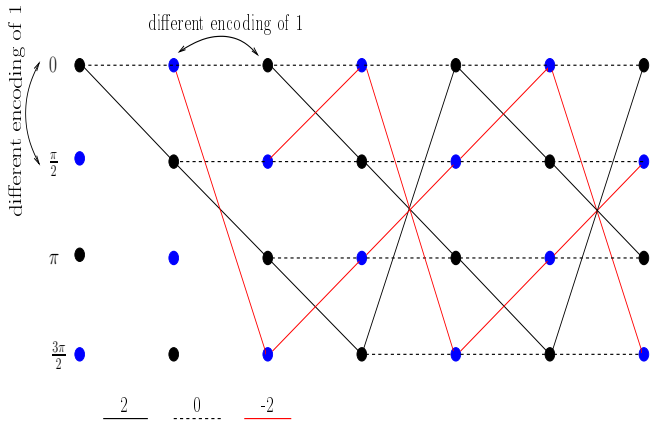

Figure 2.3: The phase trellis of a full response CPM modulation with h=1/4 (the proposed scheme).

- a high minimum distance (Information rate).
- the absence of transitions from 2 to -2 and vice versa (spectrum occupation).

The adopted strategy was to increase the IR through higher minimum distance while keeping roughly constant the spectrum occupancy. Our proposed precoder is simply defined by

$$a_n = b_n a_{n-d}(-1)^{d+1}, \tag{2.10}$$

where a_{n-d} is the latest symbol such that $|a_{n-d}| = 2$. In Figure 2.2, we plotted the power spectrum densities of a binary CPM, a ternary CPM and the proposed precoded CPM. We considered a rectangular frequency pulse with $L = 1$ and $h = 1/4$. We observe that the proposed scheme achieves almost the same spectrum occupancy as the binary CPM. Transitions from +2 to -2 and vice versa are prohibited thanks to the precoding rules. Concerning the information rate improvement, the proposed precoder has an optimized minimum distance compared to the binary CPM. This is due to the first merge. The first merge occurs at $t = (L+1)T$ for the binary CPM case [10] and at $t = (L+2)T$ for the proposed scheme. In Figure 2.3, we illustrated the proposed precoded ternary CPM design through the phase tree representation of different modulated sequences for the same modulation format as in Figure 2.2.

The minimum distance is given by the error event $\boldsymbol{e}_{min} = (2, -2)$ of length $2T$ in the case of binary CPM with full response. In the proposed precoded ternary CPM scheme the minimum distance is given by the error event $\tilde{e}_{min} = (2, 0, -2)$ of length $3T$. The multiplicity of the minimum distance is the same in both cases. We plotted in Figure 2.4 the minimum distance as a function of h for the proposed precoded ternary CPM, the full-response binary CPM as well as the binary CPM with $L = 2$ for which the first merger occurs at $t = 3T$. We observe that the proposed scheme outperforms the full-response binary CPM in terms of d_{min} over the whole range of $h([0, 1])$, while it exhibits a lower minimum distance from $h \simeq 0.78$ compared to the binary case with $L = 2$. We can thus predict an IR improvement.

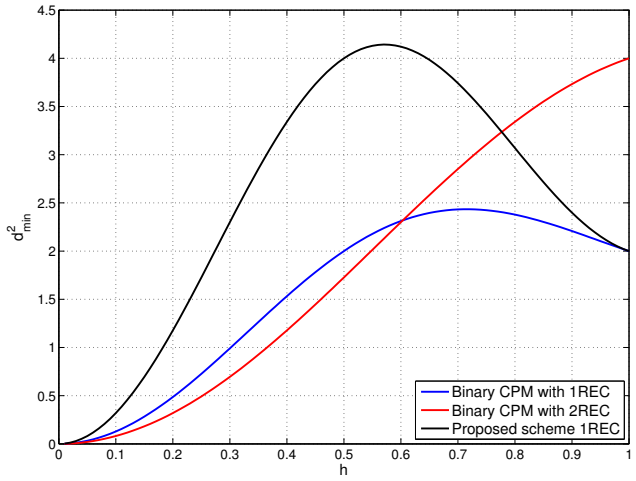

Figure 2.4: The minimum distance comparison

2.4 Corresponding Detector

In this part we describe the detection rule adapted to the proposed precoder. Let us consider a length-N binary sequence. It can take on 2^N values. However depending on the initialization, the precoder has 2^{N+1} possible output. For instance, for $N = 3$, we have 16 possible precoded sequences: $\{000, 020, 200, 220, 002, 0-20, -200, -2-20, 00-2, 022, 20-2, 222, 000, 0-2-2, -202, -2-2-2\}$ [2]. Given a transition from state $\sigma_i(n)$ to $\sigma_{i+1}(n)$, there exist two different encoding of the bit '1' depending on the preceding encoding of '1'. The number of the phase states is thus double as compared to a classic ternary CPM. We denote by $\overline{\theta}$ the complementary state of θ that satisfies $\overline{\theta} \equiv -\theta + 2\pi$. Let us consider a full response CPM ($L = 1$) with a modulation index $h = 1/3$. The diagram of the *phase state* is shown in Figure 2.5 and the trellis is represented in Figure 2.6. Starting from the state 0, we have three possible next states 0, $\frac{2\pi}{3}$ and $\overline{\frac{2\pi}{3}}$ depending on whether the transmitted symbol equals 0, 2 and -2 respectively. It is important to mention that when p is even, $\theta_i(n)$ and $\overline{\theta_i(n)}$ will have the same encoding of '1' and then the branch metrics going out from these two states will be equal. This implies that the two states $\theta_i(n)$ and $\overline{\theta_i(n)}$ can be combined into one state $\theta_i(n)$. As an example, for $L = 1$ and $h = 1/4$, the trellis is illustrated in Figure 2.3. Thus, the number of states is $p([p]_2 + 1)2^{L-1}$ where $[.]_2$ denotes the "modulo 2" operator. For the same precoder, the precoded ternary CPM will be represented by a trellis with a state number equal to the state number of the binary CPM for even values of p and double for odd values of p.

[2]The all-zero sequence is repeated twice, one is preceded by '2' and the other by '-2' and we will see later that the two resulting sequences can be considered different.

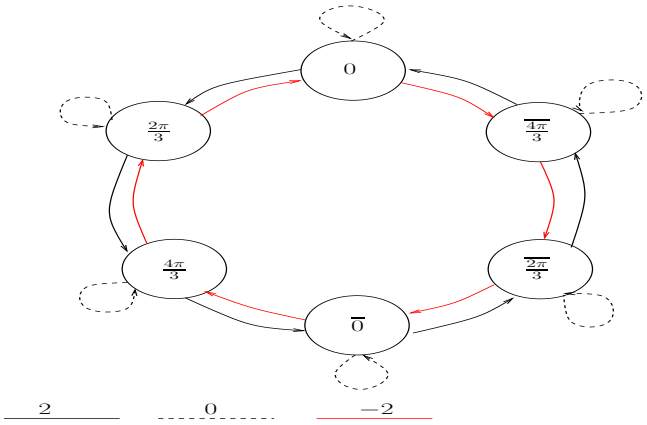

Figure 2.5: Phase state diagram of the precoded ternary CPM in the case of $h = 1/3$ (odd modulation index denominator).

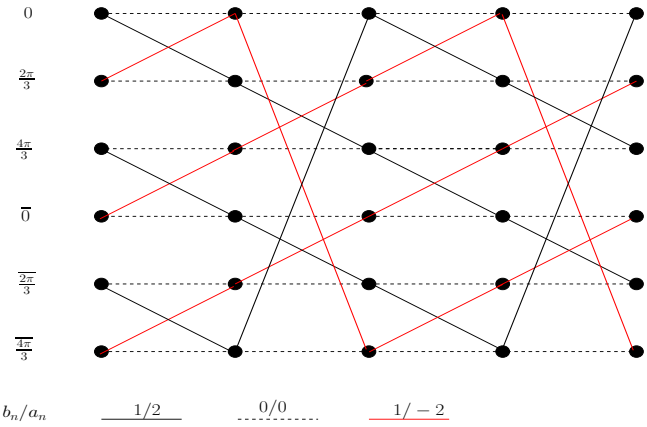

Figure 2.6: The phase trellis of a full response precoded ternary CPM modulation for odd modulation index denominator for $h = 1/3$.

2.5 Simulation Results

2.5.1 Spectral Efficiency

The variation of the information rate as a function of E_s/N_0 is plotted in Figure 2.7, for a *rectangular* frequency pulse with length $L = 1$ and different modulation indices $h = \frac{1}{7}$, $\frac{1}{4}$ and $\frac{1}{5}$. In Figure 2.8, the IR comparison is carried out for *raised cosine* frequency pulse with length $L = 2$ and different modulation indices $h = \frac{1}{4}$, $\frac{2}{7}$ and $\frac{1}{3}$. We observe again the gain thanks to the proposed precoder. In both cases, we observe a significant information rate improvement with the proposed scheme, especially in the medium SNR range ($[0, 4]$ dB). Concerning the spectral efficiency, the bandwidth which contains 99% of the overall power was adopted as bandwidth of interest. The resulting computed bandwidth values are reported in Table 2.1 for the same modulation formats as in Figures 2.7 and 2.8. From the information rate in Figures 2.7 and 2.8 and the computed bandwidth in Table 2.1, we plotted in Figures

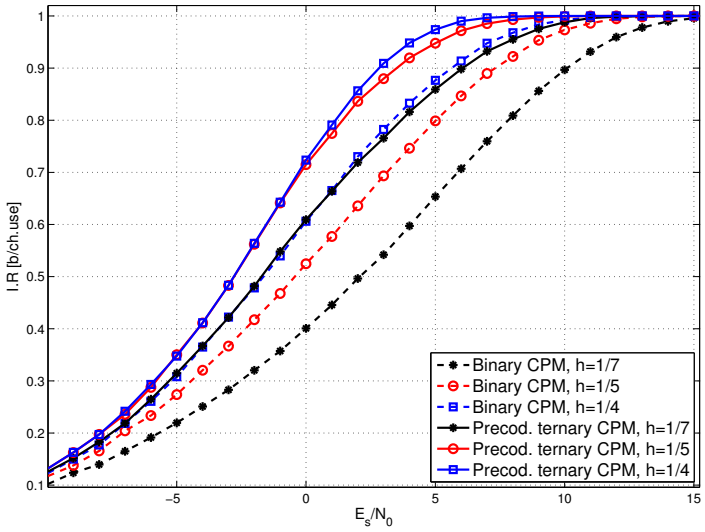

Figure 2.7: Information rate for 1REC modulation with the different modulation indices $h = \{\frac{1}{5}, \frac{1}{7}, \frac{1}{4}\}$ proposed scheme (solid curves) and classic CPM (dashed curves)

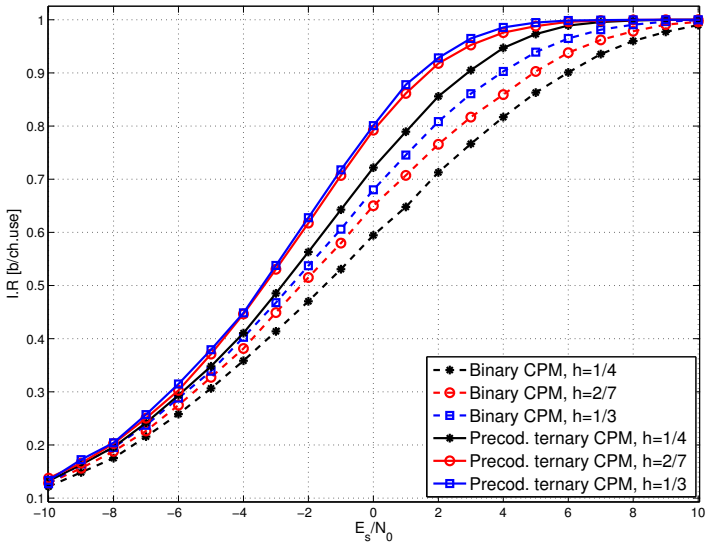

Figure 2.8: Information rate for 2RC modulation with the different modulation indices $h = \{\frac{1}{4}, \frac{2}{7}, \frac{1}{2}\}$ proposed scheme (solid curves) and classic CPM (dashed curves)

2.9 and 2.10 the corresponding spectral efficiency. We observe that the proposed precoded ternary CPM achieves a higher spectral efficiency than the corresponding binary CPM. The percentage of the SE improvement for 1REC and 2RC modulation formats respectively at $E_s/N_0 = 5$ dB and 1 dB is summarized in Table 2.2.

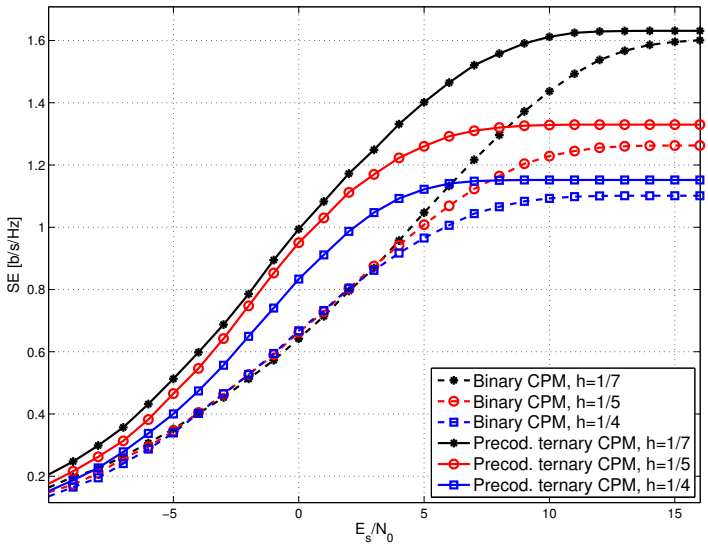

Figure 2.9: Spectral efficiency for 1REC modulations with different modulation indices.

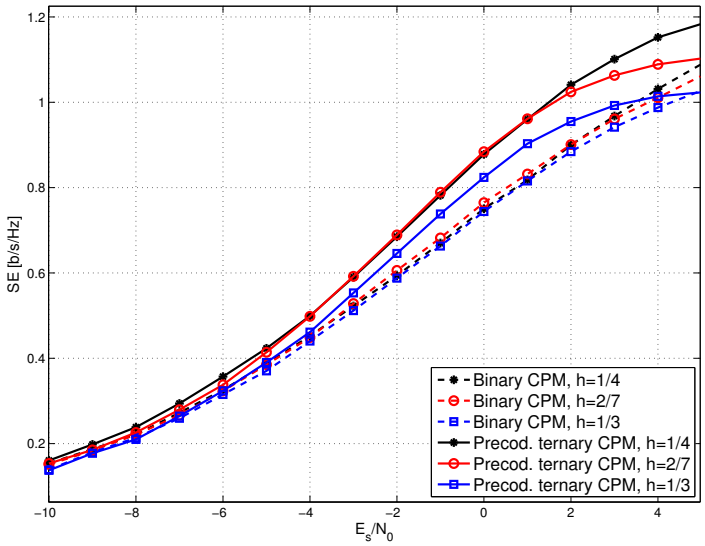

Figure 2.10: Spectral efficiency for 2RC modulations with different modulation indices.

2.5.2 Asymptotic Bit Error probability

We consider the performance of the precoded ternary CPM scheme when transmitted over the AWGN channel. No channel coding is used. We focus on the asymptotic performance for high values of E_b/N_0. Let us denote by $\boldsymbol{e} = \boldsymbol{a} - \hat{\boldsymbol{a}}$ the sequence representing the difference between the transmitted sequence $\boldsymbol{a}$ and the erroneous one $\hat{\boldsymbol{a}}$. The probability of bit error for the optimal MAP sequence detector (implemented

Table 2.1: 99% Bandwidth for some of the considered schemes

	1REC			2RC		
h	1/5	1/7	1/4	2/7	1/4	1/3
Binary CPM	0.792	0.624	0.908	0.85	0.792	0.914
Precod. ternary CPM	0.752	0.613	0.868	0.896	0.822	0.972

Table 2.2: Percentage of the SE improvement for some of the considered schemes

	1REC ($E_s/N_0 = 5$ dB)			2RC ($E_s/N_0 = 1$ dB)		
h	1/5	1/7	1/4	2/7	1/4	1/3
SE improvement	25 %	33.81 %	13.96 %	15.55 %	17.38 %	10.72 %

through the Viterbi algorithm) is well approximated by [33]

$$P_b \approx \frac{n_{\boldsymbol{e}_{min}} m_{\boldsymbol{e}_{min}}}{2^{R_{\boldsymbol{e}_{min}}}} \mathrm{Q}\left(\sqrt{d^2_{min} E_b/N_0}\right) \tag{2.11}$$

where

$$d_{min} = \min_{\boldsymbol{e}} d(\boldsymbol{e})\,. \tag{2.12}$$

$$\boldsymbol{e}_{min} = \operatorname*{argmin}_{\boldsymbol{e}} d(\boldsymbol{e})\,, \tag{2.13}$$

$n_{\boldsymbol{e}_{min}}$ is the number of bit errors (i.e., on the sequence $\{b_n\}$) caused by the error event $\boldsymbol{e}_{min}$, $m_{\boldsymbol{e}_{min}} = 2\prod_{i=0}^{R_{\boldsymbol{e}_{min}}-1}(2 - \frac{|e_{min,i}|}{2})$, $R_{\boldsymbol{e}_{min}}$ is the span of symbol times where $\boldsymbol{e}_{min}$ is different from zero and $\mathrm{Q}(x)$ is the Gaussian Q function. The coefficient $\frac{n_{\boldsymbol{e}_{min}} m_{\boldsymbol{e}_{min}}}{2^{R_{\boldsymbol{e}_{min}}}}$ is often called *multiplicity* of the error event with minimum distance. The only task is the identification of the error events corresponding to d_{min}. This can be done by working on the phase tree. We considered different modulation formats and computed the corresponding parameters $n_{\boldsymbol{e}_{min}}$, $m_{\boldsymbol{e}_{min}}$, $R_{\boldsymbol{e}_{min}}$, and d_{min}, for both the classical binary schemes and the proposed precoded ternary one. The results are reported in Table 2.3. In Figure 2.11, we considered a modulation format with a rectangular phase pulse of length $L = 1$. The analytical approximation and the simulated error rate curves coincide. It can be observed from Figure 2.11 that at a BER $= 10^{-5}$, the proposed precoded ternary CPM scheme achieves a gain of 4.2 dB for $h = 2/7$ and a gain of 3.8 dB for $h = 1/3$. For the 2REC modulation in Figure 2.12, the gain is of about 4.3 dB and 4.1 dB for respectively $h = 1/4$ and $h = 2/5$ at BER $=10^{-4}$.

2.5.3 Serial Concatenation with an outer encoder

Turbo codes have been discovered by C. Berrou et al. in 1993 [34]. This code family offers high power performance nearly closed to the theoretical Shannon limit [35]. It marked a revolution in information theory community. Since their introduction, numerous research relating to turbo codes, and more generally to concatenated

Table 2.3: Parameters for the computation of the asymptotic bit error rate.

		$\boldsymbol{e}_{min}$	$n_{\boldsymbol{e}_{min}}$	$m_{\boldsymbol{e}_{min}}$	d^2_{min}
1REC	Binary CPM	(2,-2)	2	2	1.173
$h = 1/3$	Precod. ternary CPM	(2,0,-2)	2	4	2.673
1REC	Binary CPM	(2,-2)	2	2	0.913
$h = 2/7$	Precod. ternary CPM	(2,0,-2)	2	4	2.136
2REC	Binary CPM	(2,-2,0)	2	4	0.492
$h = 1/4$	Precod. ternary CPM	(2,0,-2,0)	2	8	1.453
2REC	Binary CPM	(2,-2,0)	2	4	1.177
$h = 2/5$	Precod. ternary CPM	(2,0,-2,0)	2	8	3.064

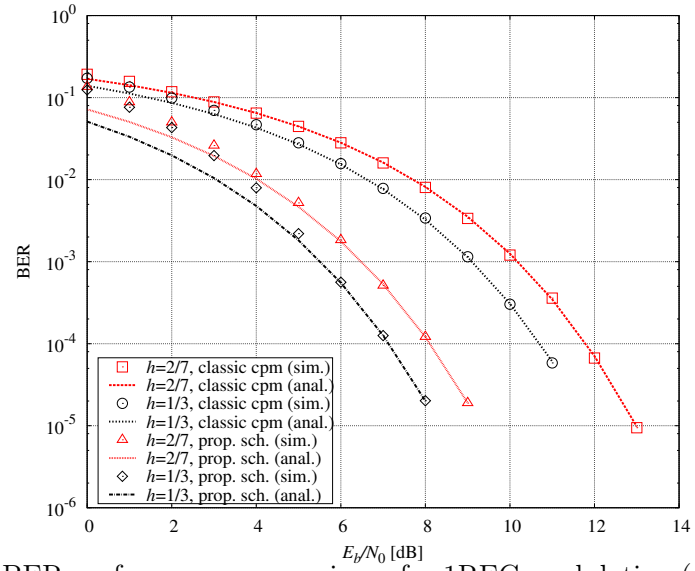

Figure 2.11: BER performance comparisons for 1REC modulation (simulations and closed-form asymptotic expressions).

codes have been carried out in order to understand and analyze their behavior and improve their performance. The proposed encoding scheme in [34] consists in the parallel concatenation of two systematic and recursive convolutional codes. The information bits are first encoded by the first convolutional encoder. These bits are then interleaved before passing into the second encoder. The two considered codes have to be systematic and recursive [36]. The interleaver is an essential element in turbo code schemes, its absence affects strongly the performance of these schemes. The interleaving can be carried out in a random manner, however, it is possible to achieve an extra power gain thanks to the optimization of the interleaver [37], [38]. In general, the power gain increases with the size of the interleaver. For the CPM signal, the Rimoldi decomposition approach [12] is usually adopted to split the coded CPM scheme into a recursive continuous phase encoder (CPE) and a memoryless mapper(MM).

The combination of continuous phase modulation (CPM) and bit interleaved

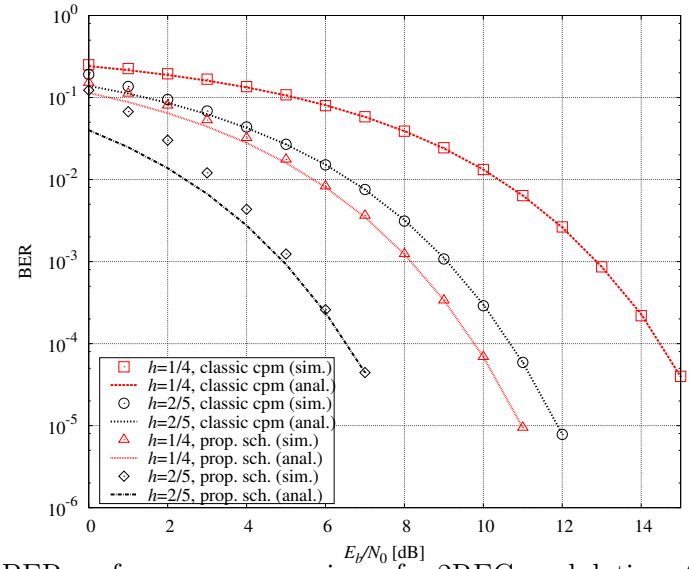

Figure 2.12: BER performance comparisons for 2REC modulations (simulations and closed-form asymptotic expressions).

coded modulation (BICM) is referred to as BIC-CPM. The strong analogy between the behavior of a CPM modulator and that of a non-recursive systematic convolutional code with coding rate $1/n_0$, n_0 is an integer is shown in [39]. The diagram of the serial concatenation of a convolutional code and a CPM with an interleaver between the two coding modules is illustrated in Figure 2.13 (a). The transmitted bits $\boldsymbol{b} = \{b_n\}$, are encoded using a convolutional channel encoder. Then, the coded bits $\boldsymbol{c} = \{c_n\}$ are interleaved and mapped to an M-ary alphabet to define a modulated sequence denoted by $\boldsymbol{a} = \{a_n\}$. The serially concatenated CPM signals with iterative decoding were first studied in [29]. The iterative BIC-CPM decoder is shown in Figure 2.13 (b). At each iteration, the proposed soft CPM demodulator computes extrinsic LLRs $\Lambda_{\text{dem}}^{\text{ext}}$ from the channel observations $r(t)$ and *a priori* LLRs L_A which are then passed through the bit interleaver, to become *a priori* information for the decoder. The latter feeds back in turn extrinsic LLRs $\Lambda_{\text{dec}}^{\text{ext}}$ which are deinterleaved to become new *a priori* information for the proposed soft CPM demodulator. Here, we consider the serial concatenation of the proposed ternary CPM with a binary convolutional encoder (CC) with generators (7,5) (octal notation) through a pseudo-random interleaver of size 4096. In the simulations we used a 1REC frequency pulse. In Figure 2.14, we plotted the BER curve for both $h = \frac{3}{8}$ and $h = \frac{1}{4}$. For a BER of 10^{-4}, we observe a gain of 0.6 dB and 1.55 dB for respectively $h = \frac{3}{8}$ and $\frac{1}{4}$.

2.5.4 Performance Analysis through EXIT Chart

This section provides numerical results to analyse the performance of the FEC-encoded precoded CPM ternary scheme thanks to the *extrinsic* information transfer (EXIT) chart [40]. The front end and the back end of the receiver which are the proposed CPM demodulator and the channel decoder exchange soft information and

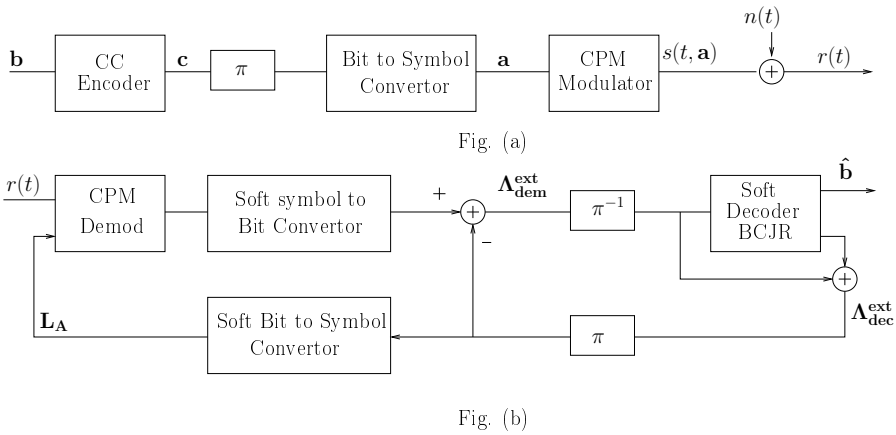

Figure 2.13: Serial concatenation of a CPM with an outer encoder

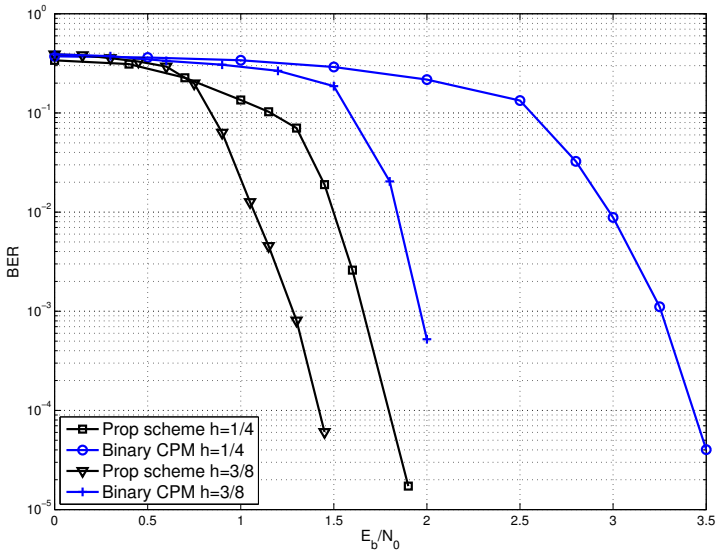

Figure 2.14: Serial concatenation with an outer code CC(7,5) via a pseudo random interleaver with length 4096 for 1REC modulation for $h = \frac{1}{4}$ and $\frac{3}{8}$.

the convergence behavior of the iterative process can be predicted from EXIT chart. Given a soft input soft output device, the input log likelihood ratio defines the *a priori* information while the difference of log likelihood ratio between its output and input corresponds to the *extrinsic* information. The input (respectively output) mutual information is the mutual information between the data bits and the *a priori* (respectively *extrinsic*) information. Let us denote by C the binary data sequence and by L the information either *a priori* (L_A) or *extrinsic* (L_E). Then the mutual

information between C and L reads [41]

$$I(\mathrm{L},\mathrm{C}) = \frac{1}{2}\sum_{\mathrm{C}=\pm 1}\int_{-\infty}^{+\infty} P(\mathrm{L}|\mathrm{C})\log_2\left[\frac{P(\mathrm{L}|\mathrm{C})}{(1/2)[P(\mathrm{L}|\mathrm{C}=-1)+P(\mathrm{L}|\mathrm{C}=+1)]}\right] dP(\mathrm{L}). \tag{2.14}$$

For most practical channels, the conditional densities $P(\mathrm{L}|\mathrm{C})$ are symmetric with respect to 0, i.e. $P(\mathrm{L}|\mathrm{C}=+1) = P(-\mathrm{L}|\mathrm{C}=-1)$. This yields the following simpler expression for the mutual information

$$\begin{aligned} I(\mathrm{L},\mathrm{C}) &= 1 - \int_{-\infty}^{+\infty} P(\mathrm{L}|\mathrm{C}=-1)\log_2\left[1+\frac{P(\mathrm{L}|\mathrm{C}=+1)}{P(\mathrm{L}|\mathrm{C}=-1)}\right] d\mathrm{L} \\ &= 1 - \mathrm{E}_{\mathrm{L}|-1}\{\log_2[1+\frac{P(\mathrm{L}|\mathrm{C}=+1)}{P(\mathrm{L}|\mathrm{C}=-1)}]\} \\ &= 1 - \mathrm{E}_{\mathrm{L}|-1}\{\log_2(1+e^{\mathrm{L}})\} \end{aligned} \tag{2.15}$$

Experimental evidence suggests that the *extrinsic* LLRs exchanged across the iterative process are well approximated by independent and identically distributed Gaussian random variables [42]. Hence, the conditional density $P(\mathrm{L}|\mathrm{C}=-1)$ can be conveniently modelled by a Gaussian distribution with mean $-\alpha_A$ and variance $2\alpha_A$. So, the input mutual information I_A is:

$$\mathrm{I}_A = 1 - \mathrm{E}_{\mathrm{L}_A|-1}\log_2(1+\exp(\mathrm{L}_A)) \tag{2.16}$$

Given the channel output and the *a priori* information, the *extrinsic* information measured at the output is used to compute I_E. We denote by T the transfer characteristic function such that $\mathrm{I}_E = T(\mathrm{I}_A, channel)$. Its drawing enables to obtain the EXIT chart. To illustrate the convergence analysis through EXIT charts, we consider the 2RC modulation format. First, for a transmission with $h = \frac{1}{4}$, the *extrinsic* information transfer is computed for two values of $E_b/N_0 = \{0.5, 2\}$. Figure 2.15 shows that the proposed precoded ternary CPM scheme performs better than the binary CPM scheme. It can be shown that the binary CPM receiver requires additional iterations to converge compared to the proposed scheme receiver. The initial output *extrinsic* information for no *priori* information $\mathrm{I}_E(\mathrm{I}_A = 0)$ is also higher in the case of the proposed precoded ternary CPM scheme.

The same remarks can be drawn for $h = \frac{1}{7}$ (see Figure 2.16). The binary CPM receiver requires a E_b/N_0 greater than 3 dB to converge. The proposed ternary CPM scheme receiver can achieve convergence even for $E_b/N_0 = 0.5$ dB.

2.6 Conclusions

In this chapter, we developed a precoded ternary CPM scheme. We discussed the different design approaches of the precoder. We pointed out that the precoder is designed in such a way to increase the information rate and maintain the same spectral occupancy. The information rate improvement is achieved through the increase

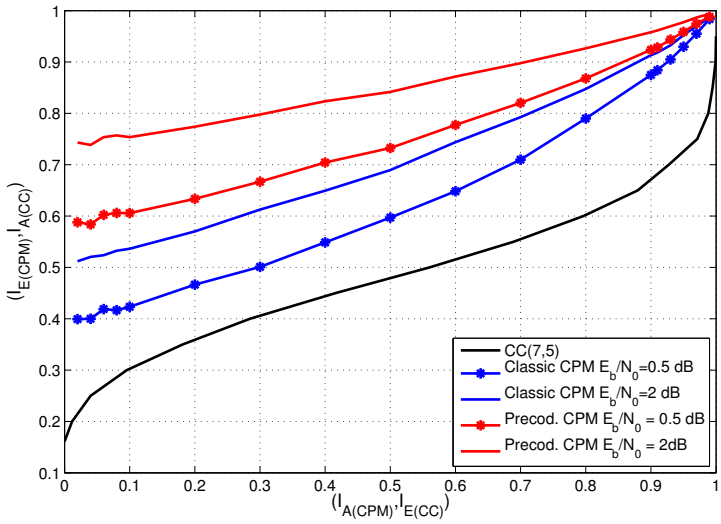

Figure 2.15: EXIT chart for the SCCPM scheme for *raised cosine* CPM with $L = 2$, CC(7,5) $h = \frac{1}{4}$, $\frac{E_b}{N_0} \in \{0.5, 2\}$ dB.

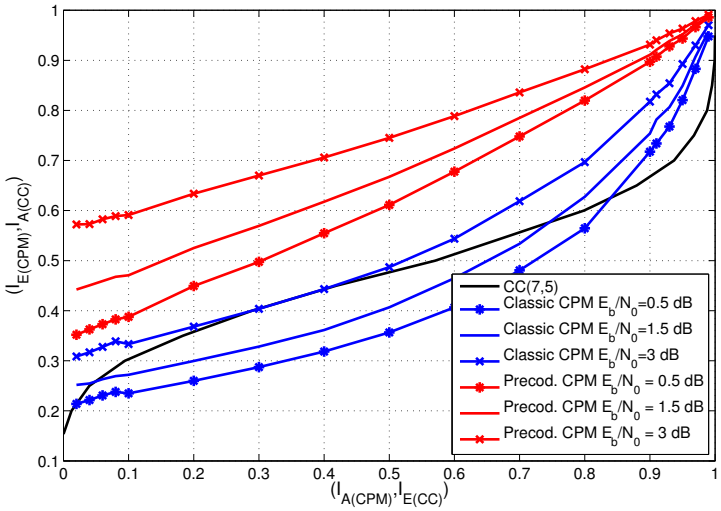

Figure 2.16: EXIT chart for the SCCPM scheme for *raised cosine* CPM with $L = 2$, CC(7,5) $h = \frac{1}{7}$, $\frac{E_b}{N_0} \in \{0.5, 1.5, 3\} dB$.

of the minimum distance by delaying the first merger. However, thanks to the prohibition of the transitions from +2 to -2 and vice versa we get almost the same spectral occupancy as the binary CPM. Thereafter, we considered the serial concatenation of the proposed precoded ternary CPM with an outer encoder through a pseudo-random interleaver. We also analyzed the convergence of serially concatenated CPM through an EXIT-chart analysis and showed that the theoretical limits (SNR threshold, $\mathrm{I}_E(\mathrm{I}_A = 0)$) are higher than the binary CPM scheme.

In this chapter, we applied MLSE demodulation of the CPM without paying attention to the receiver complexity. However depending on the value of h the number of trellis states can be too high to be implemented in practice, above all in the kind of applications targeted by this thesis. In the next chapter we address the CPM demodulation complexity and we propose a CPM receiver working on a trellis with reduced state number which performs close to the MLSE.

Chapter 3

Reduced Complexity Receiver for CPM signals

Contents

3.1 Introduction

This chapter deals with a reduced-complexity per survivor processing-based CPM demodulation. It relies on a trellis with reduced state number and defined from a rational modulation index possibly different from the transmit modulation index and referred to as virtual receiver modulation index. The virtual receiver modulation index should be chosen so as to achieve a tradeoff between error-rate performance and complexity reduction. After describing the demodulation principale and giving some performances of the resulting reduced-state receiver, we focus on the choice of the virtual receiver modulation index. We give guidelines to discard the values of the virtual receiver modulation index, that degrade the error-rate performance. Two criteria are used. The first one considers the uncoded CPM case and is based

[0]This chapter is the subject of the publication:
-Brevet francais n^o 13/54723 "Procédé de démodulation et démodulateur d'un signal modulé à phase continue, et programme d'ordinateur correspondant" Karine AMIS, Frédéric GUILLOUD et Malek MESSAI.
-M. Messai, K. Amis, and F. Guilloud, "On the optimization of a PSP-based CPM detection" *IEEE Trans. Wireless Commun*

on an approximation of the minimal Euclidean distance. The second one is related to the bit interleaved coded CPM case and resorts to an EXIT chart to analyse the convergence of the iterative receiver.

3.2 Previous Works on Reduced Complexity Detectors for CPM

The maximum likelihood sequence estimation (MLSE) of a CPM signal can be achieved by the Viterbi algorithm [13]. The objective of the Viterbi receiver is to find the sequence that maximizes the correlation with the received signal. To achieve optimal performance, it requires an exact knowledge of the modulation index. Indeed any mismatch will cause errors that will accumulate over the observation interval. In addition, the Viterbi algorithm relies on a trellis representation of the CPM where the number of states is proportional to the denominator of the modulation index and thus the Viterbi algorithm requires that h be rational. The Viterbi receiver complexity which is related to the number of states remains important in practice (see Chapter 1). Therefore, several approaches for reducing the receiver complexity, applied to the coherent detection of CPM signals, have been presented in the literature. The reduction of complexity is generally obtained by decreasing the number of trellis states and/or the number of matched filters (MF). As for only reducing the number of processed trellis states, a reduced-search algorithm performed on the full trellis has been proposed in [43]. In [44] a decision feedback equalizer is used on a smaller trellis. Neither of these methods has any impact on the number of MFs. Svensson and Aulin [45] proposed a detector based on a CPM scheme simpler than the one used at the transmitter. The main idea is to deform the frequency pulse response so as to obtain a shorter frequency pulse response length, thereby reducing the number of trellis states and the number of MFs simultaneously. This is called a mismatched detector, since the internal signal model in the detector is mismatched (different frequency pulse length and shape) with respect to the signal produced by the transmitter. Other works are based on the exact decomposition of the CPM signal on an orthonormal basis. The complexity reduction is achieved at the receiver by using a subset of orthonormal basis functions instead of the entire set. In [46], the Gram-Schmidt procedure is applied to obtain the orthonormal basis functions. Other approaches have used sampling functions [47],[48], Walsh functions [49], and regularly spaced sinusoids [46]. Another interesting representation of CPM was introduced by Laurent in 1986 [25]. In his paper, Laurent showed that any binary CPM signal can be exactly represented by a linear combination of pulse amplitude modulated (PAM) waveforms. The PAM representation of CPM has received a lot of attention in the literature. It has been exploited by Kaleh to design reduced-complexity detectors [50]. These detectors are based on a small subset of pseudo-symbols and pulses yielding a reduction of the MFs number. The PAM decomposition was extended later to the M-ary single-h CPM modulation in [51], This type of detector was described by Colavolpe [52] for M-ary single-h CPM and

by Perrins [53] for M-ary multi-h CPM. Each of the previously described methods requires the modulation index used at the reception to be the same as the one used at the transmission, and requires h to be rational. The solution presented in this chapter is to construct a trellis by using a rational modulation index h_v chosen so as to achieve near optimal demodulation with the smallest trellis state number. So the MLSE-based detection of CPM modulated data becomes possible without any restriction concerning the modulation index.

3.3 Reduced-State Trellis-Based CPM Receivers

[1] The reduced-complexity receiver relies on the decomposition of h in the form $h = h_v + \Delta_h$ with $h_v = \frac{l_v}{p_v}$ being a rational number. h_v is referred to as a virtual receiver modulation index. The key idea is to use either the Viterbi or the BCJR algorithm with modified branches and state metrics on a trellis designed upon h_v. It takes into account a phase difference proportional to Δ_h and computed on a per survivor processing (PSP) basis [54].

3.3.1 Design of a Trellis with a Reduced State Number

Thanks to the decomposition of h in the form $h = h_v + \Delta_h$, the information-bearing phase given in (1.8), can be expressed as a function of h_v and Δ_h:

$$\begin{aligned}
\phi(t,h,\boldsymbol{a}) &= \pi h \sum_{i=0}^{n-L} a_i + 2\pi h \sum_{i=n-L+1}^{n} a_i q(t-iT), \\
&= \pi h_v \sum_{i=0}^{n-L} a_i + \pi \Delta_h \sum_{i=0}^{n-L} a_i + 2\pi h_v \sum_{i=n-L+1}^{n} a_i q(t-iT) \\
&\quad + 2\pi \Delta_h \sum_{i=n-L+1}^{n} a_i q(t-iT), \\
&= \underbrace{\phi_{h_v,n} + \phi_{h_v,n}(t)}_{\phi(t,h_v,\boldsymbol{a})} + \underbrace{\Delta\phi_n + 2\pi\Delta_h \sum_{i=n-L+1}^{n} a_i q(t-iT)}_{\phi(t,\Delta_h,\boldsymbol{a})}, \qquad (3.1)
\end{aligned}$$

with $\Delta\phi_n = \pi\Delta_h \sum_{i=0}^{n-L} a_i$.
The first two terms in (3.1) are tracked by the Viterbi algorithm and the third term is the resulting phase difference which is accumulated at every symbol. This accumulation is calculated using the PSP technique by associating to each state $i, i \in \{0, 1, ..., p_v - 1\}$ an additional parameter $\Delta\phi_n^i$. The last term of (3.1) is

[1] This Section has been presented in the conference (EUSIPCO 2014):
M. Messai, F. Guilloud, and K. Amis, "A low complexity coherent CPM receiver with modulation index estimation," *in Proc. European Signal Processing Conf., 2014.*

calculated at the output of the matched filter. We can write the following relation:

$$\begin{aligned} \phi_h^i &= \Delta\phi_n^i + i\frac{l_v}{p_v}\pi, \qquad i = \{0, 1, 2, ..., p_v - 1\}, \\ &= \Delta\phi_n^i + \phi_{h_v}^i. \end{aligned} \tag{3.2}$$

The modified branch metric is equal to the scalar product which is calculated as follows:

$$\Omega_{k,i}^{\text{modified}} = \Re\big(e^{-j\Delta\phi_n^k} \int_{nT}^{(n+1)T} r(t) e^{-j\phi_{k,i}(t,h_v)} . e^{-j\psi_{k,i}(t,\Delta_h)} dt\big). \tag{3.3}$$

where

$$\phi_{k,i}(t, h_v) = \phi_{h_v,n}^k + 2\pi h_v \sum_{\ell=n-L+1}^{n-1} a_\ell^k q(t - \ell T) + 2\pi h_v a_n^i q(t - nT) \tag{3.4}$$

$$\psi_{k,i}(t, \Delta_h) = 2\pi\Delta_h \sum_{\ell=n-L+1}^{n-1} a_\ell^k q(t - \ell T) + 2\pi\Delta_h a_n^i q(t - nT). \tag{3.5}$$

3.3.1.1 PSP-based Modified Viterbi Algorithm

The only additional task that needs to be performed on the Viterbi algorithm is the PSP update of the phase difference for each state, $\Delta\phi_n^i$. The update equation is given by:

$$\Delta\phi_{n+1}^i = \Delta\phi_n^{k^*} + a_{(k^*,i)}\pi\Delta_h, \tag{3.6}$$

where k^* is selected from the M previous states of $\boldsymbol{x}_{(n+1)}^i$, as the index of the maximum cumulative metric and $a_{(k^*,i)}$ is the last component of the state vector $\boldsymbol{x}_n^{k^*}$. We apply (3.3) to compute the scalar product between the received signal and the signal corresponding to the transition $\boldsymbol{x}_n^k \to \boldsymbol{x}_{n+1}^i$ used in the modified Viterbi algorithm:

$$\left(\phi_{h_v}^k(\Delta\phi_n^k), a_{n-1}^k, a_{n-2}^k, ..., a_{n-L+1}^k\right) \xrightarrow{a_n} \left(\phi_{h_v}^i(\Delta\phi_{n+1}^i), a_n^i, a_{n-1}^i, , ..., a_{n-L+2}^i\right),$$

with $a_n^i = a_n$, $a_{n-1}^i = a_{n-1}^k$, $\cdots$, $a_{n-L+2}^i = a_{n-L+2}^k$.

3.3.1.2 PSP-based Modified BCJR Algorithm

The optimal coherent soft output detection which minimizes the symbol error probability is achieved by *maximum a posteriori* (MAP) symbol detection of the information symbol a_n.
The corresponding symbol-by-symbol MAP detector maximizes the *a posteriori* probability (APP) $p(a_n|r(t))$:

$$\hat{a}_n = \arg\max_{a\in\mathcal{M}} \; p(a_n = a|r(t)). \tag{3.7}$$

In the modified BCJR algorithm, we first carry out the forward recursion α_n, where the branch metric between states $\boldsymbol{x}_n^k$ and $\boldsymbol{x}_{n+1}^i$ is modified as follows:

$$\gamma_n(\boldsymbol{x}_n^k, \boldsymbol{x}_{n+1}^i) \propto \exp\left(\frac{\Omega_{k,i}^{\text{modified}}}{2N_0}\right) p(\boldsymbol{x}_n^k | \boldsymbol{x}_{n+1}^i), \tag{3.8}$$

where the term $\Delta\phi_{n+1}^i$ is calculated recursively according to (3.6), with index k^* defined as $k^* = \arg\max_k\{\alpha_n(\boldsymbol{x}_n^k)\gamma_n(\boldsymbol{x}_n^k, \boldsymbol{x}_{n+1}^i)\}$, and $a_{(k^*,i)}$ defined as the last component of the state vector $\boldsymbol{x}_n^{k^*}$. Here, it is important to mention the main difference between the original BCJR algorithm for which the forward and backward recursions are calculated in parallel: in the trellis with a reduced number of states, the backward recursion is carried out once the forward recursion is over. It is thus necessary to keep track of the survivor associated to each transition at each epoch in the forward recursion of $\alpha_n(\boldsymbol{x}_n^k)$. Then, these survivors are used in the backward recursion of $\beta_n(\boldsymbol{x}_n^k)$. It means that the value of $\gamma_n(\boldsymbol{x}_n^k, \boldsymbol{x}_{n+1}^i)$ will be saved during the forward recursion to be used in the backward recursion. In fact, the PSP approach is only incorporated in the forward recursion. The reasons for that are twofold: first, the accumulated phase $\Delta\phi_N$ associated to last symbol period is unknown, whereas the accumulated phase $\Delta\phi_0$ is known and equals zero; second, since the branch metric depends on the accumulated phase state (computed by the PSP process), using the PSP in both the forward and the backward recursions would produce different branch metrics for the same transition, which is not acceptable.

The proposed algorithm is summarized below:

PSP-based modified BCJR algorithm

- Step 1: Initialization ($n = 0$)
  $\Delta\phi_0^k = 0$, for all states $\boldsymbol{x}_0^k$,
  $\alpha_0(\boldsymbol{x}^0) = 1$, $\alpha_0(\boldsymbol{x}^k) = 0$, $k \neq 0$.

- Step 2: Forward Recursion $n : 0 \to N-1$
  Calculate for all possible transitions $\boldsymbol{x}_n^k \to \boldsymbol{x}_{n+1}^i$ in the reduced state number trellis, the branch metrics $\gamma_n(\boldsymbol{x}_n^k, \boldsymbol{x}_{n+1}^i)$ according to (3.8). Then, for each $\boldsymbol{x}_{n+1}^i$, update $\Delta\phi_{n+1}^i$ according to (3.6).

- Step 3 : Backward Recursion $n : N \to 0$
  Initialize $\beta_N(\boldsymbol{x}_N^k) = \frac{1}{N_s}\ \forall\ k$, where N_s denotes the number of states.
  Update backward-accumulated metric β_n by using the branch metrics calculated in the forward step.

3.3.2 Simulations

This section provides numerical results to assess the performance of the studied algorithms with reduced state number on an AWGN channel for the uncoded CPM

case. They also illustrate the need for optimization developed in Section 3.5. The hard Viterbi and the soft BCJR detection provides exactly the same performances. $h = h_v$ means an optimum CPM demodulation algorithm (either Viterbi or BCJR), working on the trellis with full state number, whereas $h \neq h_v$ means a CPM demodulation with the help of the PSP-based modified algorithm (either Viterbi or BCJR), working on a trellis with reduced state number. In the text, we refer to the receiver based on a trellis with the full state number (respectively the receiver based on a trellis with a reduced state number) as *full-state receiver* (respectively *reduced-state receiver*).

We have carefully chosen a modulation format often used in the literature: The first example refers to the continuous phase frequency shift keying (CPFSK) modulation defined by a *rectangular* frequency pulse of duration T) [55]. The second modulation is the binary 3GFSK modulation with $BT = 0.5$ used in the Bluetooth BR [20], [56] and the last one is the quaternary 2RC modulation [57], [51].

As the main purpose is the complexity reduction, therefore, h_v should be selected so as to have fewer phase states $\phi_{h_v,n}$. Hence the choice of $h_v \in \{2/3, 1/2, 2/5, ...\}$.

CPFSK modulation

Here we consider the demodulation of a binary CPFSK signal transmitted with a modulation index $h = 5/8$. This modulation index results in an effective trellis size of 16 states and 32 branch metrics to be computed at each time symbol. Three different modulation indices $h_v \in \{\frac{1}{2}, \frac{2}{3}, \frac{2}{5}\}$ are used in the reception. This results in a simple trellis with 3, 4 and 5 states respectively for $h_v = \frac{2}{3}$, $\frac{1}{2}$ and $h_v = \frac{2}{5}$. As can be seen, from Figure 3.1, the *reduced-state receiver* based upon modulation index of $\frac{2}{3}$ results in insignificant performance degradation (less than 0.8 dB) at BERs below than 10^{-3}. Whereas, receiving with $h = \frac{1}{2}$, leads to significant performance degradation (more than 1 dB). However, with $h_v = \frac{2}{5}$, the *reduced-state receiver* achieves optimal performance with only 5 states (respectively 10 branch metrics) instead of 16 states (respectively 32 branch metrics). At higher BERs, optimum performance is achieved whatever the virtual reception modulation index.

Note that here, the performance loss is more important with the 4 states receiver ($h_v = \frac{1}{2}$) than with the 3 states receiver ($h_v = \frac{2}{3}$): So the complexity-performance trade-off is no so obvious.

Binary 3GFSK modulation

The proposed *reduced-state receiver* can be applied to the Bluetooth standard which uses a binary 3 GFSK modulation with $BT = 0.5$ and the modulation index can vary from 0.28 to 0.35 [20]. The complexity of the *full-state receiver* quickly becomes prohibitive: $p = 100$ for $h = 0.29 = \frac{29}{100}$ yields a high number of states equal to $2 \times 100 \times 2^2$. Full state sequence detection is not feasible for all the Bluetooth modulation indexes $0.28 \leq h \leq 0.35$. However, *reduced-state receiver* enables

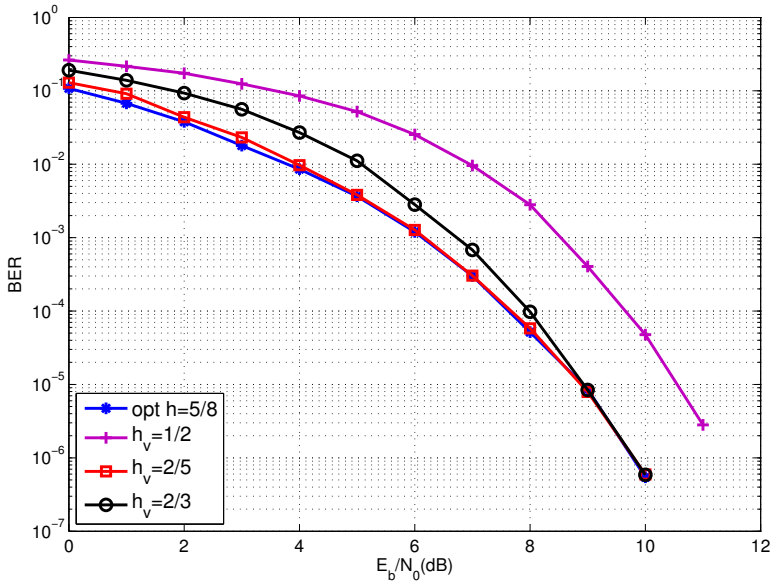

Figure 3.1: BER performance of CPFSK modulation with $h = \frac{5}{8}$ detected using *reduced-state receiver* based upon modulation index $h_v = \frac{2}{3}$, $\frac{1}{2}$ and $\frac{2}{5}$.

to drastically reduce the complexity. In the case of $h = 0.28 = \frac{7}{25}$, for instance, the original Viterbi requires 200 states which is not feasible in practice. As shown in Figure 3.2, the *reduced-state receiver* used with $h_v = \frac{2}{5}$ achieves optimal demodulation with only 20 states in the reception trellis, and with insignificant degradation at low SNR with $h_v = \frac{1}{2}$ or $\frac{2}{3}$. The same comment holds for a transmission with $h = 0.3$ and $h = 0.35$ (see Figures 3.3 and 3.4).

Quaternary 2RC modulation

Now we consider a Quaternary and partial response CPM with raised-cosine frequency pulse of length $L = 2$ where the transmission modulation index is taken rational to have a fair comparison with the optimal one, which is an example often used in the literature [51], [57]. In Figure 3.5, two transmission modulation indices are considered $h = \frac{1}{4}$ and $\frac{3}{8}$. For $h = \frac{1}{4}$, we can receive optimally using one of the virtual reception modulation indices $h_v \in \{1/2, 2/3, 2/5\}$. Whereas in the case of $h = \frac{3}{8}$, the proposed receiver algorithm retains optimal performance with $h_v = \frac{2}{5}$ and exhibits near-optimal with $h_v = \frac{1}{2}$. A trellis built with $h_v = \frac{2}{5}$ has 20 states and using $h_v = \frac{1}{2}$ allows to have only 16 states. Whereas, for the *full-state receiver*, the trellis has 64 states. However, the use of $h_v = 2/3$ at the receiver side yields a higher BER degradation of about 2 dB at BER $= 10^{-3}$.

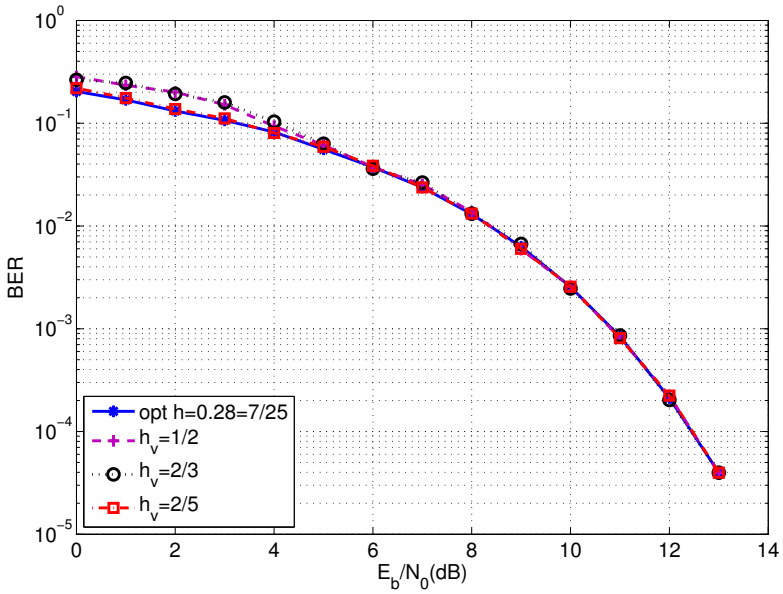

Figure 3.2: BER performance of Bluetooth standard for $h = 0.28 = \frac{7}{25}$ detected using *reduced-state receiver* based upon modulation index $h_v = \frac{2}{3}$, $\frac{1}{2}$ and $\frac{2}{5}$.

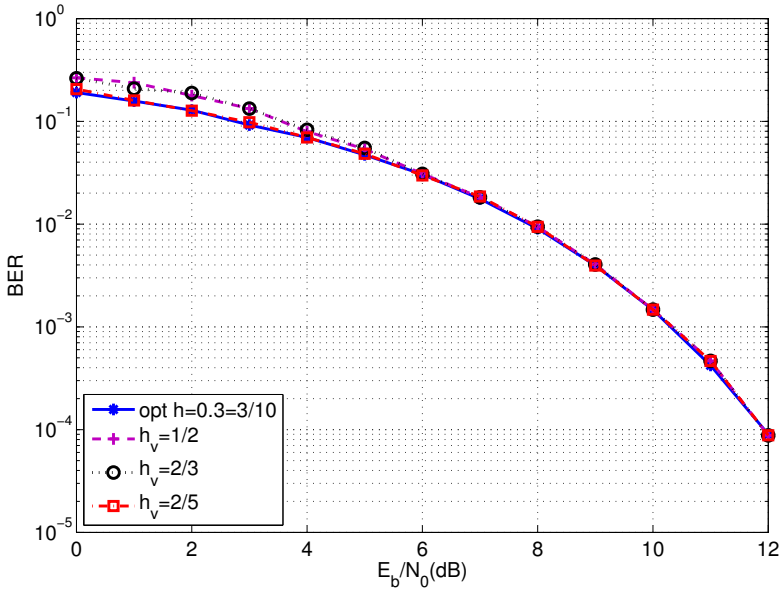

Figure 3.3: BER performance of Bluetooth standard for $h = 0.3 = \frac{3}{10}$ detected using *reduced-state receiver* based upon modulation index $h_v = \frac{2}{3}$, $\frac{1}{2}$ and $\frac{2}{5}$.

Comparison with Existing Reduced Complexity Receivers

The proposed receiver is compared with two algorithms described in [45] and

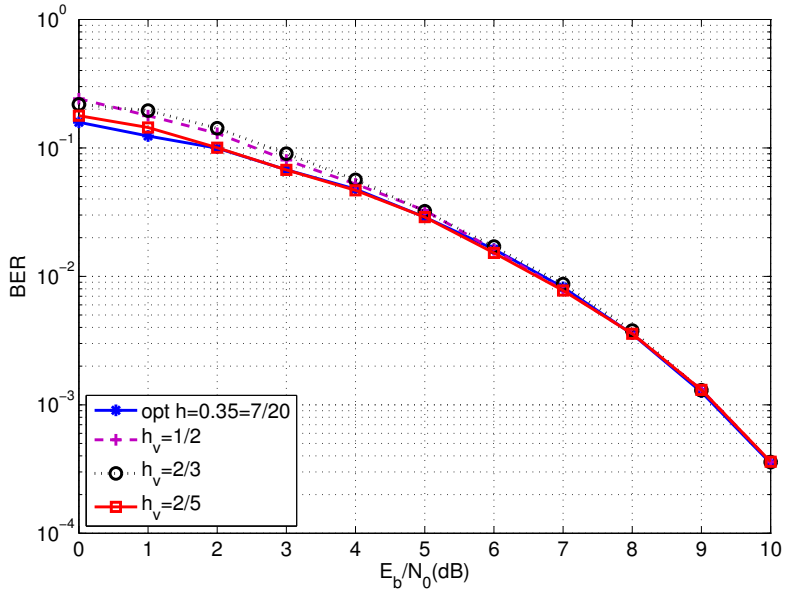

Figure 3.4: BER performance of Bluetooth standard for $h = 0.35 = \frac{7}{20}$ detected using *reduced-state receiver* based upon modulation index $h_v = \frac{2}{3}$, $\frac{1}{2}$ and $\frac{2}{5}$.

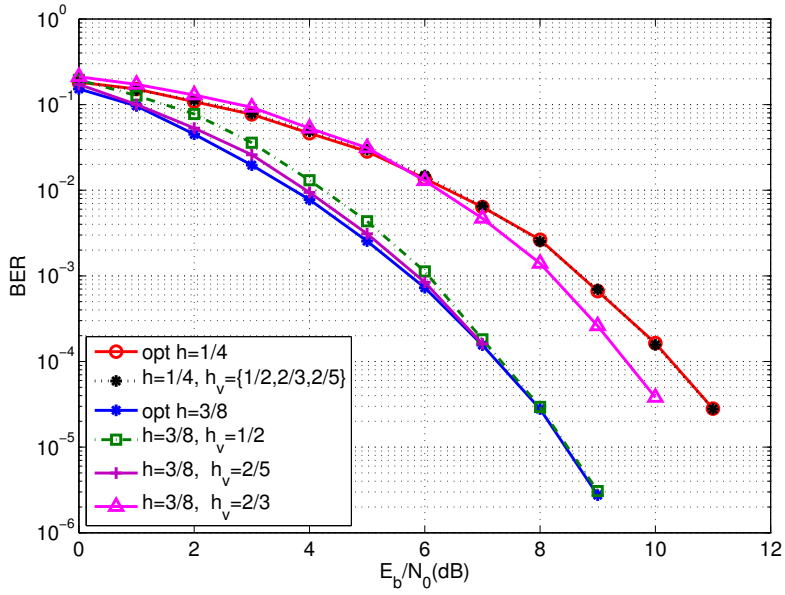

Figure 3.5: BER performance of Quaternary 2RC modulation with $h = \frac{1}{4}$ and $\frac{3}{8}$ detected using *reduced-state receiver* based upon modulation index $h_v = \frac{2}{3}$, $\frac{1}{2}$ and $\frac{2}{5}$.

[58]. The key idea of [45] is to use a receiver with a modified frequency pulse having a shorter length compared to the frequency pulse used at the transmitter. For

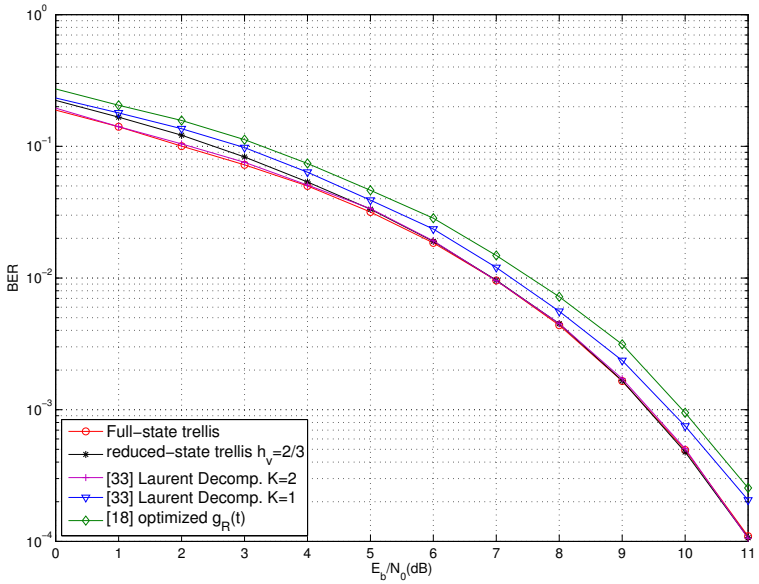

Figure 3.6: BER performance comparison for binary 3RC modulation with $h = \frac{3}{8}$.

example, the binary 3RC transmitted signal is demodulated using a trellis of the binary 2REC modulation. In [58], the Laurent decomposition into a superposition of PAM waveforms is considered with K principal components. Hence, both [45] and [58] consider a signal space at the receiver side which is different from the transmitter side. Note that this is not the case in the proposed receiver where the signal space is unchanged.

For this comparison, we considered the modulation format used in [45], namely a binary 3RC modulation with h set to $\frac{3}{8}$. The BER performance is illustrated in Figure 3.6, and a comparison of the complexities in terms of number of states is given in Table 3.1.

Compared to the *full-state receiver*, the proposed *reduced-state receiver* based upon $h_v = \frac{2}{3}$, has 12 states instead of 64 and allows to have a negligible loss for low E_b/N_0 and optimum performance from $E_b/N_0 = 4$ dB. However, the algorithm proposed in [45] based on a trellis of 32 states, performs 0.6 dB away from the optimum performance at BER $= 10^{-2}$. For the receiver proposed in [45], the approximation of the signal by its two principal components leads to achieve optimal demodulation for each E_b/N_0 with a trellis of 32 states. The approximation of the signal by only its principal component leads to a degradation of 0.3 dB at BER $= 10^{-2}$ with a trellis of 16 states.

Table 3.1: Complexity reduction vs performance degradation for Binary 3RC modulation, $h = 3/8$

	Number of states	Reduction percentage	Loss (dB) at BER $= 10^{-2}$
Full-state receiver	64	–	–
Proposed receiver ($h_v = 2/3$)	12	81.25%	0
[45]	32	50%	0.6
[58], $K = 2$	32	50%	0
[58], $K = 1$	16	75%	0.3

3.4 Iterative Reduced-Complexity detection for bit interleaved coded CPM

[2] This section provides numerical results to assess the performance of the studied algorithms with reduced state number on an AWGN channel for both uncoded CPM and BIC-CPM cases. They also illustrate the need for optimization developed in Section 3.5. In the simulations of the BIC-CPM, we use a binary convolutional code defined by its polynomials (7,5) in octal and a pseudo-random interleaver. The interleaver length (equal also to the binary coded sequence length), denoted by K, takes on its values in $\{4096, 20000\}$. We consider a quaternary and partial response CPM with a raised-cosine frequency pulse of length $L = 2$. The transmission modulation index is assumed to be rational to enable a comparison with the optimum CPM demodulation. In the figure legends, *uncoded* refers to the uncoded scheme, where hard Viterbi-based detection is carried out; *coded* refers to the BIC-CPM with soft BCJR-based detection involved in the iterative decoding process; working on the trellis with full state number, whereas $h_v \neq h$ means a CPM demodulation with the help of the PSP-based modified algorithm (either Viterbi or BCJR), working on a trellis with reduced state number. We consider two reduced-state receivers. The first designed with $h_v = \frac{2}{5}$, has a 20-state trellis, while the second designed with $h_v = \frac{2}{3}$ has a 12-state trellis. The question to be answered is: should we always choose the h_v yielding the lowest number of states whatever h? Partial answer is illustrated by the simulation results given below whereas Section 3.5 will provide a deeper analysis. In Figure 3.7 (respectively Figure 3.8), we have plotted the BER curve for both uncoded CPM and BIC-CPM cases, when the transmission modulation index is set to $h = \frac{1}{4}$ (respectively $h = \frac{2}{5}$).

Let us first focus back on the uncoded case. We observe that for $h = \frac{1}{4}$, both reduced-state receivers achieve the same performance as the full-state receiver. For $h = \frac{2}{5}$, the receiver with $h_v = \frac{2}{5}$ becomes the reference full-state receiver and it

[2] This Section has been presented in the conference (ISTC 2014):
M. Messai, K. Amis, and F. Guilloud, "A Low Complexity Iterative Soft Detection for Bit Interleaved Coded CPM," *Turbo Codes and Iterative Information Processing (ISTC), 2014 8th International Symposium on.*

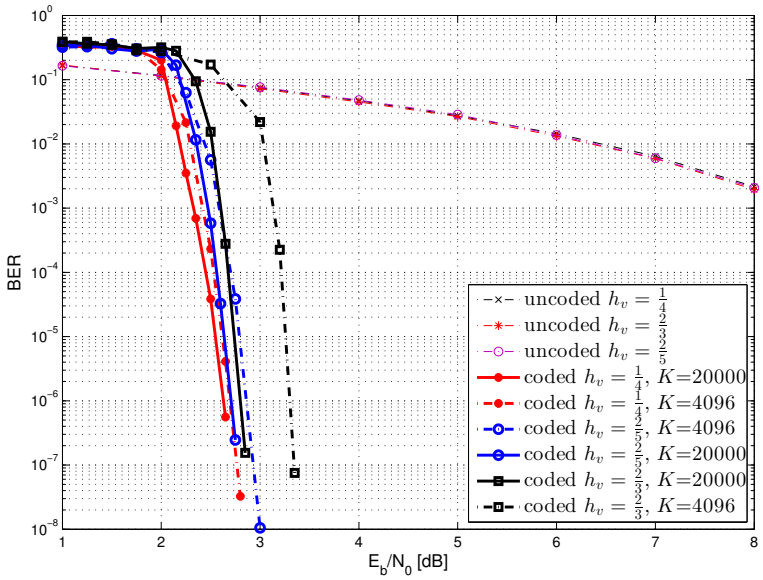

Figure 3.7: BER performance of the reduced-state receiver for a Quaternary raised cosine CPM with $L = 2$ and $h = \frac{1}{4}$. BIC-CPM: CC(7,5), pseudo-random interleaver and $K \in 4096, 20000$.

performs 0.75 dB better than the reduced-state receiver.

Let us now consider the BIC-CPM case and analyze the receiver convergence depending on h_v and K. For the BIC-CPM with $h = \frac{2}{5}$ (cf. Figure 3.8), the BER performance of the reduced-receiver is significantly poor compared to the full-sate receiver performance for both interleaver sizes, which was predictable from the uncoded case observation. The SNR gap is of roughly 1 dB as long as BER $< 10^{-3}$ and it keeps increasing below BER $= 10^{-3}$ due to a change of slope beyond around 3 dB. This change of slope is a typical BER shape for iterative receivers. There is first a slow decrease of the BER: the initial BER is too high to enable the iterative process to converge. As soon as the iterative process gain is engaged, the BER decreases quickly with the SNR (the cliff effect): this behaviour can be analysed by computing the iterative transfer of extrinsic information (EXIT charts). Then, from a given SNR value, one observes a change of slope (called the error floor), which corresponds to the convergence of the receiver towards the lower union bound. The union bound depends on the minimum distance of the BIC-CPM scheme and the error floor is all the lower as the minimum distance is high, where the minimum distance is the minimal Euclidean distance between two different coded and modulated sequences. In the case of the BIC-CPM with $h = \frac{1}{4}$ and $K = 4096$ (cf. Figure 3.7), the convergence of the full-state receiver occurs after 8 iterations. Comparatively, the reduced-state receiver with $h_v = \frac{2}{5}$ (respectively $h_v = \frac{2}{3}$) converges to its steady state after 15 iterations (respectively 20 iterations) with a loss of 0.2 dB (respectively 0.65 dB) at BER $= 10^{-5}$. In the case of $K = 20000$, the convergence of the full-state

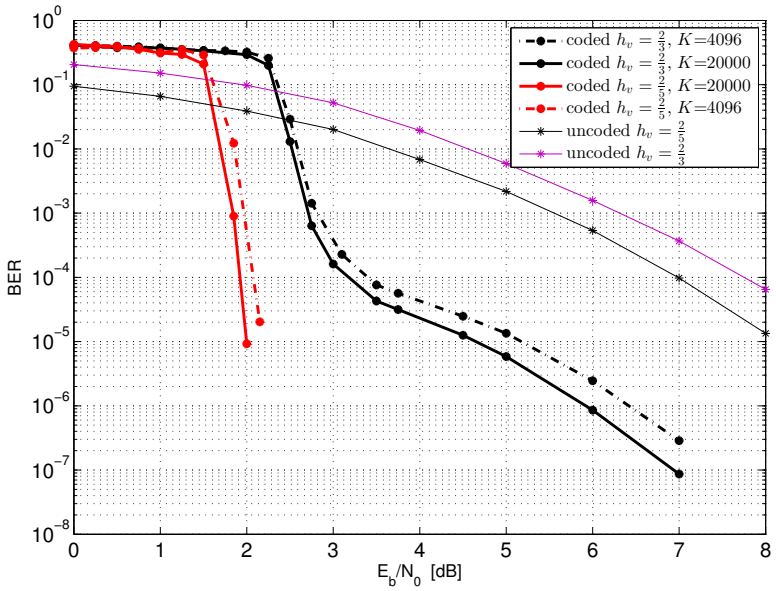

Figure 3.8: BER performance of the reduced-state receiver for a Quaternary raised cosine CPM with $L = 2$ and $h = \frac{2}{5}$. BIC-CPM: CC(7,5), pseudo-random interleaver and $K \in 4096, 20000$.

receiver is achieved after 10 iterations. The reduced-state receiver used with $h_v = \frac{2}{5}$ (respectively $h_v = \frac{2}{3}$) performs close to the full-state receiver with a slight loss of 0.1 dB (respectively 0.2 dB) at BER $= 10^{-5}$ and with convergence occurring after 14 iterations (respectively 20 iterations). We deduce that in that particular case, $h_v = \frac{2}{5}$ (respectively $h_v = \frac{2}{3}$) achieves a good tradeoff between error rate and complexity (iteration number required to converge and trellis state number) for medium codeword lengths (respectively high codeword lengths).

Conclusion: The proposed receiver has a lower number of states compared to the MLSE receiver, and compared to popular state reduction techniques from the state of the art. The state reduction results from the suppression of parallel paths in the *full-state trellis*. Two distinct symbol sequences $\boldsymbol{a}$ and $\boldsymbol{b}$ correspond to parallel paths in the *full-state trellis* from $t = nT$ if their respective states $x_{h,n}^{(a)} = (\phi_{h,n}^{(a)}, a_{n-1}, ..., a_{n-L+1})$ and $x_{h,n}^{(b)} = (\phi_{h,n}^{(b)}, b_{n-1}, ..., b_{n-L+1})$ satisfy $\phi_{h,n}^{(a)} \neq \phi_{h,n}^{(b)}$ and $a_i = b_i$ for $i \geq n - L + 1$. These two parallel paths in the *full-state trellis* can superimpose in the *reduced-state trellis* (i.e. the path with the lowest metric is suppressed), if the accumulated phase state of the path $\boldsymbol{a}$, $\Delta\phi_n^{(a)} = \pi\Delta_h \sum_{i=0}^{n-L} a_i$ (resp. of the path $\boldsymbol{b}$, $\Delta\phi_n^{(b)} = \pi\Delta_h \sum_{i=0}^{n-L} b_i$) satisfy:

$$\begin{aligned} \phi_{h,n}^{(a)} &= [\phi_{h_v,n} + \Delta\phi_n^{(a)}]_{2\pi} \\ \phi_{h,n}^{(b)} &= [\phi_{h_v,n} + \Delta\phi_n^{(b)}]_{2\pi} \end{aligned} \tag{3.9}$$

Since parallel paths correspond to the same transmitted symbols but may have

different metrics, the suppression of parallel paths has more impact on the symbol-by-symbol decoder than on the sequence decoder.

We can conclude that h_v shall not always be chosen to minimize the trellis state number. Depending on h, some h_v values may be discarded. Values of h_v discarded for the uncoded CPM receiver should also be discarded for the BIC-CPM reduced-state receiver. However, as observed hereinbefore, some values of h_v suitable for the uncoded CPM reduced-state receiver should be discarded for the BIC-CPM reduced-state receiver. In Section 3.5, rules to help discarding bad h_v values are derived.

3.5 On the optimization of a PSP-based CPM detection

We have seen in Section 3.4, that the error rate performance of the receiver based on the trellis with reduced state number may be more or less affected by the chosen virtual receiver modulation index h_v. If two different receiver modulation indices yield the same performance of the reduced-state receiver for the uncoded CPM scheme, this is not necessary the case for the BIC-CPM. Hence, the objective of this section is to study the choice of the virtual receiver modulation index in the cases of both uncoded and coded CPM, and to derive rules to skip some h_v values that would lower the error rate performance.

3.5.1 Uncoded CPM Case: Minimum Distance Analysis

In this section, we focus on the choice of h_v to build the trellis with reduced state number in the case of uncoded CPM. More precisely, we derive a rule to discard h_v values that will surely yield degradations of the error rate performance compared to the optimum performance. Since an analytical expression of the error probability achieved by the MLSE demodulation cannot be obtained, a criterion based on the minimum Euclidean distance is usually used to evaluate the performance of trellis-based CPM demodulation [10]. In the following our reasoning to discard any values of h_v is based on an approximation of an upper bound of the minimum Euclidean distance. This section is organized as follows: we first recall some materials of performance analysis based on the minimum Euclidean distance [10] and we underline how to adapt the analysis to the proposed *reduced-state receiver*. Then we apply this analysis to define rules for discarding values of h_v and illustrate the method through simulations.

3.5.1.1 Minimum Euclidean Distance Analysis [10]

The MLSE detection consists in finding the CPM sequence located at the minimum Euclidean distance denoted $d_{\min}$ from the received sequence. When an error occurs at high signal to noise ratio, it corresponds to a decided CPM sequence located at minimum Euclidean distance from the true CPM sequence. For high E_b/N_0, the bit

error probability P_b under MLSE detection is well approximated by

$$P_b \approx \mathrm{Q}\Big(\sqrt{\frac{E_b}{N_0} d^2_{\min}}\Big). \tag{3.10}$$

Thus the error rate will be all the lower as the minimum Euclidean distance is high. The minimum normalized squared Euclidean distance $d^2_{\min}$ is defined by (1.28).

Using the decomposition of the modulation index $h = h_v + \Delta_h$, the normalized squared Euclidean distance defined in (1.27) can be rewritten as:

$$d^2(\boldsymbol{e}) = \frac{\log_2(M)}{T} \int_0^{NT} \Big(1 - \cos\big(\underbrace{\phi(t, \Delta_h, \boldsymbol{e})}_{(T1)\text{:PSP process}} + \underbrace{\phi(t, h_v, \boldsymbol{e})}_{(T2)\text{:reduced trellis}} \big)\Big) dt \tag{3.11}$$

where the first term (T1) is computed using the PSP technique and where the second term (T2) is tracked by the reduced-state trellis.

The minimization in (1.28) is infeasible since the number of difference sequences $\boldsymbol{e}$ satisfying $e_0 \neq 0$ grows exponentially with N and M: $\mathrm{card}(\{\boldsymbol{e} | e_0 \neq 0\}) = (M-1) \times M^{N-1}$. The term inside the integral in (3.11) is positive, so $d^2(\boldsymbol{e})$ increases with N. This suggests that the difference sequence $\boldsymbol{e}$ corresponding to the minimum distance should have a short duration, that is to say the time interval over which $\boldsymbol{e}$ differs from the all-zero sequence should be limited, thus reducing the integration interval in (3.11). Hence, an upper bound denoted by d_B on the minimum distance $d_{\min}$ can be found by using only the difference sequences of short duration: the upper bound is then defined on a particular subset of difference sequences denoted by Γ_f. This can be summarized as:

$$\underbrace{\min_{\boldsymbol{e}, e_0 \neq 0} \big\{ d^2(e) \big\}}_{d^2_{\min}} \leq \underbrace{\min_{\boldsymbol{e} \in \Gamma_f} \big\{ d^2(e) \big\}}_{d^2_B} \tag{3.12}$$

The set of the difference sequences having a short duration Γ_f is evaluated thanks to the so-called phase tree built upon h_v. This tree is formed by the set of phase trajectories having a common start phase, say zero, at time $t = 0$. We assume that the data symbols for all the phase trajectories in the tree before this time are equal. The phase trajectories do not coincide over the first symbol interval ($e_0 \neq 0$). However, when going further into the tree, it is always possible to find a pair of phase trajectories which coincide (modulo 2π) at a specific time. This instant is referred to as a merger. Let τ denote the instant where the two phase trajectories merge. The calculation of the Euclidean distance between both signals can be reduced to the interval $[0, \tau]$. The mergers are easily identified in the phase difference tree, since they correspond to a phase difference trajectory which is identically equal to zero for all $t \geq \tau$. The mergers can be classified by sorting the values of τ in ascending order. The first order mergers correspond to the smallest values of τ, and the upper bound d^2_B defined in (3.12) can be found by using only the difference sequences corresponding to the first order mergers. The more orders, the tighter the bound.

We denote by t_k a k-th merger and we assume $t_k = mT$. Let $\boldsymbol{a}$ and $\boldsymbol{b}$ be one pair of sequences with phase trajectories merging at time t_k. Then $e_i = a_i - b_i$ takes on values in $\mathcal{A} = \{0, \pm 2, \pm 4, ..., \pm 2(M-1)\}$. The difference phase reads

$$\phi(t, h_v, \boldsymbol{e}) = 2\pi h_v \sum_{i=-\infty}^{m-1} e_i q(t - iT), \tag{3.13}$$

with $e_i \in \mathcal{A}$ for $i = 0, 1, ..., m-1$ and $e_i = 0$ for $i < 0$.

According to (3.11), $d(\boldsymbol{e})$ is a function of $\cos(\phi(t, h_v, \boldsymbol{e}))$, which is an even function. From (3.13), we observe that each sequence $\boldsymbol{e}$ has its opposite in the set of phase difference sequences. Thus, for the calculation of the upper bound of the minimum distance, it is sufficient to consider the phase difference tree, using the difference sequences $\boldsymbol{e} = (e_0, ..., e_{N-1})$ taken in Γ_m defined as:

$$\Gamma_m = \{\boldsymbol{e} | \underset{0 \le i \le m-1}{e_i \in \mathcal{A}}, \quad \underset{i \ge m}{e_i = 0}, \quad e_0 > 0, \quad e_{m-L} \neq 0\} \tag{3.14}$$

Assuming $\boldsymbol{e} \in \Gamma_m$, the two phase trajectories merge at t_k and coincide beyond if the following condition is satisfied:

$$\begin{aligned} \exists \ell \in \mathbb{Z}, \phi(t, h, \boldsymbol{e}) &= 2\ell\pi, \ t \ge t_k \\ \Leftrightarrow \exists \ell \in \mathbb{Z}, \quad 2\pi h_v \sum_{i=0}^{m} e_i q(t - iT) &= 2\ell\pi, \ t \ge t_k \\ \Leftrightarrow \exists \ell \in \mathbb{Z}, \pi h_v \sum_{i=0}^{m-L} e_i + 2\pi h_v \sum_{i=m-L+1}^{m} e_i q(t - iT) &= 2\ell\pi, \ t \ge t_k \end{aligned} \tag{3.15}$$

Let $\boldsymbol{b}$ and $\hat{\boldsymbol{b}}$ be the pair of sequences yielding a phase difference trajectory corresponding to a k-th merger. The paths merge at $t_k = mT$ at a state $x_m^j = (\phi_{h_v,m}^j(\Delta\phi_{m+1}^j), a_m^j, a_{m-1}^j, ..., a_{m-L+1}^j)$. It means that $(b_m, b_{m-1}, ..., b_{m-L+1}) = (a_m^j, a_{m-1}^j, ..., a_{m-L+1}^j)$ and that $(\hat{b}_m, \hat{b}_{m-1}, ..., \hat{b}_{m-L+1}) = (a_m^j, a_{m-1}^j, ..., a_{m-L+1}^j)$, and thus $(b_m, b_{m-1}, ..., b_{m-L+1}) = (\hat{b}_m, \hat{b}_{m-1}, ..., \hat{b}_{m-L+1})$, that is to say $e_i = 0, i = \{m-L+1, ..., m\}$: so the time dependent part of (3.15) is set to zero, yielding:

$$(3.15) \Leftrightarrow \exists \ell \in \mathbb{N}, \pi h_v \sum_{i=0}^{m-L} e_i = 2\ell\pi. \tag{3.16}$$

Thus, the difference sequence of a pair of sequences whose phase trajectories separate at $t = 0$ ($e_0 > 0$) and merge at t_k, always verifies

$$\begin{cases} \exists \ell \in \mathbb{N}, h_v \sum_{i=0}^{m-L} e_i = 2\ell \\ e_0 > 0 \end{cases} \tag{3.17}$$

From [10] (Chapter 3), in the case of the MLSE (full-state trellis corresponding to $h_v = h$), the upper bound on the minimal distance d_B is obtained using the difference sequences that are common to all the values of the modulation index i.e

when $\ell = 0$. The upper bound d_B is thus computed for the MLSE considering all sequences satisfying

$$\sum_{i=0}^{m-L} e_i = 0, \quad \boldsymbol{e} \in \Gamma_m. \tag{3.18}$$

The proposed algorithm working on the reduced state-number trellis suppresses more candidate paths (due to a higher merging path number per state) compared to the Viterbi algorithm working on the original trellis, yielding a possible smaller minimum Euclidean distance, and thus performance degradation. The virtual modulation index h_v will be chosen so that the k-th mergers in the trellis with reduced state number are higher than the k-th mergers in the original trellis (with full state number). An upper bound d_B of the minimum distance in the case of the trellis designed with h_v, is computed by considering all the cases described in (3.17) i.e, using the difference sequences $\boldsymbol{e}$ in Γ_m satisfying:

$$\sum_{i=0}^{m-L} e_i = \frac{2\ell}{h_v}, \quad \ell \geq 0 \tag{3.19}$$

As $h_v = \frac{l_v}{p_v}$ with l_v and p_v being relatively prime integers and, as $\sum_{i=0}^{m-L} e_i$ takes on integer values, (3.19) becomes

$$\sum_{i=0}^{m-L} e_i = 2\ell p_v, \quad \ell \geq 0. \tag{3.20}$$

3.5.1.2 Application to the Design of the Virtual Modulation Index

For a *reduced-state receiver* based upon h_v, the computation of the upper bound d_B is as follows:

- First, we determine the set of difference sequences Γ_f corresponding to the mergers of the first orders: they are identified from the reduced state trellis built upon h_v (term (T2) in (3.11)). For a fixed p_v, we determine exhaustively the possible values of m and their corresponding $\boldsymbol{e}$.
- We compute the normalized Euclidean distance $d(\boldsymbol{e})$ given by (3.11) for every difference sequence found, since $\phi(t, \Delta_h, \boldsymbol{e}) + \phi(t, h_v, \boldsymbol{e}) = \phi(t, h, \boldsymbol{e})$.
- The upper bound on the minimum distance d_B is the lower bound of all of these computed normalized Euclidean distances ($d_B = \min_{\boldsymbol{e} \in \Gamma_f} d(\boldsymbol{e})$).

We observe that the minimum value of m for which (3.20) has solutions for $\ell \neq 0$ increases with p_v. Given h, h_v will thus be chosen so that the value of m yielding to the minimum distance in the MLSE trellis be inferior to the value of m from which (3.20) has solution for $\ell \neq 0$. Among the set of h_v satisfying this condition, we will choose the one which results in the best state number reduction.

Let us illustrate this principle with the CPM parameters used in Section 3.3. The first two mergers are reported in Table 3.2 and an upper bound d_B^2 for the

Table 3.2: First two mergers in the reduced state number trellis for Quaternary 2RC

	MLSE $h_v = h$	$h_v = \frac{k}{5}$ $(k \wedge 5 = 1)$	$h_v = \frac{k}{4}$ $(k \wedge 4 = 1)$	$h_v = \frac{k}{3}$ $(k \wedge 3 = 1)$	$h_v = \frac{k}{2}$ $(k \wedge 2 = 1)$
First mergers	$m = 4$ $\sum_{i=0}^{1} e_i = 0$, $e_i \in \Gamma_4$	$m = 3$ $\sum_{i=0}^{1} e_i = 10$, $e_i \in \Gamma_3$	$m = 3$ $\sum_{i=0}^{1} e_i = 8$, $e_i \in \Gamma_3$	$m = 2$ $\boldsymbol{e} = (6, 0)$	$m = 2$ $\boldsymbol{e} = (4, 0)$
Second mergers	$m = 5$ $\sum_{i=0}^{2} e_i = 0$, $e_i \in \Gamma_5$	$m = 4$ $\sum_{i=0}^{2} e_i = 10$, $e_i \in \Gamma_4$	$m = 4$ $\sum_{i=0}^{2} e_i = 8$, $e_i \in \Gamma_4$	$m = 3$ $\sum_{i=0}^{2} e_i = 6$, $e_i \in \Gamma_3$	$m = 3$ $\sum_{i=0}^{2} e_i = 4$, $e_i \in \Gamma_3$

reduced state number trellis is plotted in Figure 3.9 for several values of h_v. We observe that d_B^2 is the same for the reduced state number trellis and for the full state number trellis when $h_v = \frac{k}{5}$ with $k \wedge 5 = 1$. $k \wedge p$ denotes the greatest common divisor of k and p. Whereas if $h_v = \frac{k}{4}$, with $k \wedge 4 = 1$ there is a slight degradation when the transmission modulation index is different from h_v and belongs to the interval $[0.51, 0.56]$. For a detection with $h_v = \frac{k}{3}$ where $k \wedge 3 = 1$ there is also a degradation when $h \neq h_v$ belongs to the modulation index intervals $[0.34, 0.44]$, $[0.59, 0.81]$, $[0.9, 1.13]$ or $[1.28, 1.43]$. Finally, by using $h_v = \frac{k}{2}$ with $(k \wedge 2 = 1)$ we observe a degradation when $h \neq h_v$ is in the modulation index intervals $[0.39, 0.67]$, $[0.87, 1.191]$ or $[1.41, 1.5]$. This is in accordance with the conclusions drawn from Figure 3.7 and Figure 3.8. We observed no error rate degradation in the case of $h = \frac{1}{4}$ and $h_v \in \{\frac{2}{3}, \frac{2}{5}\}$, whereas $h_v = \frac{2}{3}$ yielded a significant degradation in the case of $h = \frac{2}{5}$.

In order to check the validity of our approach, we added in Figure 3.9 the values of the minimum distance in the reduced-state trellis, estimated through simulations based on the fact that the bit error probability P_b for large E_b/N_0 is approximated by (3.10). For each value of h and given a large E_b/N_0, we simulated the detection of the CPM with the proposed reduced-state trellis-based receiver to estimate the BER and to deduce an estimate of $d^2_{\min}(h)$ from the inverse function of $\mathrm{Q}(x)$ (the solution is unique since the function $\mathrm{Q}(x)$ is bijective). Note that we chose the value of E_b/N_0 to ensure a low BER, depending on the value of h as follows: $E_b/N_0 = 16$ dB for $h \in \{0.1, 0.2\}$, $E_b/N_0 = 12$ dB for $h \in \{0.3, 0.4\}$ and $E_b/N_0 = 10$ dB for $h \in \{0.5, 0.6, 0.7, 0.8, 0.9\}$.

3.5.2 Coded CPM: EXIT Charts Analysis

In the case of uncoded CPM, the minimum distance is a good criterion to discard some values of the virtual reception modulation index. However, we have observed in Section 3.3 that given two different values of h_v, the performance of the two corresponding reduced-state receivers may coincide in the case of uncoded CPM and may differ in the case of BIC-CPM. Indeed, given a high enough signal to noise ratio, after the first iteration, the soft BCJR-based CPM detector of the BIC-CPM receiver

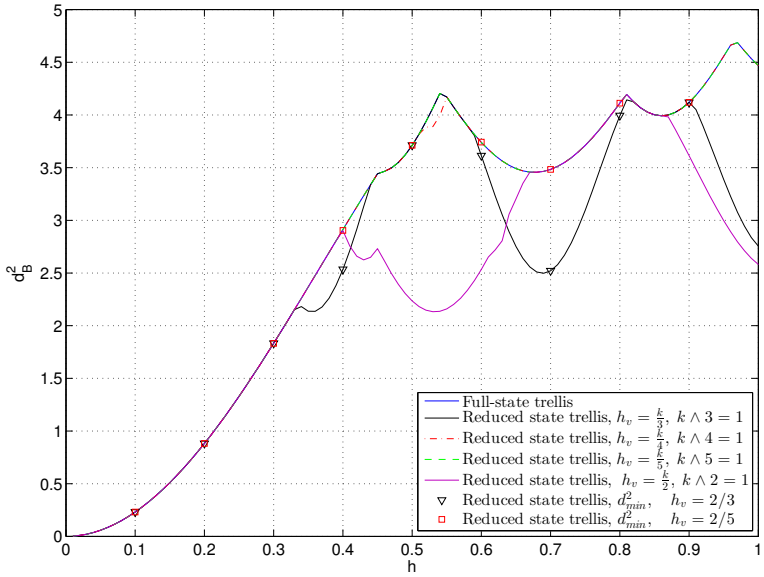

Figure 3.9: Upper bound on the minimum distance as a function of h in the reduced state number trellis for Quaternary 2RC CPM and different values of h_v

yields the same decision as the hard Viterbi-based CPM detector. The hard decision is given by applying a threshold on the log-likelihood ratio. Given two different values of h_v, the corresponding soft BCJR-based CPM detectors may deliver the same hard decisions but extrinsic information with highly different reliabilities.

In the case of BIC-CPM, the inner and the outer components of the receiver, namely the proposed CPM demodulator and the FEC decoder, exchange soft information on the encoded bits. The transfer characteristic curves can be obtained by considering the *a priori* information delivered by the proposed CPM demodulator to the decoder [40]. In the following, we intend to analyze the influence of the choice of h_v on the convergence of the reduced-state receiver from EXIT charts. Simulations are carried out with the Quaternary 2RC CPM as in previous sections.

In Figure 3.10, we have considered $h = \frac{1}{4}$ and $E_b/N_0 = 1.5$ dB. We have plotted the EXIT chart for the full-state receiver ($h_v = \frac{1}{4}$) and for two reduced-state receivers ($h_v = \frac{2}{5}$ and $h_v = \frac{2}{3}$). From Figure 3.7, we have observed that the three receivers perform roughly the same for high codeword lengthes with a higher degradation for medium lengthes with $h_v = \frac{2}{3}$. From Figure 3.10, we can also observe that for low-to-medium information values (beginning of the iterative process), the curves of the BCJR-based detectors seem parallel but shifted. The convergence threshold is thus better for $h_v = \frac{2}{5}$ than $h_v = \frac{2}{3}$. The EXIT chart enables also to complete the complexity comparison by predicting the iteration number required to converge. Table 3.3 reports the complexity comparison in terms of trellis state number and minimum iteration number required to converge. We deduce that using

$h_v = \frac{2}{5}$ at the reception allows to perform a good compromise between performance and complexity.

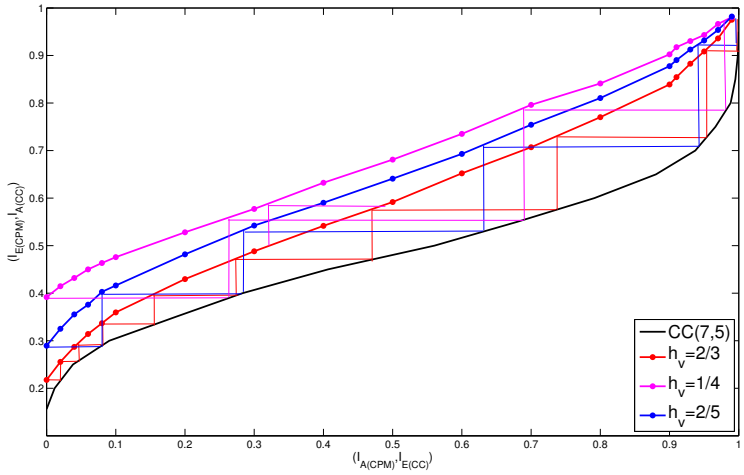

Figure 3.10: EXIT chart for the reduced-state BIC-CPM receiver ($h_v \in \{\frac{1}{4}, \frac{2}{5}, \frac{2}{3}\}$). Quaternary raised cosine CPM with $L = 2$ and $h = \frac{1}{4}$, CC(7,5), pseudo-random interleaver, $\frac{E_b}{N_0} = 1.5\ dB$.

In Figure 3.11 we have considered $h = \frac{2}{5}$ (same simulation conditions as for Figure 3.8). The EXIT chart is plotted for the full-state receiver ($h_v = \frac{2}{5}$) on the right and for the reduced-state receiver ($h_v = \frac{2}{3}$) on the left. Different values of E_b/N_0 are simulated to compare the convergence thresholds. For $E_b/N_0 = 1.5$ dB, none of the receivers will be able to converge. For $E_b/N_0 = 2$ dB, only the full-state receiver will converge. For $E_b/N_0 = 2.5$ dB, both of them will converge. The difference between the respective thresholds of convergence is quite significative. The EXIT chart analysis is thus in accordance with the conclusions drawn from Figure 3.8.

Table 3.3: Trellis state number and predicted minimum iteration number for the reduced-state BIC-CPM receiver. Quaternary 2RC with $h = \frac{1}{4}$ for $\frac{E_b}{N_0} = 1.5\ dB$

	Trellis state number	Predicted minimum iteration number
$h_v = \frac{1}{4}$	32	4
$h_v = \frac{2}{5}$	20	5
$h_v = \frac{2}{3}$	12	9

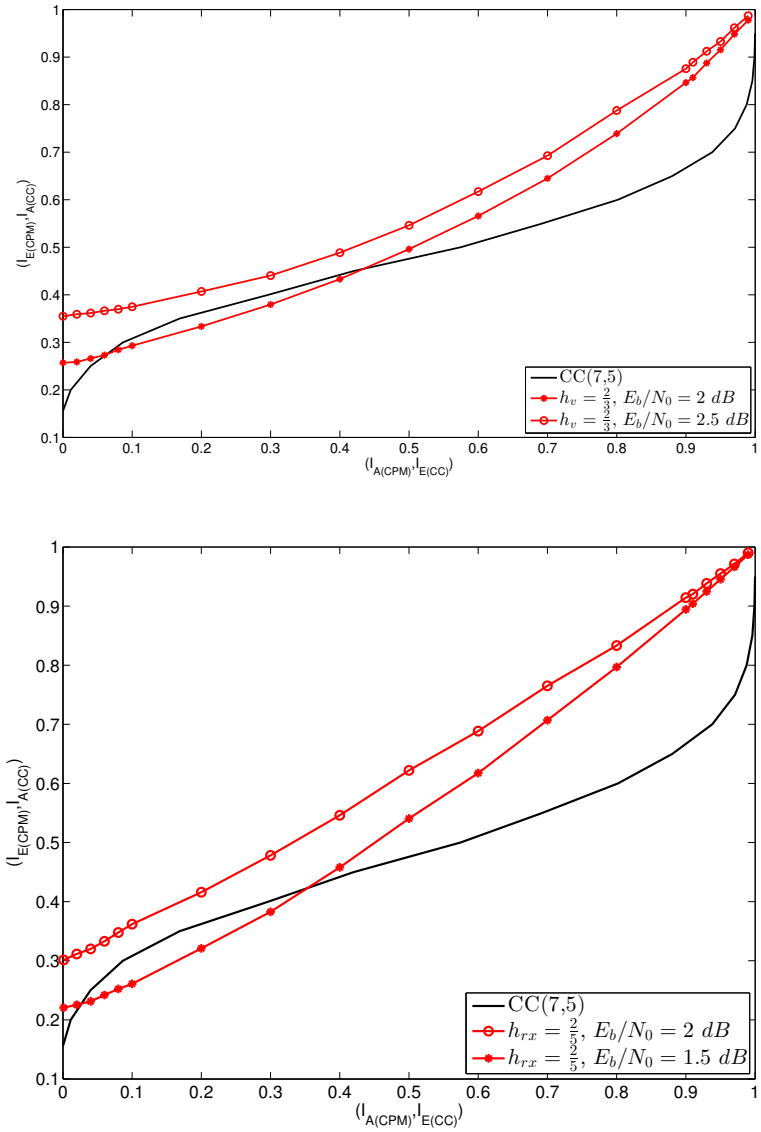

Figure 3.11: EXIT chart for the BIC-CPM receiver. Quaternary raised cosine CPM with $L = 2$ and $h = \frac{2}{5}$, CC(7,5), pseudo-random interleaver. Left side: reduced-state receiver, $h_v = \frac{2}{3}$, $\frac{E_b}{N_0} \in \{2, 2.5\}dB$. Right side: full-state receiver, $h_v = \frac{2}{5}$, $\frac{E_b}{N_0} \in \{1.5, 2\}dB$.

3.6 Conclusions

This chapter focused on low complexity algorithms for CPM demodulation. The principle is to choose a virtual modulation index at the receiver side which can be different from the modulation index of the transmitted CPM waveform, hence enabling the detection of CPM waveforms with irrational modulation indices. Depend-

ing on the virtual modulation index, a trellis with a reduced number of states can be obtained. Using modified branch metrics, both Viterbi algorithm for sequence detection and BCJR algorithm for soft-input soft-output CPM demodulation are derived. Even if a large range of modulation indices can be used at the receiver side, the complexity reduction (number of states in the trellis) is a first criterion to select a particular one. However, some modulation indices may degrade the error rate performance. We proposed two ways to discard such modulation indices. The first one is related to the uncoded CPM case (Viterbi detection) and is based on the minimal distance upper bound derivation, as a function of both the transmission modulation index and the virtual modulation index used at the receiver side to design the trellis. The second one is related to the BIC-CPM case, where an iterative receiver based on soft information exchange between the FEC decoder and the CPM detector is performed. In this case, avoiding values discarded from the minimal distance study, an EXIT chart analysis enables to discard the modulation indices which degrade the convergence of the iterative decoding algorithm. A trade-off between the remaining possible modulation indices is finally possible by balancing the convergence speed and the number of states in the trellis.
In this chapter, we considered an AWGN channel and we assumed the modulation index perfectly known at the receiver. However, in most channels such as in satellite applications, a phase noise may degrade the performance if not taken into account. Moreover in applications with low-cost transmitters which are targeted in this work, the modulation index may vary around its nominal value and it should be taken into account in the receiver to ensure high quality transmission. The next chapter addresses the problem of robustness to phase noise and modulation index mismatch and tackles it from the transmitter and the receiver sides.

Chapter 4

Robustness to Modulation Index Mismatch and Phase Noise for a binary CPM

Contents

4.1 Introduction

In this chapter, we deal with the robustness problem and particularly when the transmission modulation index is unknown at the receiver. Firstly, we resolve the problem of the unknown modulation index from the transmitter side. We design new binary schemes with enhanced robustness. They are based on the concatenation

[0]This chapter is the subject of the publication:
- M. Messai, G. Colavolpe, K. Amis and F. Guilloud, "Robust Detection of Binary CPMs with Unknown Modulation Index" *IEEE Commun. Letters.*
-M. Messai, G. Colavolpe, K. Amis and F. Guilloud, "Binary Continuous Phase Modulation Robust to a Modulation Index Mismatch" *IEEE Trans. Commun.*

of a proper precoder with binary input and a ternary CPM format as in Chapter 2. However in Chapter 2 we focused on the spectral efficiency improvement while here we aim at making the transmission robust to modulation index mismatch and to phase noise. The result is a family of CPMs formats whose phase state is constrained to follow a specific evolution. Two of these precoders are considered. We will discuss many aspects related to these schemes, as the power spectral density, the spectral efficiency, simplified detection, the minimum distance, and the uncoded performance. The adopted precoders do not change the recursive nature of CPM schemes. So these schemes are still suited for serial concatenation, through a pseudo-random interleaver, with an outer channel encoder.

Secondly, we consider the very general problem of soft-input soft-output (SISO) detection of a binary CPM signal with an unknown modulation index transmitted over a channel with phase noise. We adopt a simplified representation of the CPM signal based on the principal component of its Laurent decomposition [25] and describe the joint a-posteriori probability of the transmitted symbols, the channel phase, and the modulation index variation through a factor graph (FG) [26]. The sum-product algorithm (SPA) is then advocated to compute the a-posteriori probabilities of the transmitted symbols [26]. Due to the recursive nature of the modulator which also makes the CPM well suited for a concatenation with an outer error code, no pilots are required to bootstrap detection. Being soft-output in nature, the proposed algorithm is a good candidate to be employed in iterative detection and decoding schemes.

4.2 A Brief Review of Previous Studies

Coherent receivers performs better than Non-coherent ones, provided that the modulation index is perfectly known. Even a slight variation leads to a modification of the trellis structure with a large possible number of states. Therefore, in the case of uncertainty of the modulation index noncoherent detection is an attractive strategy. Non coherent receivers have received a keen interest in the literature for their robustness. The simplest noncoherent receivers for continuous phase modulation (CPM) are differential detectors [59], [60]. A simple differential detector makes its decision according to the sign of the estimated phase difference over a symbol period. Later, a new differential demodulation algorithm using multiple-symbol observation intervals was developed for GMSK signal in [61]. Based on the decision feedback, in [62] a multiple differential detection (MDD) sequence estimator was described for GMSK demodulation. This technique is based on a maximum-likelihood sequence estimation (MLSE) of the transmitted phases over multiple symbols rather than symbol-by-symbol detection.

Among the simple methods we can also mention the limiter discriminator [63]. It uses a limiter to restore the constant envelope property to the corrupted received signal and a discriminator to convert the phase modulation into amplitude modulation for envelope detection. The discriminator is often followed by a low-pass filter,

such as an integrate-and-dump filter. This method was improved after in [64], where the author proposed a multilevel decision method for band-limited digital FM with limiter-discriminator demodulation. The multilevel decision method is inserted after the limiter-discriminator and integrate-and-dump filter. In the two-level method the decision is made taking into account the previous detected symbol while in the four-level method, the two preceding detected symbols are considered.

A more complicated non-coherent algorithm with better performance was proposed later in [65] where a differential detection via the Viterbi algorithm strategy was derived. This algorithm estimates the phase state based on the previous observation and uses it in the decision metric of a VA coherent receiver. Nevertheless the performance is far from the MLSE receiver performance due to the differential detection approach. Then, the principle used in [65] was extended in [66] in association to the Laurent decomposition of a CPM signal to define a *multiple-symbol differential detection*. The resulting receiver performs closer to the optimum coherent receiver at the expense of a higher computational complexity. Recently, in [56], a noncoherent receiver for the Gaussian frequency shift keying (GFSK) signal adopted in the Bluetooth standard was proposed. This receiver can tolerate only a relatively small modulation index deviation. Another alternative is the introduction at the receiver of a modulation index estimation algorithm [67] coupled with a coherent receiver.

4.3 CPM Signals and Laurent Decomposition

In this section, we will briefly review the Laurent decompositions of binary and ternary CPMs [25, 68]. Based on Laurent representation, the complex envelope of a binary or a ternary CPM signal may be exactly expressed as [25, 68]

$$s(t, h, \boldsymbol{a}) = \sum_{k=0}^{K-1} \sum_{n} \alpha_{k,n} p_k(t - nT) \tag{4.1}$$

where $K = 2^{(L-1)}$ or $K = 2 \cdot 3^{(L-1)}$ for binary or ternary CPMs, respectively. The expressions of pulses $\{p_k(t)\}$ as a function of $q(t)$ and h and those of symbols $\{\alpha_{k,n}\}$ as a function of the information symbol sequence $\{a_n\}$ and h may be found in [25, 68]. By truncating the summation in (4.1) considering only the first $K < 2^{(L-1)}$ terms, we obtain an approximation of $s(t, h, \boldsymbol{a})$. In the binary case, most of the signal power is concentrated in the first component, i.e., that associated with pulse $p_0(t)$, which is called *principal component* [25]. As a consequence, the principal component may be used in (4.1) to reach a very good trade-off between approximation quality and number of signal components [57, 69]. In this case, it holds

$$\alpha_{0,n} = \alpha_{0,n-1} e^{j\pi h a_n} \tag{4.2}$$

Symbols $\{\alpha_{0,n}\}$ take on p values [25] and it can be easily observed that $\alpha_{0,n} = e^{j\phi_n}$, where ϕ_n is defined in (1.8).

In the ternary case, most of the signal power is concentrated in two principal components, corresponding to pulses $p_0(t)$ and $p_1(t)$. In this case, the corresponding

symbols can be expressed as

$$\alpha_{0,n} = e^{\jmath\pi h a_n}\alpha_{0,n-1} \tag{4.3}$$

$$\alpha_{1,n} = \frac{1}{2}\left[e^{\jmath\pi h\gamma_{0,n}} + e^{\jmath\pi h\gamma_{1,n}}\right]\alpha_{0,n-1} \tag{4.4}$$

where $\gamma_{0,n}$ and $\gamma_{1,n}$ belong to the alphabet ± 1 and are such that $a_n = \gamma_{0,n}+\gamma_{1,n}$ [68]. In this ternary case, it is again $\alpha_{0,n} = e^{\jmath\phi_n}$.

In low-cost transmitters, the value of the modulation index is often different from its nominal value which is instead assumed at the receiver [70]. In the following, we will express the modulation index at the transmitter as $h = h_{rx} + h_e$, where h_{rx} is the nominal value known at the receiver and h_e accounts for the mismatch between transmitter and receiver and is assumed unknown. This mismatch has a catastrophic effect on the performance. As observed in [67], the pulses of the principal components weakly depend on the value of the modulation index and thus on h_e. On the contrary, the effect of h_e is cumulative in the phase state and thus in $\alpha_{0,n}$. This observation motivates the schemes proposed in the next section.

We consider transmission over an additive white Gaussian noise (AWGN) channel. The complex envelope of the received signal thus reads

$$r(t) = s(t, h_{rx} + h_e, \boldsymbol{a}) + w(t) \tag{4.5}$$

where $w(t)$ is a complex-valued white Gaussian noise process with independent components, each with two-sided power spectral density N_0. In the following, we will denote by $\boldsymbol{r}$ a proper vector of sufficient statistics extracted from the continuous-time received signal $r(t)$.

4.4 Robust Precoded CPM Schemes

The schemes described in section 4.2 operate at the receiver side and no attempt to increase the intrinsic robustness of the generated signal is made. This problem is faced here. In other words, we will define new binary formats for which the performance degradation is very limited even when there is a significant modulation index mismatch between the transmitter and the receiver. These new schemes are based on the concatenation of a precoder with binary input and ternary output, and a ternary CPM scheme. The aim of the precoder is to constrain the evolution of the CPM phase state. Two precoders will be described and investigated in this section. The overall scheme resulting from the adoption of the first precoder has only two states, independently of the adopted modulation index. The second precoder generates an overall scheme with a number of states which depends on the modulation index denominator and will be introduced to avoid the presence of impulses in the power spectral density. We will show the properties of the power spectral density of these schemes and also study the uncoded performance and the spectral efficiency, which provides a benchmark on the coded performance. Suboptimal detection will be also considered.

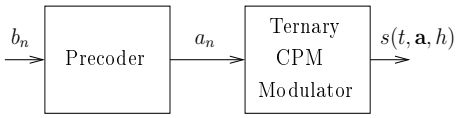

Figure 4.1: Proposed scheme.

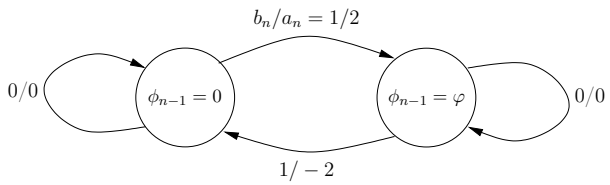

Figure 4.2: State diagram of the overall scheme in the case of AMI precoder.

4.4.1 AMI precoder

The precoded ternary CPM scheme depicted in Figure 4.1 is similar to the scheme studied in Chapter 2. The difference comes from the design criteria. In Chapter 2 we aimed at improving the spectral efficiency, while in this Chapter we try to enhance the robustness to modulation index mismatch. In both cases, the ternary CPM scheme is employed.

We design the precoder to avoid the cumulative effect on the phase state, still keeping its recursive definition. This latter property is important to have an interleaver gain when the proposed scheme is concatenated with an outer encoder through an interleaver. The classical alternate mark inversion (AMI) precoder encodes bit $b_n = 0$ as $a_n = 0$ and encodes bit $b_n = 1$ alternately as $a_n = 2$ or $a_n = -2$. By denoting $\varphi = 2\pi h$ and assuming that the initial phase state is $\phi_0 = 0$, we thus have the alternation of the phase states 0 and φ according to the state diagram shown in Figure 4.2. In this state diagram, the values of a_n are also shown. Thus, there is no accumulation effect and a possible error on h has a very limited impact on the performance, as shown in Section 4.4.6.

4.4.2 Proposed precoder

As we will see in Section 4.4.4, unless $h = 1/2, 3/2, \ldots$, the power spectral density of the signal resulting from the previous AMI-based scheme has impulses at harmonics of the signaling rate $1/T$. They can be used to help timing and frequency synchronization. In case they are considered as undesirable, another precoder can be used. We will see that these impulses are not present when $E\{\alpha_{0,n}\} = 0$, where $\alpha_{0,n}$ is the principal pseudo-symbol of its Laurent decomposition defined in 4.2. For this reason, we can define a precoder such that all phase states

$$\Big\{ -\frac{p}{2}\varphi, \big(-\frac{p}{2}+1\big)\varphi, \ldots, -\varphi, 0, \varphi, \ldots, \big(\frac{p}{2}-1\big)\varphi, \frac{p}{2}\varphi \Big\}$$

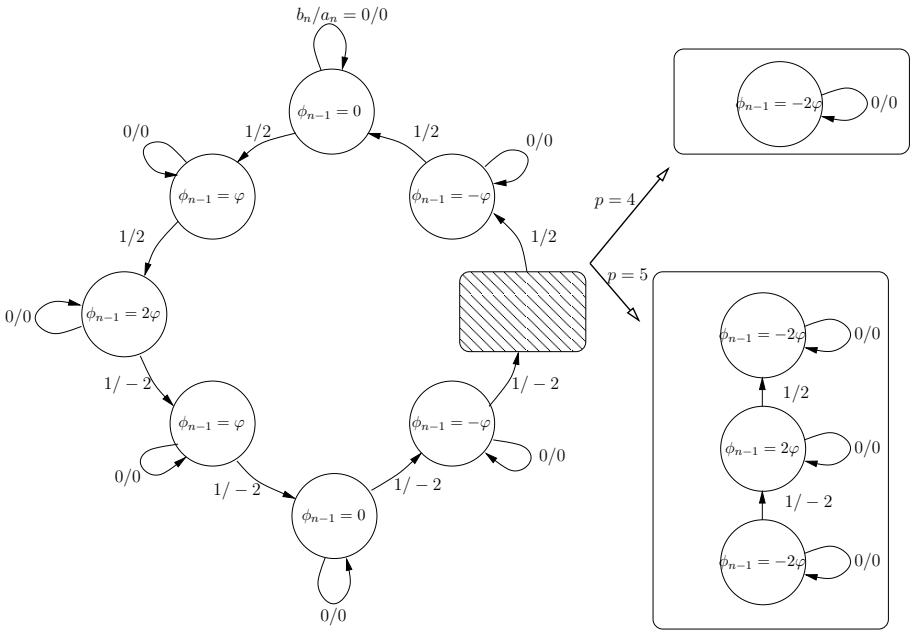

Figure 4.3: State diagram of the overall scheme in the case of second proposed precoder for $p = 4$ or $p = 5$.

when p is even and

$$\left\{ -\frac{p-1}{2}\varphi, -\frac{p-3}{2}\varphi, \ldots, -\varphi, 0, \varphi, \ldots, \frac{p-3}{2}\varphi, \frac{p-1}{2}\varphi \right\}$$

when p is odd, occur with the same probability. This precoder is based on this simple rule: bit $b_n = 0$ is again encoded as $a_n = 0$, whereas bit $b_n = 1$ as $a_n = 2$ or $a_n = -2$. This time, however, the encoder provides at its output a block of p symbols $a_n = 2$ followed by a block of p symbols $a_n = -2$, one after the other. Without loss of generality, let us assume that initial phase state of the encoder is $\phi_0 = -\frac{p}{2}\varphi$ if p is even or $\phi_0 = -\frac{p-1}{2}\varphi$ if p is odd. The state of the overall scheme is not only related to the actual CPM phase state ϕ_{n-1} but also to the sign of the block of symbols we are transmitting. The state diagram of the overall scheme is shown in Figure 4.3 for $p = 4$ or $p = 5$.

4.4.3 Corresponding detector

As far as detection is concerned, we could implement the optimal receivers through a bank of proper matched filters followed by a Viterbi [13] or a BCJR [16] algorithm with a proper number of states.[1] However, a low-complexity suboptimal receiver with practically optimal performance can be implemented through a bank of two filters matched to pulses $p_0(t)$ and $p_1(t)$, followed by a Viterbi or a BCJR algorithm

[1]The Viterbi and the BCJR algorithms are used for the implementation of the maximum a posteriori (MAP) *sequence* and *symbol* detection criteria, respectively.

with branch metrics [57, 69]

$$\begin{aligned}\lambda_n(b_n,\phi_{n-1}) =& \Re\left[x_{0,n}\alpha_{0,n}^* + x_{1,n}\alpha_{1,n}^*\right]\\ =& \Re\Big\{e^{-\jmath\phi_{n-1}}\Big[x_{0,n}e^{-\jmath\pi h a_n}\\ &+ x_{1,n}\Big(\frac{e^{-\jmath\pi h\gamma_{0,n}}+e^{-\jmath\pi h\gamma_{1,n}}}{2}\Big)\Big]\Big\}\end{aligned} \tag{4.6}$$

$x_{0,n}$ and $x_{1,n}$ being the outputs at time nT of the two matched filters, having impulse response $p_0(-t)$ and $p_1(-t)$, respectively, a_n is a function of ϕ_{n-1} and b_n, as shown in Figure 4.2 or in Figure 4.3, and, as previously stated, $\gamma_{0,n}$ and $\gamma_{1,n}$ are such that $a_n = \gamma_{0,n} + \gamma_{1,n}$. These algorithms thus work on a trellis with only 2 states, independently of the value of h, in the case of the AMI precoder, whereas in the case of the second proposed encoder the number of states is $2p$ when p is even, and $2(p-1)$ when p is odd.

4.4.4 Spectrum and Spectral Efficiency

In order to gain a deeper understanding of the effect of these precoders on the overall signal, we now consider the power spectral density (PSD) of the transmitted signal in our proposed schemes. Instead of considering the exact PSD, we will consider the PSD of the signal resulting from the approximation of the transmitted signal with its two principal components.[2] Hence, we approximate the transmitted signal as

$$s(t,\boldsymbol{a},h) \simeq \overline{s}(t,\boldsymbol{a},h) = \sum_n \alpha_{0,n}p_0(t-nT) + \sum_n \alpha_{1,n}p_1(t-nT) \tag{4.7}$$

whose PSD can be expressed as

$$\begin{aligned}W_{\overline{s}}(f) =& \frac{W_{\alpha_0}(f)}{T}|P_0(f)|^2 + \frac{W_{\alpha_1}(f)}{T}|P_1(f)|^2\\ &+ \frac{2}{T}\Re\Big\{W_{\alpha_0,\alpha_1}(f)P_0(f)P_1^*(f)\Big\}\end{aligned} \tag{4.8}$$

where $W_{\alpha_0}(f)$, $W_{\alpha_1}(f)$, and $W_{\alpha_0,\alpha_1}(f)$ are the Fourier transforms of the discrete-time sequences $R_{\alpha_0}(m) = E\{\alpha_{0,n+m}\alpha_{0,n}^*\}$, $R_{\alpha_1}(m) = E\{\alpha_{1,n+m}\alpha_{1,n}^*\}$, and $R_{\alpha_0,\alpha_1}(m) = E\{\alpha_{0,n+m}\alpha_{1,n}^*\}$, respectively, whereas $P_0(f)$ and $P_1(f)$ are the Fourier transforms of pulses $p_0(t)$ and $p_1(t)$, respectively. The first two terms in (4.8) represent the PSD of the two components whereas the remaining one takes into consideration the correlation between the two components. It is straightforward to prove that, for the precoder in Figure 4.2 it is

$$\begin{aligned}\lim_{m\to\infty} R_{\alpha_0}(m) &= \frac{1}{2}(1+\cos 2\pi h)\\ \lim_{m\to\infty} R_{\alpha_1}(m) &= \frac{\cos^2\pi h}{2}(1+\cos 2\pi h)\\ \lim_{m\to\infty} R_{\alpha_0,\alpha_1}(m) &= \frac{3}{4}\cos\pi h + \frac{1}{4}\cos\pi h\cos 2\pi h\end{aligned} \tag{4.9}$$

[2] When $L = 1$, this representation with only two components turns out to be exact, i.e., in (4.7) only two components are present in this case.

This is one of the properties of the autocorrelation function [71]. However, it is sufficient to adopt a precoder such that in Figure 4.3 that makes $E\{\alpha_{0,n}\} = 0$ to avoid the presence of such impulses. In fact, for ternary CPMs, by considering all symbols $\{\alpha_{k,n}\}$ (not only those corresponding to principal components) it can be easily shown that they can be expressed as [68]

$$\alpha_{k,n} = \alpha_{0,n-\ell} f(a_n, \ldots, a_{n-\ell+1})$$

for a suitable ℓ, where $f(\cdot)$ is a suitable (nonlinear) function. Since $\alpha_{0,n-\ell}$ is independent of future symbols $a_n, \ldots, a_{n-\ell+1}$, $E\{\alpha_{0,n}\} = 0$ is a sufficient condition for having $E\{\alpha_{k,n}\} = 0$, $\forall k$. Thus we have

$$\lim_{m\to\infty} R_{\alpha_k}(m) = |E\{\alpha_{k,n}\}|^2 = 0$$
$$\lim_{m\to\infty} R_{\alpha_{k_1},\alpha_{k_1}}(m) = E\{\alpha_{k_1,n}\}E\{\alpha^*_{k_2,n}\} = 0$$

and no impulses will be present in the resulting PSD.

We also evaluated the spectral efficiency (SE) of the proposed schemes. Our aim is to understand if the proposed precoded ternary schemes have a SE comparable with that of the classical binary schemes for a same frequency pulse, and thus a similar performance has to be expected when the proposed signals are employed in coded systems. The spectral efficiency η for the considered scheme was computed in the same manner as in the Chapter 2. We took $\rho = 99.9\%$ to define the bandwidth in (2.8).

4.4.5 Uncoded Performance

We remind that the probability of bit error for the optimal MAP sequence detector (implemented through the Viterbi algorithm) is well approximated by [33]

$$P_b \approx \frac{n_{\boldsymbol{e}_{min}} m_{\boldsymbol{e}_{min}}}{2^{R_{\boldsymbol{e}_{min}}}} \mathrm{Q}\left(\sqrt{d^2_{min} E_b/N_0}\right) \tag{4.10}$$

where the different parameters $d_{min}, e_{min}, m_{\boldsymbol{e}_{min}}, R_{\boldsymbol{e}_{min}}$ are described in section 2.5.2 of Chapter 2. Now, it only remains to identify the error events corresponding to d_{min} which is also explained in Chapter 1. We considered different modulation formats and computed the corresponding parameters $n_{\boldsymbol{e}_{min}}$, $m_{\boldsymbol{e}_{min}}$, $R_{\boldsymbol{e}_{min}}$, and d_{min}, for both the classical binary schemes and the proposed ones. We considered a modulation format with a rectangular phase pulse of length $L = 1$ (1REC) and $h = 1/2$, a modulation format with raised cosine frequency pulse of length $L = 2$ (2RC) and $h = 1/4$, and a Gaussian frequency pulse with normalized bandwidth $BT = 0.5$ truncated to a length $L = 2$ (2GFSK) and $h = 1/3$ [10]. The results are reported in Table 4.1. It can be observed that the proposed schemes do not modify the minimum distance and, at most, they modify the multiplicity of the error event by a factor 2. In particular, the 2nd proposed precoder provides the same asymptotic performance as the classical scheme except for $h = 1/2$, when the multiplicity is halved.

Table 4.1: Parameters for the computation of the asymptotic bit error probability for three different phase pulses and modulation indices.

		$\boldsymbol{e}_{min}$	$n_{\boldsymbol{e}_{min}}$	$m_{\boldsymbol{e}_{min}}$	d^2_{min}	P_b
1REC $h = 1/2$	classical	$(2, -2)$,$(2, 2)$	2	4	2	$2\mathrm{Q}\left(\sqrt{2\frac{E_b}{N_0}}\right)$
	AMI precod.	$(2, -2)$	2	4	2	$2\mathrm{Q}\left(\sqrt{2\frac{E_b}{N_0}}\right)$
	2nd precod.	$(2, -2)$	2	2	2	$\mathrm{Q}\left(\sqrt{2\frac{E_b}{N_0}}\right)$
2RC $h = 1/4$	classical	$(2, 0, -2)$	2	4	0.66	$\mathrm{Q}\left(\sqrt{0.66\frac{E_b}{N_0}}\right)$
	AMI precod.	$(2, 0, -2)$	2	8	0.66	$2\mathrm{Q}\left(\sqrt{0.66\frac{E_b}{N_0}}\right)$
	2nd precod.	$(2, 0, -2)$	2	4	0.66	$\mathrm{Q}\left(\sqrt{0.66\frac{E_b}{N_0}}\right)$
2GFSK $BT = 0.5$ $h = 1/3$	classical	$(2, 0, -2)$	2	4	1.06	$\mathrm{Q}\left(\sqrt{1.06\frac{E_b}{N_0}}\right)$
	AMI precod.	$(2, 0, -2)$	2	8	1.06	$2\mathrm{Q}\left(\sqrt{1.06\frac{E_b}{N_0}}\right)$
	2nd precod.	$(2, 0, -2)$	2	4	1.06	$\mathrm{Q}\left(\sqrt{1.06\frac{E_b}{N_0}}\right)$

4.4.6 Simulation Results

We first motivate the adoption of the proposed schemes by assessing their robustness in the case of a significant modulation index mismatch. We consider uncoded transmissions, both classical and proposed schemes, and the performance of the Viterbi-based receiver working on the principal components of the Laurent decomposition and designed on the nominal modulation index.

As a first example, we consider a case inspired by the Bluetooth standard, where the 2GFSK frequency pulse with $BT = 0.5$ is employed (third row of Table 4.1). We will consider both classical and proposed schemes. We will assume that the modulation index at the transmitter can vary from 0.3 to 0.37 and that the receiver is designed for a nominal value of $h_{rx} = 1/3$. No attempt is made at the receiver to compensate for the modulation index mismatch. The results are shown in Figure 4.4. It can be observed that, whereas for the classical binary CPM format a small value of the mismatch produces a large degradation, for the proposed schemes the degradation is very limited (at most 1 dB) in the considered range.

Similarly, in Figure 4.5 we consider the case of full response CPMs with REC and RC frequency pulses. In this case, the modulation index employed at the transmitter (h) and that at used to design the receiver (h_{rx}) are explicitly reported in the caption. The results confirm our intuition about the robustness of the proposed schemes that exhibit a negligible performance loss even when the mismatch is large.

The correctness of the proposed asymptotic analysis for uncoded transmissions is addressed in Figure 4.6, where the bit error rate (BER) performance, computed through simulations, for some of the modulation formats also considered in Table 4.1 is shown and compared with the asymptotic formulas reported in the table. In this case, there is no modulation index mismatch and the receivers considered in

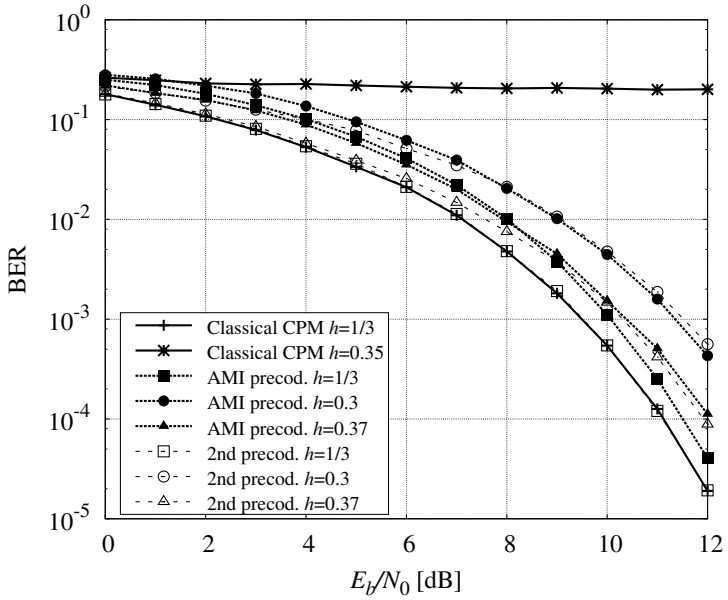

Figure 4.4: Robustness for the case of a 2GFSK frequency pulse with $BT = 0.5$.

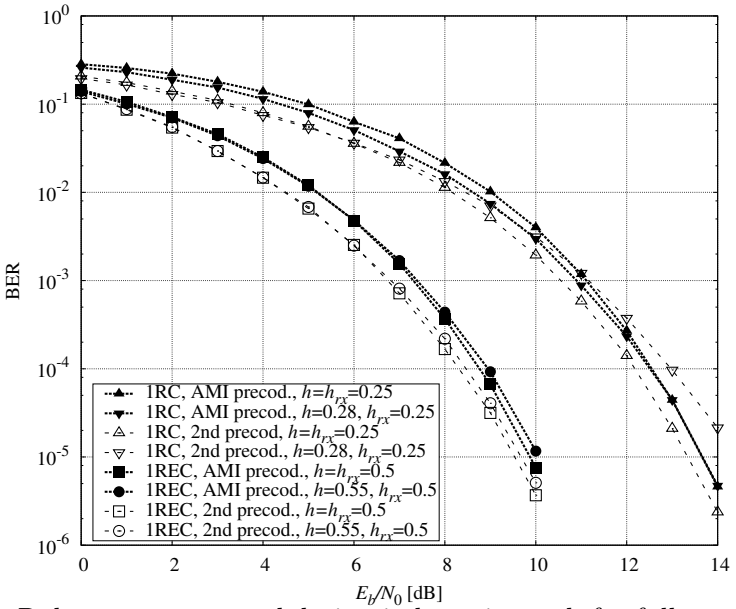

Figure 4.5: Robustness to a modulation index mismatch for full response CPMs.

the simulations are not the optimal ones but the simplified receivers based on the Laurent decomposition.

We now consider coded transmissions. In order to assess the ultimate performance limits of coded transmissions, we consider the spectral efficiency η as defined in (2.9) instead of the simple information rate, in order to also capture a possible bandwidth expansion caused by the considered precoders. In Figures 4.7 and 4.8 we report the results in case of employ of a 1REC or a 2RC frequency pulse, re-

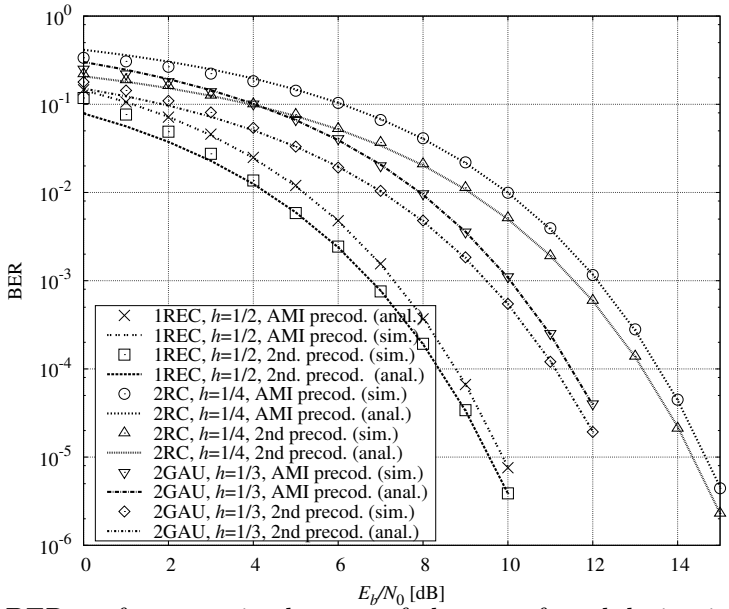

Figure 4.6: BER performance in the case of absence of modulation index mismatch (simulations and closed-form asymptotic expressions).

spectively, with different modulation indexes. The second proposed precoder has a spectral efficiency quite similar to that of classical binary CPMs. On the contrary, a significant spectral efficiency degradation is observed by using the AMI precoder. This is due to a bandwidth expansion related to the use of this precoder. This can be observed by looking at Table 4.2, where the values of 99.9%-bandwidth (defined as the bandwidth that contains 99.9% of the overall signal power) is reported for the modulation formats considered in Figures 4.5 and 4.6. If, from one side, the use of the second proposed precoder does not entail significant modifications in the bandwidth values with respect to the classical binary CPM with the same modulation index and frequency pulse, a significant bandwidth expansion is observed with the AMI precoder.

Table 4.2: 99.9%-bandwidth for some of the considered schemes.

	$B_{99.9\%}T$ for 1REC				$B_{99.9\%}T$ for 2RC			
h	1/7	1/6	2/9	1/8	2/7	1/6	1/5	1/7
Classical CPM	1.21	1.27	1.4	1.18	1.24	1.1	1.16	1.02
AMI precoder	1.51	1.8	2.2	1.39	1.76	1.32	1.43	1.24
2nd precoder	1.22	1.3	1.43	1.03	1.4	1.03	1.2	1.03

Finally, we considered BER simulations for a coded transmission system. We serially concatenated the proposed schemes with a binary convolutional encoder with generators $(7, 5)$ (octal notation) through a pseudo-random interleaver of length 1024 or 4096 bits. We used a 1REC frequency pulse with modulation index $h = 1/2$. We also report the performance related to the use, in the same concatenation, of a classi-

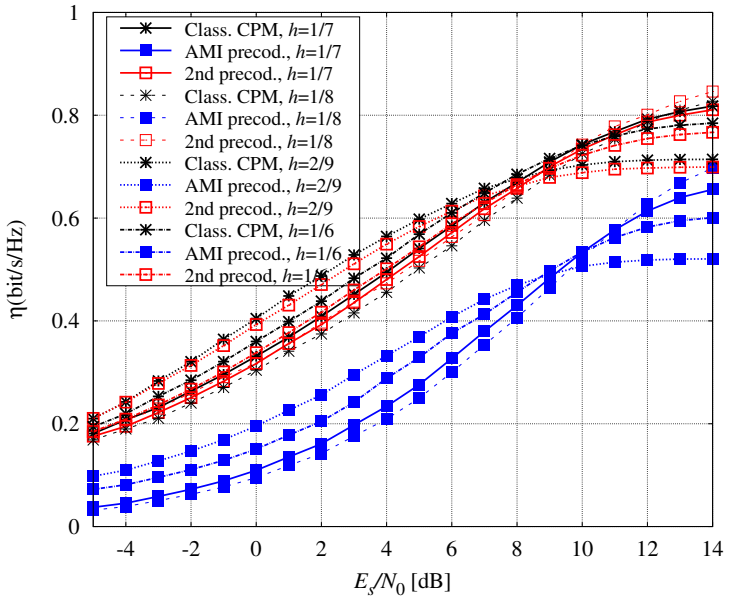

Figure 4.7: Spectral efficiency for 1REC modulations with different modulation indexes.

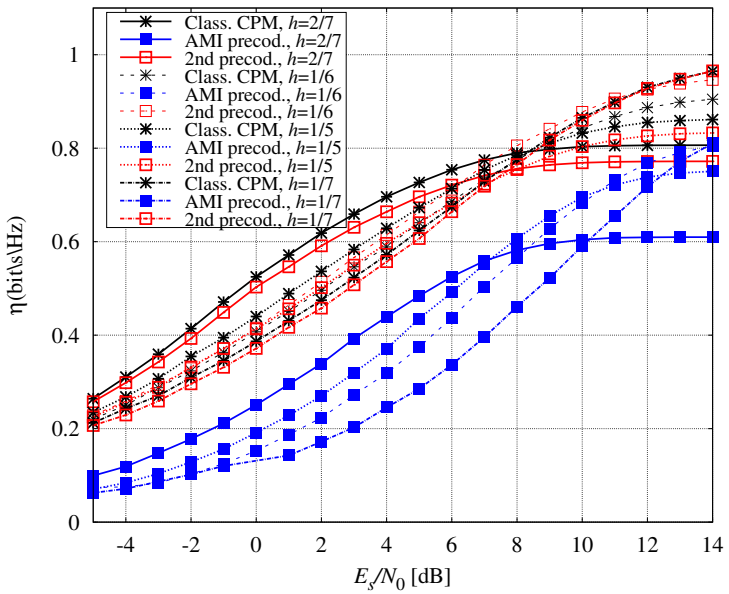

Figure 4.8: Spectral efficiency for 2RC modulations with different modulation indexes.

cal CPM scheme with the same frequency pulse and modulation index, corresponding to a minimum shift keying (MSK) modulation. For all considered schemes, a number of 16 iterations between detector and decoder is allowed. This figure demonstrates that the proposed schemes are suitable for such a kind of concatenation and an interleaver gain can be observed due to the preserved recursive nature of the

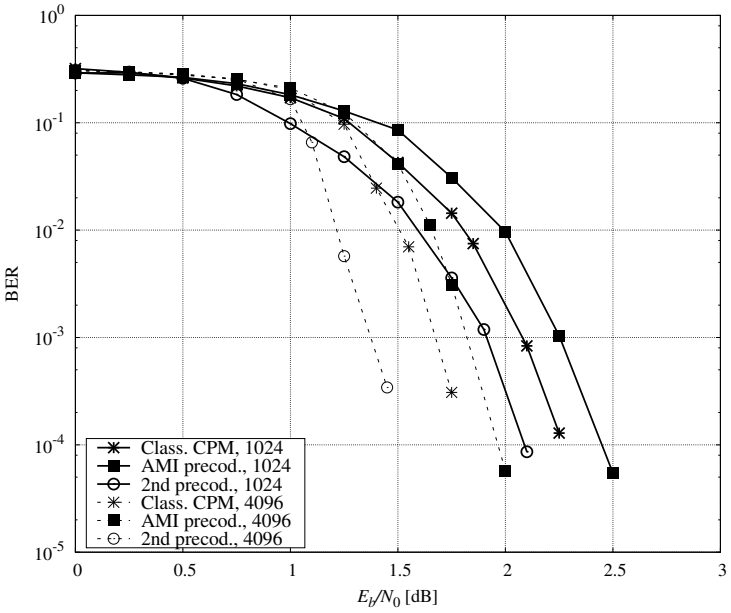

Figure 4.9: BER performance for a 1REC modulation with $h = 1/2$ serially concatenated with a convolutional encoder via a pseudo-random interleaver.

modulator.

4.5 Robust CPM Detection

In Section 4.4, we proposed new binary continuous-phase-modulated schemes for applications where low-cost transmitters are employed. The robustness issue was solved from the transmitter side. Now, we consider soft-output detection of a binary continuous phase modulation (CPM) generated through a low-cost transmitter, thus characterized by a significant modulation index uncertainty, and sent over a channel affected by phase noise. The proposed detector is designed by adopting a simplified representation of a binary CPM signal with the principal component of its Laurent decomposition and is obtained by using the framework based on factor graphs and the sum-product algorithm. It does not require an explicit estimation of the modulation index nor of the channel phase and is very robust to large uncertainties of the nominal value of the modulation index. Being soft-output in nature, this detector can be employed for iterative detection/decoding of practical bit interleaved coded CPM schemes.

4.5.1 Factor Graph and Sum Product Algorithm

Here, we describe some frameworks to be used in the remainder of this chapter. We briefly introduce particularly the FG/SPA tool, from the tutorial paper [26].

Let $x_1, x_2, ..., x_n$ a set of variables, where x_i takes its values on a finite domain denoted A_i , and let $g(x_1, x_2, ..., x_n)$ be a real multi-variable function.

Suppose that the marginal functions associated to $g(x_1, x_2, ..., x_n)$ have to be computed, defining the n functions $g_i(x_i)$ as

$$g_i(x_i) = \sum_{\sim\{x_i\}} g(x_1, x_2, ..., x_n), \tag{4.11}$$

where $\sim \{x_i\}$ indicate the *not-sum* operator [26], i.e., a sum over all variables except x_i .

The marginalization of a function is a common problem in many applications. Typically, detection issue needs the marginalization of eventually cumbersome function which depends on many variables. When the function can be expressed as the product of simpler functions, each of them depending on a subset of the variables, the marginalization can be less complex, when the function to be marginalized can be expressed as the product of simpler functions. Each function depends on a subset of variables, and so the marginalization proves to be less complex. The FGs produce a graphical description about the factorization of the "global" function into a product of many "local" functions. The SPA applied on this FG, computes either exactly or approximately the derived marginal functions from the global function.

Let us assume that $g(x_1, x_2, ..., x_n)$ can be factorized into a product of several local functions f_j, each function is defined on a subset X_j of $\{x_1, x_2, ..., x_n\}$ as argument, i.e

$$g(x_1, x_2, ..., x_n) = \prod_{j \in \boldsymbol{J}} f_j(X_j), \tag{4.12}$$

where $\boldsymbol{J}$ denotes a discrete index set. The FG of the *global* function g is a bipartite graph composed by a factor node for each function f_j, and a variable node for each variable x_i, and an edge connecting the variable node x_i with the function node f_j if and only if x_i is an argument of f_j. The SPA is a sort of message-passing algorithm operating over a FG. It evaluates the *messages* at the nodes of the bipartite graph and exchanges them along the edges. It's shown in [26] that when the FG is acyclic (it leads to have a tree representation for each variable node), the SPA accomplishes the exact marginalization of the *global* function represented by the FG. We denote by $\mu_{x\to f}(x)$ the message sent from the variable node x to the factor node f, and by $\mu_{f\to x}(x)$ the opposite direction message. The messages computed at the variable and factor node are respectively:

$$\begin{aligned} \mu_{x\to f}(x) &= \prod_{h \in n(x) \setminus f} \mu_{h\to x}(x) \\ \mu_{f\to x}(x) &= \sum_{\sim\{x\}} \left[f(X) \prod_{y \in n(f)\setminus\{x\}} \mu_{y\to f}(y) \right], \end{aligned} \tag{4.13}$$

$n(x)$ represents the set of functions f having as argument x, and $X = n(f)$ represents the set of arguments of the function f. When the graph is cycle-free,

its representation has the form of a tree and the SPA begins the evaluation of the messages from the leaf nodes. If the leaf is a variable node, it transmits to its neighbor nodes corresponding to a factor node, the identity message $\mu_{x\to f}(x)$. The other nodes are activated when receiving the messages from their incident edges, then, each one sends a message to the remaining edge. When two messages in opposite direction, have been passed over every edge, the SPA finishes and the marginal functions can be computed as

$$g_i(x_i) = \prod_{f\in n(x_i)} \mu_{f\to x_i}(x_i), \tag{4.14}$$

Even if the underlying FG has cycles, the SPA can be also used, leading to an iterative algorithm. In such case, the convergence to the exact marginalization is not ensured, and depends on the adopted schedule (an order of messages evaluation) and on the structure of the considered graph. There are several graphical techniques described in [26] to remove the cycles in the graph, at the price of an increase in the complexity of the SPA algorithm. Nevertheless, for several relevant problems characterized by FGs with cycles, the SPA tries to provide good convergence properties and a valuable alternative to the exact solution, with an excellent performance/complexity trade-off.

4.5.2 Proposed Receiver

h_e is assumed unknown and modeled as a random variable with known distribution. We consider transmission over an additive white Gaussian noise (AWGN) channel possibly affected by phase noise. The complex envelope of the received signal thus reads

$$r(t) = e^{j\theta(t)} s(t, \boldsymbol{a}, h_{rx} + h_e) + w(t) \tag{4.15}$$

where $w(t)$ is a complex-valued white Gaussian noise process with independent components, each with two-sided power spectral density N_0, and $\theta(t)$ is the phase noise introduced by the channel, modeled as a continuous-time Wiener process with incremental variance over a signaling interval equal to σ_Δ^2.

Approximating the useful signal through its principal component only and exploiting the feature that the pulse of the principal component weakly depends on the modulation index, we can express the received signal as

$$r(t) \backsimeq e^{j\theta(t)} \sum_n \alpha_{0,n}^{(h_{rx})} \alpha_{0,n}^{(h_e)} \hat{p}_0(t - nT) + w(t), \tag{4.16}$$

where we denoted by $\hat{p}_0(t)$ the pulse of the principal component for the nominal value of the modulation index (h_{rx}) and having exploited the property, easily derived from (4.2), that symbol $\alpha_{0,n}$ related to the transmitted signal can be expressed as the product of symbol $\alpha_{0,n}^{(h_{rx})}$ corresponding to the nominal CPM signal and symbol $\alpha_{0,n}^{(h_e)}$ corresponding to a CPM signal with modulation index h_e.

Under the assumption that the channel phase $\theta(t)$ is slowly varying such that it can be considered constant over the duration of pulse $\hat{p}_0(t)$, an approximate sufficient statistic may be obtained through a filter matched to pulse $\hat{p}_0(t)$. We will define

$$x_n = \int_{-\infty}^{+\infty} r(t)\hat{p}_0(t - nT)\, dt \tag{4.17}$$

as the output, sampled at time nT, of the filter matched to $\hat{p}_0(t)$. Defining also $\theta_n = \theta(t)|_{nT}$, $\phi_n = \arg[\alpha_{0,n}^{(h_{rx})}]$, $\delta_n = \arg[\alpha_{0,n}^{(h_e)}]$, and $\psi_n = \theta_n + \phi_n + \delta_n$, collecting the samples of ψ_n into a vector $\boldsymbol{\psi}$, and representing the received signal onto an orthonormal basis and denoting by $\boldsymbol{r}$ its vector representation, we can express, exploiting the constant envelope property of any CPM signal, [69]

$$p(\boldsymbol{r}|\boldsymbol{\psi}) \,\widetilde{\propto}\, \prod_n G_n(\psi_n) \tag{4.18}$$

with

$$G_n(\psi_n) = \exp\left\{\frac{1}{N_0}\mathrm{Re}[x_n e^{-j\psi_n}]\right\}. \tag{4.19}$$

Samples θ_n satisfy the discrete-time Wiener model

$$\theta_n = \theta_{n-1} + \Delta_n \tag{4.20}$$

where $\{\Delta_n\}$ are real, independent, and identically distributed Gaussian random variables, with mean zero and variance σ_Δ^2, and θ_0 is assumed uniformly distributed in $[0, 2\pi)$. The stochastic model for h_e depends on the considered standard. As an example, in the case of Bluetooth BR [20] h_e follows a uniform distribution in the interval $[0.28 - h_{rx}, 0.35 - h_{rx}]$, whereas in the case of the AIS standard [72], it follows a Gaussian distribution with mean $0.5 - h_{rx}$ and variance $\sigma_{h_e}^2$ [70].

We can thus write

$$\begin{aligned}\psi_n &= \theta_n + \phi_n + \delta_n \\ &= \theta_{n-1} + \Delta_n + \phi_{n-1} + \pi h_{rx} a_n + \delta_{n-1} + \pi h_e a_n \\ &= \psi_{n-1} + \Delta_n + \pi h_{rx} a_n + \pi h_e a_n\,.\end{aligned} \tag{4.21}$$

Assuming that h_e has mean zero (this is always possible by properly choosing h_{rx}) and an even probability density function (pdf), given a_n the random variable $\pi h_e a_n$ is statistically equivalent to πh_e. We may thus write

$$\begin{aligned}p(\boldsymbol{\psi}|\boldsymbol{a}) &= \prod_n p(\psi_n|\psi_{n-1}, a_n) \\ &= \prod_n H_n(a_n, \psi_{n-1}, \psi_n)\end{aligned} \tag{4.22}$$

where

$$H_n(a_n, \psi_{n-1}, \psi_n) = f(\psi_n - \psi_{n-1} - \pi h_{rx} a_n) \tag{4.23}$$

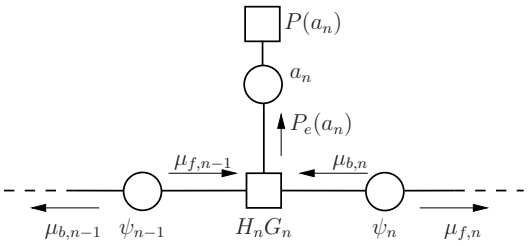

Figure 4.10: Portion of the FG corresponding to equation (4.25).

$f(y_n)$ being the pdf of the random variable $y_n = \Delta_n + \pi h_e$ that can be easily computed from the a-priori information available at the receiver (i.e., the distributions of Δ_n and h_e and the fact that they are independent). As an example, when h_e has uniform distribution in $[-\varepsilon, \varepsilon]$, we have

$$f(y_n) = \frac{1}{2\pi\varepsilon}\left[\mathrm{Q}\Big(\frac{y_n - \pi\varepsilon}{\sigma_\Delta}\Big) - \mathrm{Q}\Big(\frac{y_n + \pi\varepsilon}{\sigma_\Delta}\Big)\right] \tag{4.24}$$

We are now ready to derive the optimal MAP symbol detection strategy. The a-posteriori joint distribution of vectors $\boldsymbol{a}$ and $\boldsymbol{\psi}$ can be expressed as

$$\begin{aligned} p(\boldsymbol{a}, \boldsymbol{\psi}|\boldsymbol{r}) &\propto p(\boldsymbol{r}|\boldsymbol{\psi}) p(\boldsymbol{\psi}|\boldsymbol{a}) P(\boldsymbol{a}) \\ &= \prod_n G_n(\psi_n) H_n(a_n, \psi_{n-1}, \psi_n) P(a_n)\,. \end{aligned} \tag{4.25}$$

This joint distribution can be represented through a FG. One section of it is shown in Figure 4.10.

We can observe that it is cycle-free. Hence, the application of the SPA with a non-iterative forward-backward schedule, produces the exact marginal a-posteriori probabilities (APPs) of symbol a_n (except for the approximation related to the use of the principal components only). With reference to the messages in the figure, by applying the updating rules of the SPA, messages $\mu_{f,n}(\psi_n)$ and $\mu_{b,n}(\psi_n)$ can be recursively computed by means of the following forward and backward recursions:

$$\begin{aligned} \mu_{f,n}(\psi_n) = \sum_{a_n} P(a_n) \int \mu_{f,n-1}(\psi_{n-1}) H_n(a_n, \psi_{n-1}, \psi_n) \\ \cdot G_n(\psi_n)\, d\psi_{n-1} \end{aligned} \tag{4.26}$$

$$\begin{aligned} \mu_{b,n-1}(\psi_{n-1}) = \sum_{a_n} P(a_n) \int \mu_{b,n}(\psi_n) H_n(a_n, \psi_{n-1}, \psi_n) \\ \cdot G_n(\psi_n)\, d\psi_n \end{aligned} \tag{4.27}$$

The extrinsic APPs of bits $\{a_n\}$, i.e., $P_e(a_n) = P(a_n \boldsymbol{r})/P(a_n)$ can be finally computed as

$$\begin{aligned} P_e(a_n) = \iint \mu_{f,n-1}(\psi_{n-1}) \mu_{b,n}(\psi_n) \\ \cdot H_n(a_n, \psi_{n-1}, \psi_n) G_n(\psi_n)\, d\psi_{n-1} d\psi_n \end{aligned} \tag{4.28}$$

This strategy involves integration and computation of continuous pdfs, and it is not suited for direct implementation. A solution to this problem consists in the use of canonical distributions, i.e., the pdfs $\mu_{f,n}(\psi_n)$ and $\mu_{b,n}(\psi_n)$ computed by the algorithm are constrained to be in a certain "canonical" family, characterized by some parametrization. Hence, the forward and backward recursions reduce to propagating and updating the parameters of the pdf rather than the pdf itself. A very straightforward solution to implement (4.26)-(4.28) is obtained by discretizing the channel phase [69]. In this way, the pdfs $\mu_{f,n}(\psi_n)$ and $\mu_{b,n}(\psi_n)$ become probability mass functions (pmfs) and the integrals in (4.26)-(4.28) become summations. When the number D of discretization levels is large enough, the resulting algorithm becomes optimal (in the sense that its performance approaches that of the exact algorithm).

4.6 Simulation Results

The performance of the proposed detector is assessed by computer simulations in terms of bit error rate (BER) versus E_b/N_0, E_b being the received signal energy per information bit. In all cases we used a value $D = 20$. No performance improvement has been observed with a larger value of D.

We first consider an uncoded binary transmission using the GFSK format described in the Bluetooth standard in BR mode. In this case, the modulation index can take its value in the interval $[0.28, 0.35]$, randomly, but we will assume that $h = 0.28$. At the receiver side, for the proposed detector we considered both cases of $h_{rx} = 0.3$ and $h_{rx} = 1/3$. In Figure 4.11, we compare the performance of the proposed algorithm with that of the noncoherent detector in [56]. In this latter case, the modulation index is estimated using an estimation period of $N_e = 50$ symbols and parameters α and β described in [56] have been optimized by simulations. The BER performance is compared for different values of phase noise standard deviation σ_Δ. We can observe that the proposed algorithm performs better than that in [56] and, when the value of σ_Δ is low, it performs quite close to the receiver which perfectly knows the modulation index and the channel phase (also shown in the figure).

We now consider the serial concatenation, through a pseudo-random interleaver of length 2048 bits, of a binary convolutional encoder with generators $(7, 5)$ (octal notation), and a binary CPFSK modulation with an irrational transmission modulation index of $h = \frac{\pi}{5}$. In this case, we compare, for different values of the phase noise standard deviation, the performance of the detection algorithm here proposed when assuming $h_{rx} = 5/8$, with that of the algorithm [73] which assumes a perfect knowledge of the channel phase and the modulation index. When the modulation index is irrational, a trellis description is not possible and thus we have no performance reference. For this reason, we also considered the performance of the optimal detector when $h = h_{rx} = \frac{5}{8}$ (a value very close to the considered irrational modulation index) and the channel phase is perfectly known at the receiver. For all considered receivers, a number of 12 iterations between detector and decoder is al-

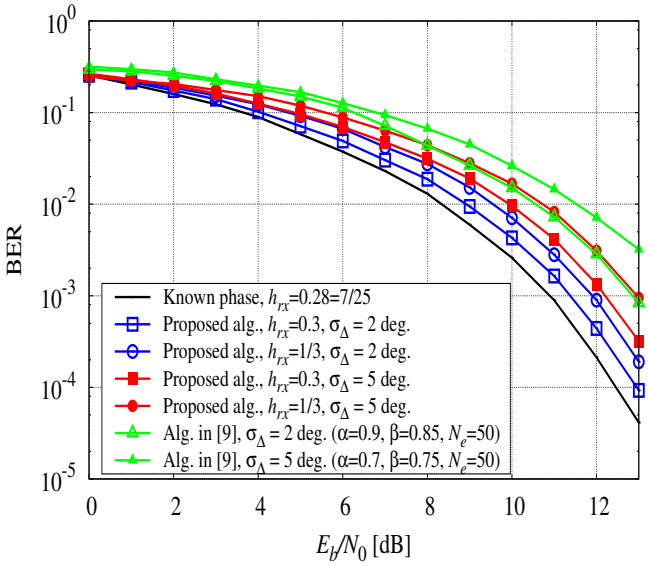

Figure 4.11: Bluetooth (BR) detection in the presence of phase noise with standard deviation equal to 2 and 5 degrees, $h = 0.28$.

lowed. One may observe that the performance of the proposed algorithm is very close to that in [73] although this latter receiver has a perfect knowledge of h and the channel phase. The proposed algorithm is thus able to perform detection even when the modulation index is irrational and not perfectly known and when there is a significant phase noise.

4.7 Conclusions

In this chapter, the robustness issue was solved from the transmitter and the receiver sides separately. Firstly, we proposed new precoded continuous-phase-modulated schemes based on the concatenation of a proper precoder with binary input and a ternary CPM format as in chapter 2. However in chapter 2 we focused on the spectral efficiency improvement while here we aimed at making the transmission robust to modulation index mismatch. The result is a family of CPMs formats whose phase state is constrained to follow a specific evolution. Two of these precoders are considered. The overall scheme resulting from the adoption of the first precoder-based on the AMI principle that has only two states, independently of the adopted modulation index. The second precoder generates an overall scheme with a number of states which depends on the modulation index denominator and avoids the presence of impulses in the power spectral density. If not properly taken into account at the receiver through the use of techniques for estimation and compensation, a modulation index mismatch can severely degrade the performance of classic schemes. The proposed precoded schemes are, instead, almost insensitive to this mismatch.

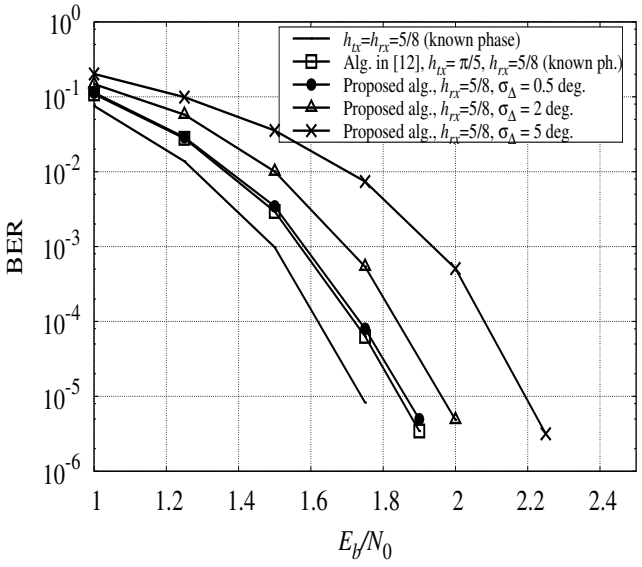

Figure 4.12: BER Performance of a binary CPFSK modulation serially concatenated with CC(7,5) via a pseudo-random interleaver of length 2048, with irrational modulation index $\frac{\pi}{5}$ in the presence of phase noise with standard deviation σ_Δ.

Secondly, we derived a robust soft-output detector for binary CPM signals. The proposed algorithm was derived based on the Laurent representation of a CPM signal where only the principal component was considered. Detection in the presence of an unknown modulation index and a time-varying phase noise was performed based on the sum-product algorithm working on a properly defined factor graph. We observed a high robustness of the proposed receiver towards modulation index mismatch and phase noise.

In this chapter we addressed the problem of robustness to modulation index mismatch and phase noise in the case of simple-user low-cost transmitter systems. In the next chapter we generalize the issue to multi-user systems and we extend the schemes proposed in this chapter.

Chapter 5

Robust CPM-based Multi-user Systems

Contents

5.1 Introduction

In this chapter, we address the robustness problem in a CPM-based multi-user system. Each user's binary CPM signal is generated through a low-cost transmitter, which may lead to a modulation index error.

Firstly, we tackle the robustness issue from the transmitter side. A new multiple access technique based on CPM is derived. We propose, a multi-user communication system with the same bandwidth as a single user system which allows a significant increase in the spectral efficiency. The proposed CPM-based multiuser scheme resorts to the concatenation of an AMI precoder with a ternary CPM per user followed by a multiuser separation device based on a phase rotation. Thus a robust CPM-based system for synchronous users is obtained.

[0]M. Messai, F. Guilloud, K. Amis, and G.Colavolpe, "Robust Multiuser Binary CPM Detection with Unkown modulation index", *Proc. European Signal Processing Conf., 2015.*

Secondly, we address the robustness issue from the receiver side. The Factor Graph and Sum Product algorithm framework is used in a double way. In addition to its use for the derivation of an efficient multi-user receiver with reduced complexity [74], it is also used to perform detection in the presence of unkown modulation index[1] and of a time varying phase noise as studied for single user transmission in Chapter 4. The resulting robust multi-user detector is referred to as "*robust* FG-MUD". In brief, we derive a robust multiuser binary CPM detector for frequency-division-multiplexed FDM-CPM systems where the spectral efficiency (SE) of FDM systems can be increased by reducing the spacing between adjacent users [11]. The proposed algorithm is derived based on the Laurent representation of a CPM signal where only the principal component is considered.

5.2 Literature Review on Multi-user CPM systems

Personal communications have been increasing throughout the world over the past two decades, making critical the design of efficient multiuser systems. In this section, we discuss some interesting work on CPM-based multi-user systems. In [75], the authors have derived a reduced complexity multiuser detection algorithm for GMSK signals transmitted through a common channel. The reduced complexity maximum a posteriori (MAP) coherent detector for the transmitted bits is derived by approximating each CPM signal by its primary Laurent component.

In [76], [29] a multiuser serially-concatenated-continuous-phase-modulation (SC-CPM) was developed using a carrier frequency offset between the users. Consequently, with an iterative decoder it was shown that the power/bandwidth efficiencies are better than for single-user SC-CPM system. Then, a separation between users was made in [77, 78, 79] by introducing a phase offset separation in addition to the carrier frequency offset. This algorithm assumes the absence of carrier offset and can be applied only for MSK-type modulations ($h = \frac{1}{2}$ and $L = 1$) with a few number of users.

In [80], a CPM-based spread-spectrum system for multi-user communications was proposed. PSD smoothness was obtained using multi-h CPM modulation with a long enough sequence of modulation indices. It was pointed out that it is possible to set the spectral spreading of the CPM signal by considering the highest value of modulation index. The separation between users was reached by associating to each multi-h CPM user a sequence of modulation indices thus defining a new multiple-access technique.

Using the FG and SPA frameworks, a reduced-complexity multiuser detection algorithm for a frequency division multiplexed (FDM) system was derived in [74]. This FDM system uses continuous phase modulation in serially concatenated schemes. The algorithm proposed in [74] allows to effectively reduce the frequency spacing between adjacent users and thus increasing the spectral efficiency with an effective

[1] The modulation index error generated by the k-th low cost transmitter $h_e^{(k)}$ is assumed unkown and modeled as a random variable with known distribution.

compromise in terms of performance and computational complexity. In [81], the FG and SPA frameworks were used to design a new approximate MU detection algorithm. In this algorithm, the approximation of a suitable set of sum-product messages by a Gaussian distribution allows to significantly reduce the memory size requirements and computational complexity as compared to a straightforward application of the sum-product rules. The described algorithm achieves a good error performance.

5.3 Robust multiple-access technique based on synchronous AMI precoded ternary CPM

5.3.1 Multiuser System based on phase-shifted AMI precoded ternary CPM

We recall that the information-carrying phase of a binary CPM during the n-th time interval, $t \in [nT, (n+1)T]$, can be written according to the Rimoldi decomposition [12] as:

$$\begin{aligned} \phi(t, h, \boldsymbol{b}) &= 4\pi h \sum_{i=0}^{n} b_i q(t - iT), \\ &= 2\pi h \sum_{i=0}^{n-L} b_i + 4\pi h \sum_{i=n-L+1}^{n} b_i q(t - iT), \\ &= \phi_{h,n} + \phi_{h,n}(t). \end{aligned} \tag{5.1}$$

In the binary CPM case the phase state $\phi_{h,n}$ takes on p values. For example if $h = 3/8$, $\phi_{h,n} \in \{0, \frac{\pi}{4}, \frac{\pi}{2}, \frac{3\pi}{4}, \pi, \frac{5\pi}{4}, \frac{6\pi}{4}, \frac{7\pi}{4}\}$. Therefore the detection of the sum of two or more CPM signals becomes quickly too complex, all the more as p is high.

We have seen in Chapter 4 that the concatenation of a ternary CPM modulator with an AMI precoder reduces the phase state number to two, that is to say $\theta_n \in \{0, 2\pi h\}$. Thus, based on the fact that the phase state takes only two values instead of p, a multiple access technique is obtained by shifting each user's AMI precoded CPM signal with a carrier phase ψ_k. The signal model is a K-user CPM system where all users share a common carrier frequency and symbol period. The common carrier frequency assumption makes it possible to consider the sum of K complex baseband CPM signals transmitted simultaneously in the same frequency bandwidth:

$$\begin{aligned} S(t, \boldsymbol{A}) &= \sum_{k=1}^{K} e^{j\psi_k} s^{(k)}(t, h^{(k)}, \boldsymbol{a}^{(k)}) \\ &= \sum_{k=1}^{K} e^{j\psi_k} \sqrt{\frac{E_b^{(k)}}{T}} e^{j\phi(t, h^{(k)}, \boldsymbol{a}^{(k)})}, \end{aligned} \tag{5.2}$$

where ψ_k is the shifted phase of the k-th signal, T is the common symbol period shared by the K users and $E_b^{(k)}$ is the energy per bit of the k-th user. We assume that

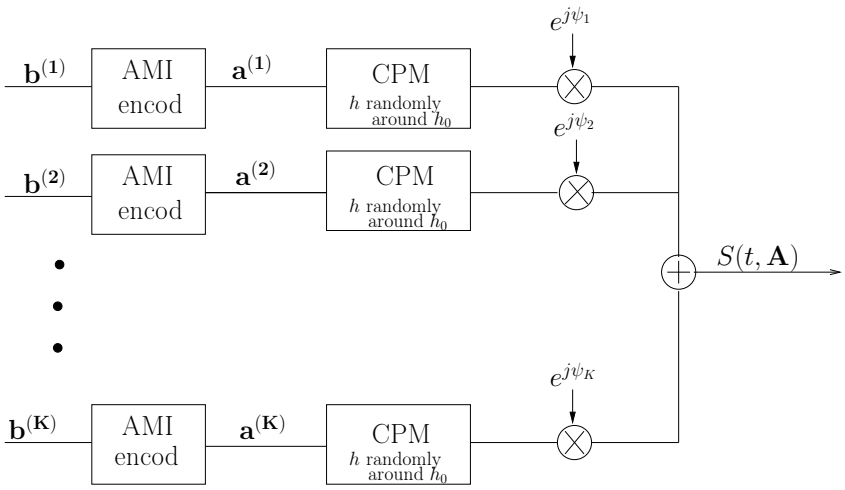

Figure 5.1: Multi-users System Model

the users have the same energy per bit that is to say $E_b^{(k)} = E_b$. $h^{(k)}$ takes its value randomly around a nominal value h_0 i.e $h^{(k)} = h_0 + h_e^{(k)}$ where the modulation index error of the k-th user $h_e^{(k)}$ follows a uniform distribution in the interval $[-\varepsilon, \varepsilon]$. ($h_e^{(k')}$ and $h_e^{(k)}$ are assumed independent for $k' \neq k$). The sequence of symbols transmitted by the k-th user is the AMI encoder output $\boldsymbol{a}^{(k)} = [a_k(0), a_k(1), ..., a_k(N-1)]$ with $a_k(i)$ being the i-th symbol from the k-th user, whose value is drawn from the set $\{0, \pm 1\}$ [2]. The KxN matrix of transmitted symbols $\boldsymbol{A}$ in (5.2) is $\boldsymbol{A} = [\boldsymbol{a}^{(1)^T}, \boldsymbol{a}^{(2)^T}, ..., \boldsymbol{a}^{(K)^T}]$. The transmitted system model is shown in Figure 5.1.

5.3.2 Corresponding Multi-user Joint Detector

In this section, we discuss the MLSE joint detector for CPM signaling, based on the signal model in (5.2). The receiver consists of K sets of front-end matched filters followed by a Viterbi algorithm. The complexity of the implementation can be significantly reduced by approximating each ternary signal by the two main pulses of its PAM decomposition [68] as done in chapter 4. Thus the multi-user low complexity receiver would have only 4^K states. In this study we focus on the scheme feasibility and consider the optimum multiuser receiver which simultaneously detect the K user signals (join detection). The received signal reads

$$r(t) = S(t, \boldsymbol{A}) + w(t), \tag{5.3}$$

The MAP detector of $\boldsymbol{A}$ searches $\hat{\boldsymbol{A}}$ such that

$$\hat{A} = \underset{\boldsymbol{A}}{\operatorname{argmax}} \; P(\boldsymbol{A}|r(t)) \tag{5.4}$$

[2]For ternary CPM, the use of $\{0, \pm 1\}$ data alphabet with the tilted phase is equivalent to the use of $\{0, \pm 2\}$ with the classic phase format

which is equivalent to

$$\begin{aligned}\hat{A} &= \underset{\boldsymbol{A}}{\operatorname{argmin}}\{\int_{-\infty}^{+\infty}|r(t)-S(t,\boldsymbol{A})|^2dt\}\\ &= \underset{\boldsymbol{A}}{\operatorname{argmax}}\ \{\ 2\Re\{\int_{-\infty}^{+\infty}\{r(t)S(t,\boldsymbol{A})^*dt\}-\int_{-\infty}^{+\infty}|S(t,\boldsymbol{A})|^2dt\}\end{aligned} \tag{5.5}$$

By expanding the last term in (5.5) we obtain

$$\int_{-\infty}^{+\infty}|S(t,\boldsymbol{A})|^2dt=\int_{-\infty}^{+\infty}|\sum_{k=1}^{K}e^{j\psi_k}s^{(k)}(t,h^{(k)},\boldsymbol{a}^{(k)})|^2dt \tag{5.6}$$

and then,

$$\begin{aligned}\int_{-\infty}^{+\infty}|S(t,\boldsymbol{A})|^2dt=\int_{-\infty}^{+\infty}2\Re\{\sum_{k_1=1}^{K}\sum_{k_2=1}^{k_1-1}e^{j\psi_{k_1}}e^{-j\psi_{k_2}}s_{k_1}(t,h^{(k_1)},\boldsymbol{a}^{(k_1)})\\ s_{k_2}(t,h^{(k_2)},\boldsymbol{a}^{(k_2)})^*dt\}+\int_{-\infty}^{+\infty}\sum_{k_1=1}^{K}|s_{k_1}(t,h^{(k_1)},\boldsymbol{a}^{(k_1)})|^2dt\end{aligned} \tag{5.7}$$

As each signal $s_{k_1}(t,h^{(k_1)},\boldsymbol{a}^{(k_1)})$ has a constant modulus, the last term is a constant. Therefore the MAP estimate of A can be written as

$$\hat{A}=\underset{\boldsymbol{A}}{\operatorname{argmax}}\ \Re\Bigg\{\int_{-\infty}^{+\infty}r(t)S(t,\boldsymbol{A})^*dt-\int_{-\infty}^{+\infty}\sum_{k_1=1}^{K}\sum_{k_2=1}^{k_1-1}e^{j\psi_{k_1}}e^{-j\psi_{k_2}}s_{k_1}(t,h^{(k_1)},\boldsymbol{a}^{(k_1)}) \tag{5.8}$$

$$s_{k_2}(t,h^{(k_2)},\boldsymbol{a}^{(k_2)})^*dt\Bigg\} \tag{5.9}$$

5.3.3 Simulations Results

The BER performance of the uncoded case is shown in Figure 5.2 from one to 5 users, where the shifted phases are chosen as shown in Table 5.1. The value of ψ_k have been set empirically and a theoretical optimization could be done but here our goal is to show the feasibility of the proposed scheme. All users have the same modulation format which is $1RC$ with the nominal modulation index $h_0 = 3/8$. $h^{(k)}$ follows a uniform distribution in the interval $[h_0-0.05, h_0+0.05]$. The performance criterion is the BER averaged over all users.

The performance degradation from 1 to 2 users is negligible. For two users, the quasi-orthogonality between the signals is mainly due to the accumulated phase caused by the modulation index mismatch. We can also note that the performance loss between k and $k+1$ users is not constant. For instance at BER $= 10^{-4}$, the degradation between 2 and 3 users is around 3 dB while between 3 and 4 users it is about 2 dB. It's seen also that there is no error floor as the user number increases and this may be related to the use of an optimal multiuser detector.

The coded case is shown in Figure 5.4. Each AMI precoded CPM is concatenated with a rate-1/2 CC(7,5). All users employ a pseudo-random interleaver of length 4092 bits, (16 iterations were used).

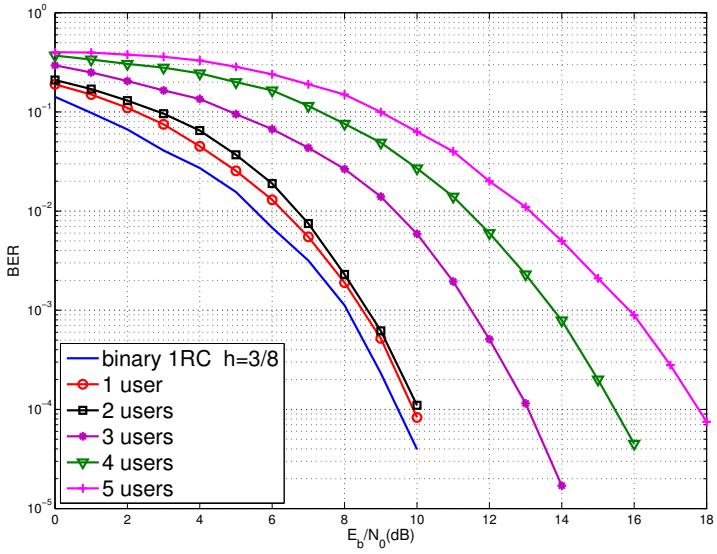

Figure 5.2: BER performance of the uncoded case, all the users have the same modulation $1RC$ and the same nominal modulation index $h_0 = 3/8$

	ψ_1	ψ_2	ψ_3	ψ_4
$K=2$	$\frac{3\pi}{8}$	-	-	-
$K=3$	$\frac{\pi}{4}$	$\frac{\pi}{2}$	-	-
$K=4$	$\frac{3\pi}{16}$	$\frac{3\pi}{8}$	$\frac{9\pi}{16}$	-
$K=5$	$\frac{3\pi}{20}$	$\frac{6\pi}{20}$	$\frac{9\pi}{20}$	$\frac{12\pi}{20}$

Table 5.1: Phase shifted ψ_k for each user chosen such that $\psi_k = k\frac{\frac{3\pi}{4}}{K}$, all users have the same modulation format $1RC$ with $h_0 = 3/8$.

5.3.4 Summary

In Section 5.3, we proposed a robust multiuser system based on AMI precoded ternary CPM user signals separated thanks to a phase shift. Our aim was to demonstrate the feasibility of such a scheme and its optimization through the choice of $\{\psi_k\}$ remains to be done as well as its theoretical evaluation (the maximum user number). Let us remark that such a technique can be combined with the FDM-CPM scheme studied in next section.

5.4 Robust FG-based detection for FDM-CPM systems

In frequency division multiplexed (FDM) systems, the spectral efficiency (SE) can be increased by reducing the spacing between adjacent users, thus allowing overlap in frequency and hence admitting a certain amount of interference. This aspect has been investigated in [11] from an information-theoretic point of view for continuous

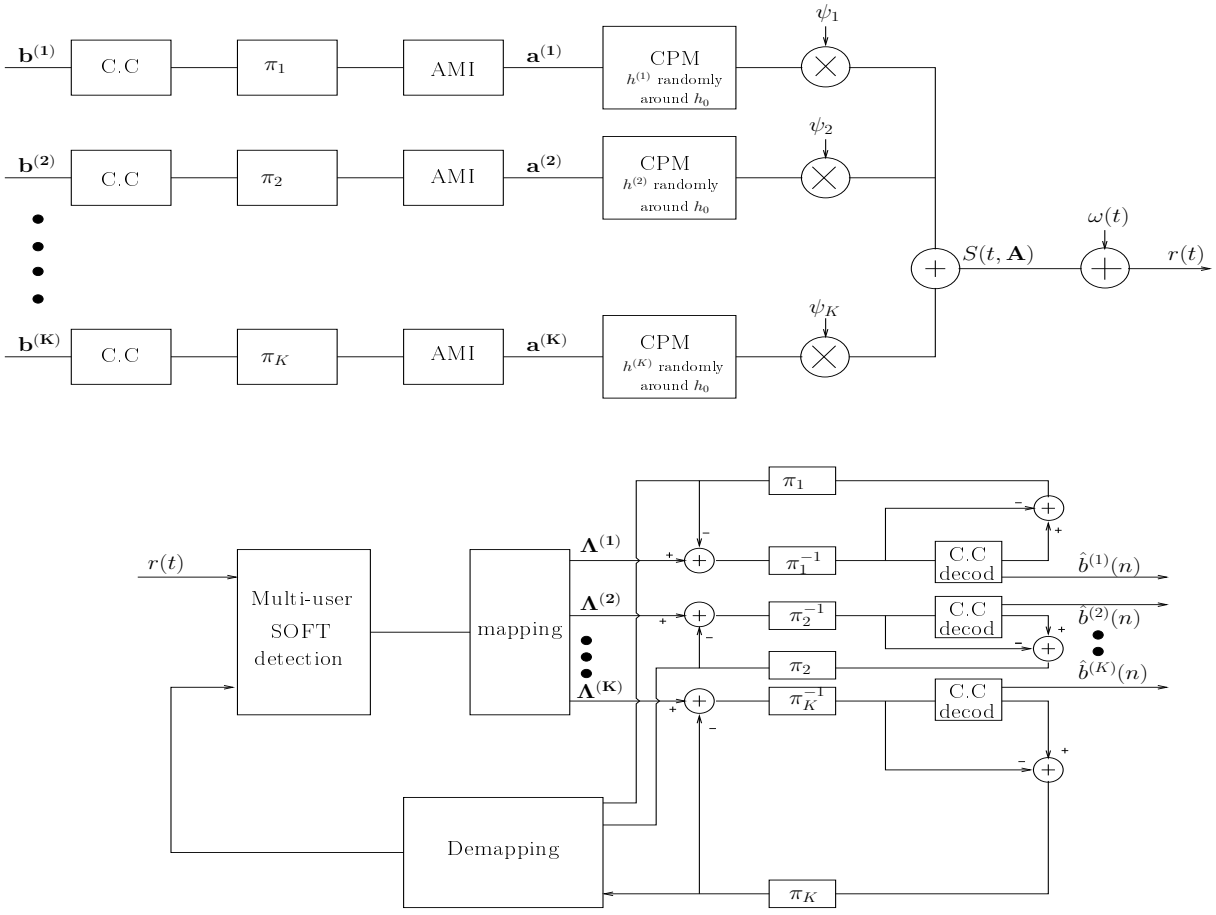

Figure 5.3: Multi-users serial concatenated system

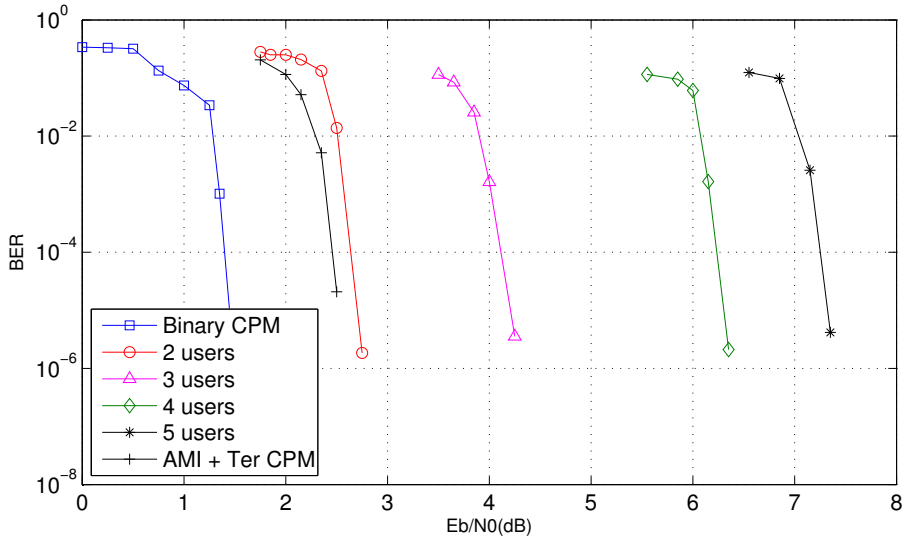

Figure 5.4: Serial concatenated multi-users with CC (7,5) and a pseudo random interleaver with length 4096 for 1RC modulation with $h = 3/8$

phase modulations (CPMs), showing that a significant improvement can be obtained even for a single-user detector. The benefits in terms of spectral efficiency can be even larger when a multiuser receiver is adopted that is to say when the multi-user interference is taken into account. Optimal multiuser detectors have a complexity which increases exponentially with the number of users, therefore suboptimal detection schemes are required. Recently a reduced-complexity MUD algorithm for an additive white Gaussian noise (AWGN) channel has been derived in [74] based on factor graphs (FGs) and the sum-product algorithm (SPA) [26]. The algorithm designed in [74] outperforms all other suboptimal MUD algorithms both from performance and complexity points of view. In this section we adapt the MUD detection proposed in [74] so as to make it robust to modulation index uncertainties and phase noise.

5.4.1 System Model

We consider a synchronous K-user CPM system in which all users share the same modulation format and transmit at the same power. The extension to the case of asynchronous users, possibly with different powers and modulation formats can be pursued as described in [74]. We assume that each user transmits N information bits and we denote by $a_n^{(k)}$ the n-th symbol from the k-th user, whose value is drawn from the set $\{-1, 1\}$. The sequence of symbols transmitted by the k-th user is $\boldsymbol{a}^{(k)} = (a_0^{(k)}, a_1^{(k)}, ..., a_{N-1}^{(k)})$. We define $\boldsymbol{a}_n = (a_n^{(1)}, a_n^{(2)}, ..., a_n^{(K)})$ and we denote by $\boldsymbol{a} = (\boldsymbol{a}_0^T, \boldsymbol{a}_1^T, ...\boldsymbol{a}_{N-1}^T)^T$ the $K \times N$ matrix of transmitted symbols. The complex

envelope of the received signal can be written as

$$r(t) = \sum_{k=1}^{K} s^{(k)}(t, h^{(k)}, \boldsymbol{a}^{(k)}) \exp\left(j2\pi f^{(k)} t\right) + \omega(t) \tag{5.10}$$

where $\omega(t)$ is a complex zero-mean circularly symmetric white Gaussian noise with power spectral density $2N_0$, $f^{(k)}$ is the difference between the carrier frequency of user k and the reference frequency. $s^{(k)}(t, h^{(k)}, \boldsymbol{a}^{(k)})$ is the binary CPM information-bearing signal of user k which is given by

$$s(t, h^{(k)}, \boldsymbol{a}^{(k)}) = \sqrt{\frac{2E_b}{T}} \exp\{j2\pi h^{(k)} \sum_{n=0}^{N-1} a_n^{(k)} q(t - nT)\}. \tag{5.11}$$

5.4.2 FG-Multiuser Detection Based on Laurent decomposition

We denote by $\boldsymbol{r}$ the vector of all received samples defined by $\boldsymbol{r} = (\boldsymbol{r}_0^T, \boldsymbol{r}_1^T, ..., \boldsymbol{r}_{N-1}^T)^T$ with $\boldsymbol{r}_n^T = (r_{n,0}, r_{n,1}, ..., r_{n,N_s-1})$ and $r_{n,m}$ denotes the m-th received sample $(m = 0, 1, ..., N_s - 1)$ of the n-th interval. Based on the application of the FG/SPA framework, a suitable factorization of the probability mass function $P(\boldsymbol{a}, \boldsymbol{\alpha}_0|\boldsymbol{r})$ can be derived as follows

$$P(\boldsymbol{a}, \boldsymbol{\alpha}_0|\boldsymbol{r}) \propto p(\boldsymbol{r}|\boldsymbol{a}, \boldsymbol{\alpha}_0) P(\boldsymbol{\alpha}_0|\boldsymbol{a}) P(\boldsymbol{a}) \tag{5.12}$$

where $\boldsymbol{\alpha}_0 = (\boldsymbol{\alpha}_0^{(1)}, \boldsymbol{\alpha}_0^{(2)}, ..., \boldsymbol{\alpha}_0^{(K)})$ with $\boldsymbol{\alpha}_0^{(k)} = (\alpha_{0,0}^{(k)}, \alpha_{0,1}^{(k)}, ..., \alpha_{0,N-1}^{(k)})$. Each term can be further factored as follows:

$$\begin{aligned}
P(\boldsymbol{a}) &= \prod_{k=1}^{K} \prod_{n=0}^{N-1} P(a_n^{(k)}) \\
P(\boldsymbol{\alpha}_0|\boldsymbol{a}) &= \prod_{k=1}^{K} P(\alpha_{0,0}^{(k)}) \prod_{n=0}^{N-1} P(\alpha_{0,n+1}^{(k)}|a_n^{(k)}, \alpha_{0,n}^{(k)}) \\
p(\boldsymbol{r}|\boldsymbol{a}, \boldsymbol{\alpha}_0) &\propto \prod_{n=0}^{N-1} F_n(\boldsymbol{a}_n, \boldsymbol{\alpha}_{0,n}) \prod_{k=1}^{K} H_n^k(a_n^{(k)}, \alpha_{0,n}^{(k)})
\end{aligned} \tag{5.13}$$

where

$$\begin{aligned}
P(\alpha_{0,n+1}^{(k)}|a_n^{(k)}, \alpha_{0,n}^{(k)}) &\propto I_n^{(k)}(\alpha_{0,n+1}^{(k)}, \alpha_{0,n}^{(k)}, a_n^{(k)}) \\
F_n(\boldsymbol{a}_n, \boldsymbol{\alpha}_{0,n}) &= \prod_{i=1}^{K-1} \prod_{j=i+1}^{K} \exp\{-\frac{1}{\xi^2} \Re[\boldsymbol{s}_n^{(i)H} \boldsymbol{s}_n^{(j)}]\} \\
H_n^k(a_n^{(k)}, \alpha_{0,n}^{(k)}) &= \exp\{\frac{1}{\xi^2} \Re[\boldsymbol{r}_n^H \boldsymbol{s}_n^{(k)}]\}
\end{aligned} \tag{5.14}$$

with $I_n^{(l)}(\alpha_{0,n+1}^{(l)}, \alpha_{0,n}^{(l)}, a_n^{(l)})$ being the indicator function equal to one if $a_n^{(l)}$, $\alpha_{0,n}^{(l)}$ and $\alpha_{0,n+1}^{(l)}$ satisfy the trellis constraint for user l, and equal to zero otherwise. Hence,

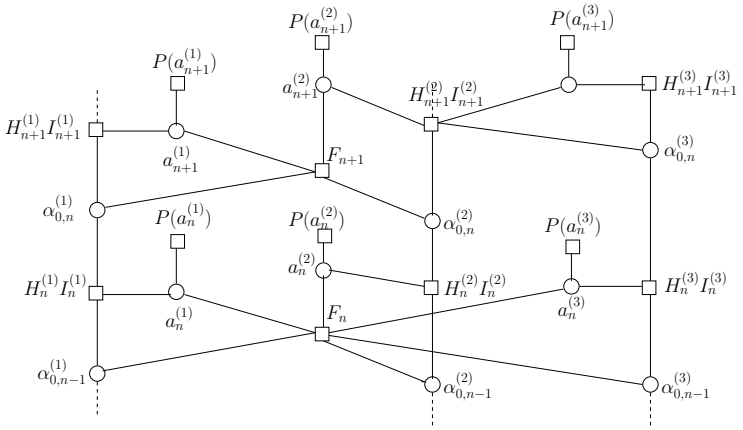

Figure 5.5: FG corresponding to (5.15) for $K = 3$ users.

we finally have

$$P(\boldsymbol{a}, \boldsymbol{\alpha}_0|\boldsymbol{r}) \propto \Big[\prod_{k=1}^{K} P(\alpha_{0,0}^{k})\Big] \prod_{n=0}^{N-1} F_n(\boldsymbol{a}_n, \boldsymbol{\alpha}_{0,n})$$
$$\prod_{k=1}^{K} H_n^k(a_n^{(k)}, \alpha_{0,n}^{(k)}) I_n^{(k)}(\alpha_{0,n+1}^{(k)}, \alpha_{0,n}^{(k)}, a_n^{(k)}) P(a_n^{(k)}) \tag{5.15}$$

The resulting FG, shown in Figure 5.5, has cycles of length four. The application of the SPA to a FG with cycles allows an approximate (due to the presence of cycles) computation of the a posteriori probabilities $P(a_n^{(k)}|\boldsymbol{r})$ required for the implementation of the MAP symbol detection strategy [82]. However, the presence of short cycles of length four makes the convergence of the SPA to good approximations of the a posteriori probabilities $P(a_n^{(k)}|\boldsymbol{r})$ very unlikely [82]. It is possible to remove these short cycles by stretching $\alpha_{0,n}^{(k)}$ in $(a_n^{(k)}, \alpha_{0,n}^{(k)})$. In other words, instead of representing variables $a_n^{(k)}$ alone, we define a new variable given by the couple $(a_n^{(k)}, \alpha_{0,n}^{(k)})$. This transformation does not involve approximations, since the resulting graph preserves all the information of the original graph. The resulting FG has cycles of length twelve. Since cycles are still present, the SPA applied to this graph is iterative and still leads to an approximate computation of the a posteriori probabilities $P(a_n^{(k)}|\boldsymbol{r})$ [82]. However, the absence of short cycles allows us to obtain very good approximations. As shown in [74], the resulting algorithm outperforms all other suboptimal MUD algorithms both from performance and complexity points of view.

5.4.3 Presence of Modulation Index Mismatch and Phase Noise

We now consider the FDM-CPM scheme assuming low cost transmitters and satellite-type channel. The user signals can thus be affected by a significant modulation index uncertainty denoted by $h_e^{(k)}$. ($h_e^{(k')}$ and $h_e^{(k)}$ are assumed independent

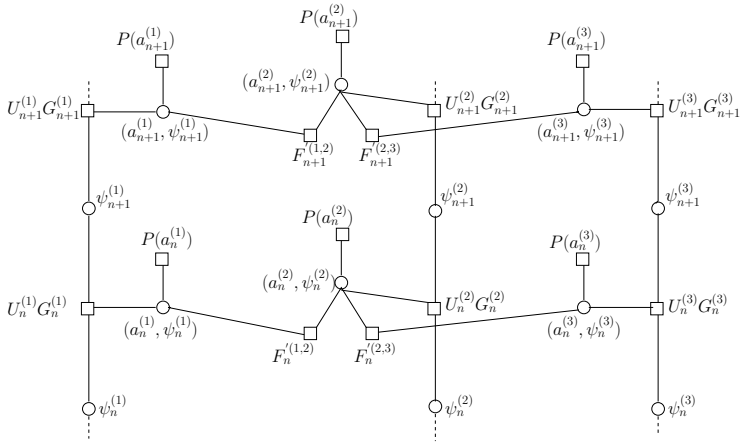

Figure 5.6: FG corresponding to (5.21) and resulting from the approximation (5.24) for $K = 3$ users.

for $k' \neq k$). The transmission also suffers from the phase noise. Here, the framework of FG and SPA will be used in a double way. In addition to the derivation of an efficient multi-user receiver with reduced complexity [74] as reminded in Section 5.4.2, it will also be used to perform detection in the presence of unkown modulation index[3] and of a time varying phase noise as proposed for a single user transmission in [83], to derive finally a robust multi-user detector named "*robust* FG-MUD". In this case, the complex envelope of the received signal can be expressed as

$$r(t) = \sum_{k=1}^{K} e^{j\theta^{(k)}(t)} s^{(k)}(t, \boldsymbol{a}^{(k)}, h + h_e^{(k)}) e^{j2\pi f^{(k)} t} + \omega(t) \tag{5.16}$$

where $\theta^{(k)}(t)$ is the phase noise affecting user k ($\theta^{(k)}(t)$ and $\theta^{(k')}(t)$ are assumed independent for $k \neq k'$) introduced by the channel, modeled as a continuous-time Wiener process with incremental variance over a signaling interval equal to σ_Δ^2. Approximating the signal through its principal component only and exploiting the feature that the pulse of the principal component weakly depends on the modulation index [67], we can express the received signal as

$$\begin{aligned} r(t) \backsimeq & \sum_{k=1}^{K} e^{j\theta^{(k)}(t)} e^{j2\pi f^{(k)} t} \\ & \Big(\sum_{n} \alpha_{0,n}^{(k)}(h) \alpha_{0,n}^{(k)}(h_e^{(k)}) \hat{p}_0(t - nT) \Big) + \omega(t) \end{aligned} \tag{5.17}$$

where we have denoted by $\hat{p}_0(t)$ the pulse of the principal component for the nominal value of the modulation index h and we have exploited the property, easily derived from (4.2), that symbol $\alpha_{0,n}^{(k)}$ related to the transmitted signal can be expressed

[3] The modulation index error generated by the k-th low cost transmitter $h_e^{(k)}$ is assumed unkown and modeled as a random variable with known distribution.

as the product of symbol $\alpha_{0,n}^{(k)}(h)$ corresponding to the nominal CPM signal and symbol $\alpha_{0,n}^{(k)}(h_e^{(k)})$ corresponding to a CPM signal with modulation index $h_e^{(k)}$. Under the assumption that the channel phase $\theta^{(k)}(t)$ is slowly varying such that it can be considered constant over the duration of pulse $\hat{p}_0(t)$, an approximate sufficient statistic may be obtained through a filter matched to pulse $\hat{p}_0(t)$. We define

$$x_n^{(k)} = \int_{-\infty}^{+\infty} r(t)\hat{p}_0(t-nT)e^{-j2\pi f^{(k)}t}\,dt \tag{5.18}$$

as the output, sampled at time nT, of the filter matched to $\hat{p}_0(t)$. We define also $\theta_n^{(k)} = \theta^{(k)}(nT)$, $\phi_n^{(k)} = \arg[\alpha_{0,n}^{(k)}(h)]$, $\delta_n^{(k)} = \arg[\alpha_{0,n}^{(k)}(h_e^{(k)})]$, and $\psi_n^{(k)} = \theta_n^{(k)} + \phi_n^{(k)} + \delta_n^{(k)}$, collecting the samples of $\psi_n^{(k)}$ into a vector $\boldsymbol{\psi}_n = \left(\boldsymbol{\psi}_n^{(1)}, \psi_n^{(2)}, ..., \psi_n^{(K)}\right)^T$, $\boldsymbol{\psi} = \left(\boldsymbol{\psi}_0^T, \boldsymbol{\psi}_1^T, ..., \boldsymbol{\psi}_{N-1}^T\right)$, representing the received signal onto an orthonormal basis and denoting by $\boldsymbol{r}$ its vector representation. As the samples $\theta_n^{(k)}$ satisfy the discrete-time Wiener model

$$\theta_n^{(k)} = \theta_{n-1}^{(k)} + \Delta_n^{(k)} \tag{5.19}$$

where $\{\Delta_n^{(k)}\}$ are real, independent, and identically distributed Gaussian random variables, with zero mean and variance σ_Δ^2, and $\theta_0^{(k)}$ is assumed uniformly distributed in $[0, 2\pi)$, it is thus

$$\begin{aligned}\psi_n^{(k)} &= \theta_n^{(k)} + \phi_n^{(k)} + \delta_n^{(k)} \\ &= \theta_{n-1}^{(k)} + \Delta_n^{(k)} + \phi_{n-1}^{(k)} + \pi h a_n^{(k)} + \delta_{n-1}^{(k)} + \pi h_e^{(k)} a_n^{(k)} \\ &= \psi_{n-1}^{(k)} + \Delta_n^{(k)} + \pi h a_n^{(k)} + \pi h_e^{(k)} a_n^{(k)}\,.\end{aligned} \tag{5.20}$$

Discarding the terms independent of symbols and states and taking into account that a CPM signal has a constant envelope, the joint distribution $p(\boldsymbol{a}, \boldsymbol{\psi}|\boldsymbol{r})$ can be factored as

$$\begin{aligned}p(\boldsymbol{a}, \boldsymbol{\psi}|\boldsymbol{r}) \propto \Big[\prod_{k=1}^{K} P(\psi_0^{(k)})\Big] \prod_{n=0}^{N-1} F_n'(\boldsymbol{\psi}_n) \\ \prod_{k=1}^{K} U_n^{(k)}(\psi_n^{(k)}) G_n^{(k)}(\psi_{n+1}^{(k)}, \psi_n^{(k)}, a_n^{(k)}) P(a_n^{(k)})\,.\end{aligned} \tag{5.21}$$

where

$$\begin{aligned}F_n'(\boldsymbol{\psi}_n) &= \prod_{k=1}^{K-1} \prod_{i=k+1}^{K} \exp\Big\{ -\frac{1}{\xi^2} \Re\left(e^{j(\psi_n^{(k)} - \psi_n^{(i)})}\right) \Big\} \\ U_n^{(k)}(\psi_n^{(k)}) &= \exp\Big\{ \frac{1}{\xi^2} \Re\left(x_n^{(k)} e^{-j\phi_n^{(k)}}\right) \Big\} \\ G_n^{(k)}(\psi_{n+1}^{(k)}, \psi_n^{(k)}, a_n^{(k)}) &= v(\psi_{n+1}^{(k)} - \psi_n^{(k)} - \pi h a_n^{(k)})\,.\end{aligned} \tag{5.22}$$

The stochastic model for $h_e^{(k)}$ depends on the considered standard. As an example, in the case of Bluetooth BR [20] $h_e^{(k)}$ follows a uniform distribution in the interval $[0.28-h, 0.35-h]$, whereas in the case of the AIS standard [72], it follows a Gaussian distribution with mean $0.5-h$ and variance $\sigma_{h_e}^2$. Assuming that $h_e^{(k)}$ has mean zero (this is always possible by properly choosing h) and an even probability density function (pdf), given $a_n^{(k)}$ the random variable $\pi h_e^{(k)} a_n^{(k)}$ is statistically equivalent to $\pi h_e^{(k)}$. We will also assume that the random variables $y_n^{(k)} = \Delta_n^{(k)} + \pi h_e^{(k)}$ are independent[4]. The pdf $v(y_n^{(k)})$ of the random variable $y_n^{(k)}$ can be easily computed from the a-priori information available at the receiver (i.e., using the distributions of $\Delta_n^{(k)}$ and $h_e^{(k)}$ and the fact that they are independent). As an example, when $h_e^{(k)}$ has uniform distribution in $[-\varepsilon, \varepsilon]$, we have

$$v(y_n) = \frac{1}{2\pi\varepsilon}\left[\mathrm{Q}\Big(\frac{y_n - \pi\varepsilon}{\sigma_\Delta}\Big) - \mathrm{Q}\Big(\frac{y_n + \pi\varepsilon}{\sigma_\Delta}\Big)\right] \tag{5.23}$$

The FG corresponding to (5.21) has cycles of length four. As shown in the previous section we can remove these short cycles by stretching the variables $a_n^{(k)}$ and $\psi_n^{(k)}$ in $(a_n^{(k)}, \psi_n^{(k)})$ and thus obtain a graph with shortest cycles of length twelve. As in [74], we assume that the interference among non-adjacent users is negligible. Then, $F_n^{'}(\boldsymbol{\psi}_n)$ in (5.22) can be approximated as

$$F_n^{'}(\boldsymbol{\psi}_n) \backsimeq \prod_{k=1}^{K-1} F_n^{'(k,k+1)}(\psi_n^{(k)}, \psi_n^{(k+1)}) \tag{5.24}$$

where

$$F_n^{'(k,k+1)}(\psi_n^{(k)}, \psi_n^{(k+1)}) = \exp\Big\{ -\frac{1}{\xi^2}\Re\left(e^{j(\psi_n^{(k+1)} - \psi_n^{(k)})}\right)\Big\}. \tag{5.25}$$

The resulting FG is shown in Figure 5.6.

5.4.4 Simulation Results

We compare three detectors. The first one, referred to as O-MUD, is the optimal multi-user detector. The second one, referred to as FG-MUD for factor graph multi-user detection, was proposed in [74]. The third one is the proposed *robust* FG-MUD. We consider the serial concatenation of the CPM, through a pseudo-random interleaver of length 2048 bits, with a binary convolutional encoder with generators (7,5) (octal notation). The bit error rate performance is averaged over all users. We assume that all users transmit at the same power and share the same modulation format and that channels are equally spaced in frequency. For all considered receivers, a number of 12 iterations between detector and decoder is allowed. The first example corresponds to a minimum shift keying (MSK) modulation format (binary modulation with $h = 1/2$ and a rectangular frequency pulse of duration T). The normalized spacing $F = |f^{(k+1)} - f^{(k)}|$ is equal to 0.5. Two different numbers

[4]This assumption corresponds to the case when $h_e^{(k)}$ can assume independent values in different symbol intervals.

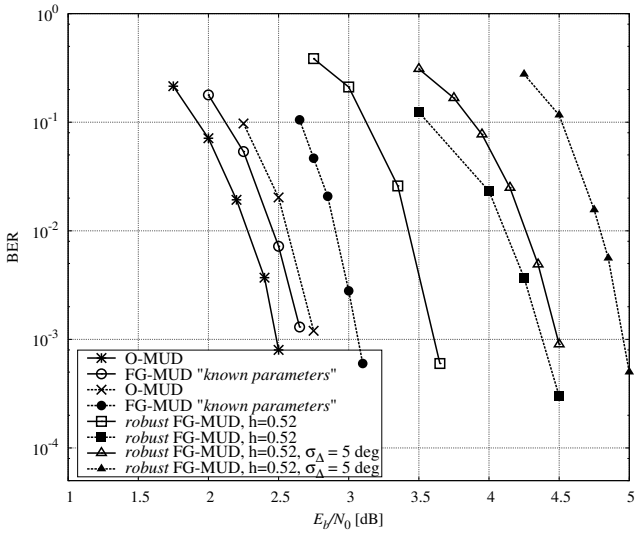

Figure 5.7: Serial concatenation with CC (5,7) via a pseudo-random interleaver with length 2048 bits with MSK modulation and a channel spacing $F = 0.5$ for two different number of users $K = 3$ (solid curves) and $K = 5$ (dashed curves)

of users are considered $K = \{3, 5\}$. The O-MUD and FG-MUD performance are plotted as reference ($h^{(k)} = 1/2$). Concerning the "*robust* FG-MUD", we assume $h^{(k)} = 0.52$ for all users and the detection considers that the modulation index of each user takes on value randomly and uniformly in the interval $[0.45, 0.55]$. From Figure 5.7, in the presence of modulation index mismatch only, at BER $= 10^{-3}$ the "*robust* FG-MUD" performs at around 1 dB (resp 1.4 dB), compared to the FG-MUD, for $K = 3$ (resp $K = 5$). In the presence of a phase noise with standard deviation $\sigma_\Delta = 5$ deg in addition to the modulation index mismatch, we observe a degradation of 1.35 dB (resp 1.85 dB), compared to the FG-MUD, for $K = 3$ (resp $K = 5$) at BER$=10^{-3}$. In the second example, the same parameters for Bluetooth (BR) system as in [56] are taken, namely Gaussian frequency-shift keying (GFSK) modulation with $BT = 0.5$ and a frequency pulse duration $L = 2$, whereas the modulation index h can vary between 0.28 and 0.35. We fix the number of users to $K = 3$ and we consider both cases: $F = 0.4$ and $F = 0.6$. The FG-MUD performance is plotted with the nominal modulation index ($h^{(k)} = 1/3$). For the "*robust* FG-MUD", we assume $h^{(k)} = 0.35$ and that the modulation index of each user takes on value randomly and uniformly in the interval $[0.28, 0.35]$. From Fig 5.8, in the presence of modulation index mismatch only the proposed algorithm performs at 0.7 dB (resp 1.15 dB) compared to the FG-MUD, for $F = 0.6$ (resp $F = 0.4$) at BER $= 10^{-3}$. In the presence of a phase noise with standard deviation $\sigma_\Delta = 5$ deg in addition to the modulation index mismatch, we observe a degradation of 1.9 dB (resp 2.5 dB), compared to the FG-MUD, for $F = 0.6$ (resp $F = 0.4$) at BER$=10^{-3}$.

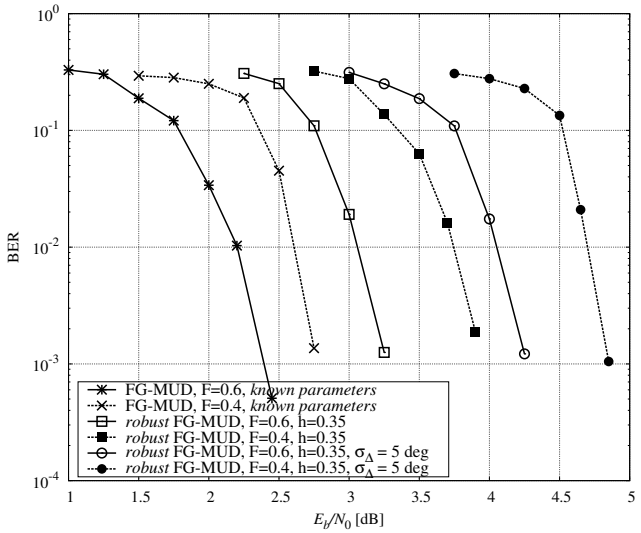

Figure 5.8: Serial concatenation with CC (5,7) via a pseudo-random interleaver with length 2048 bits with 2GFSK modulation with $BT = 0.5$ and $h = 1/3$, for a number of users K=3 and two different channel spacing $F = 0.6$ (solid curves) and $F = 0.4$ (dashed curves)

5.5 Conclusions

In this chapter, a robust CPM-based multiuser system was developed. The robustness issue was tackled first from the transmitter side where a new multiple access technique based on CPM signals was derived. This latter results from the concatenation of an AMI precoder with a ternary CPM per user followed by a multiuser separation device based on a phase rotation. The feasibility of such a scheme has been shown whereas its optimization through an optimal choice of the phase shift as well as its theoretical evaluation (the maximum user number) remains a prospect.

Then, we have derived a robust multiuser binary CPM detector for FDM-CPM systems where the spectral efficiency (SE) of frequency-division-multiplexed (FDM) systems can be increased by reducing the spacing between adjacent users. Each user's binary CPM signal is generated through a low-cost transmitter, which leads to a modulation index error, and transmitted over a channel affected by phase noise. The proposed algorithm has been derived based on the Laurent representation of a CPM signal where only the principal component has been considered. Detection in the presence of an unknown modulation index and a time-varying phase noise is performed based on the sum-product algorithm working on a properly defined factor graph (FG). Performance in terms of BER are compared to the FG-MUD detector where it's shown that an acceptable performance is obtained even in the presence of a significant phase noise and modulation index uncertainty.

Chapter 6

Conclusions & Perspectives

Conclusions

The targeted background of this work is any application that involves a huge number of low-cost transmitters, which are stand-alone devices into energy and with a limited computational capacity. We have identified the CPM as a good candidate waveform for such applications. However it is first necessary to overcome the primary disadvantages of CPM, which are its lower spectral efficiency compared to linear modulations, the complexity of its optimum receiver as well as its non-robustness to parameter mismatch around their nominal values and phase noise. The PhD goals were to find solutions to alleviate these drawbacks.

In Chapter 1, we introduced the CPM model used in this document and we described the Viterbi and BCJR algorithms that perform optimal demodulation of the CPM. We also briefly studied the influence of the defining parameters (CPM format) on the power spectrum density as well as the error rate so as to evaluate the spectral and power efficiencies of the CPM and to highlight its weaknesses.

In Chapter 2, we tackled the spectral efficiency improvement of binary CPM by proposing a precoded ternary CPM. The scheme uses an outer binary input-ternary output precoder concatenated with an inner ternary CPM. The precoder was designed so as to increase the minimum Euclidean distance and thus the information rate while keeping roughly constant the spectrum occupancy. We also studied the serial concatenation of the proposed precoded ternary CPM scheme with an outer FEC code. The EXIT chart tool was used to analyse the iterative receiver convergence. Simulations showed that the precoded ternary CPM scheme outperforms the classical binary CPM in terms of spectral and power efficiencies.

In Chapter 3, we addressed the problem of low-complexity coherent CPM demodulation. The proposed receiver relies on a trellis with reduced-state number and the application of the PSP technique in the demodulation algorithm. The trellis is built with a virtual modulation index different from the transmission modulation index. We investigated the choice of the virtual modulation index to balance the complexity reduction and the error-rate performance. We gave guidelines to discard virtual modulation index values that degrade the error-rate performance. Minimum Euclidean distance for uncoded CPM and EXIT chart for coded CPM were used as design criteria.

In Chapter 4, we dealt with the robustness to modulation index uncertainty as well as phase noise. We tackled the problem from the transmitter and the receiver

sides independently. We first proposed a precoded ternary CPM scheme, where the precoder was designed so as to impose a specific evolution of the phase state. The resulting scheme is almost insensitive to a modulation index variation around its nominal value and has almost the same spectral efficiency as the classical binary CPM. We then derived a binary CPM receiver based on the Laurent decomposition of the CPM signal as well as the sum-product algorithm application on a properly defined factor graph. The receiver is robust to both modulation index mismatch and phase noise.

In Chapter 5, we generalized the robustness issue to multi-user systems. We defined a multiple access technique based on AMI-precoded ternary CPM signals with user separation thanks to phase shifts. We proved the feasibility of such a scheme, while the phase shift optimization as well as theoretical analysis need further investigation. We then considered the FDM-CPM scheme introduced in [11] in which the frequency spacing between adjacent users is reduced in order to maximize the spectral efficiency. We adapted the multi-user joint detection proposed in [74] and based on the sum-product algorithm applied on an appropriate factor graph, we adapted it to make it robust to modulation index mismatch and time-varying phase noise. To this end we applied the Laurent decomposition to each user binary CPM signal and retained only their first principal component. Simulations proved the good performance of the robust receiver in presence of modulation index uncertainty and time-varying phase noise.

Perspectives

The optimization of the phase shifts in the multiple-access scheme proposed in Chapter 5, as well as its theoretical analysis to identify its limits are short-term perspectives. Among mid-term prospects, we can mention the implementation of the CPM as waveform for applications involving the deployment of a high number of low-cost and stand-alone communicating devices. Related to this topic, we could investigate the synchronization issue which was left aside in the PhD scope but, which would deserve deep interest if CPM were to be selected.

To conclude, although intensively studied in the early eighties, the CPM should arouse a regain of interest with the predicted invasion of device-to-device communications, which gives a glimpse of research opportunities related to CPM.

Bibliography

[1] F. Boccardi, R. Heath, A. Lozano, T. Marzetta, and P. Popovski, "Five disruptive technology directions for 5G," *Communications Magazine, IEEE*, vol. 52, no. 2, pp. 74–80, Feb. 2014. (Cited on page 3.)

[2] A. Osseiran, F. Boccardi, V. Braun, K. Kusume, P. Marsch, M. Maternia, O. Queseth, M. Schellmann, H. Schotten, H. Taoka, H. Tullberg, M. Uusitalo, B. Timus, and M. Fallgren, "Scenarios for 5G mobile and wireless communications: the vision of the METIS project," *Communications Magazine, IEEE*, vol. 52, no. 5, pp. 26–35, May 2014. (Cited on page 3.)

[3] M. Hasan, E. Hossain, and D. Niyato, "Random access for machine-to-machine communication in LTE-advanced networks: issues and approaches," *Communications Magazine, IEEE*, vol. 51, no. 6, pp. 86–93, Jun. 2013. (Cited on page 3.)

[4] K. Zheng, F. Hu, W. Wang, W. Xiang, and M. Dohler, "Radio resource allocation in LTE-advanced cellular networks with M2M communications," *Communications Magazine, IEEE*, vol. 50, no. 7, pp. 184–192, Jul. 2012. (Cited on page 3.)

[5] Ericsson, "More than 50 billion connected devices," Tech. Rep., Feb. 2011. (Cited on page 3.)

[6] CISCO, "The internet of things how the next evolution of the internet is changing everything," Tech. Rep., Apr. 2011. (Cited on page 3.)

[7] METIS, "Mobile and wireless communication enables for the twenty-twenty information society," EU 7th Framework Programme project: `http://www.metis2020.com`. (Cited on page 3.)

[8] J. Andrews, S. Buzzi, W. Choi, S. Hanly, A. Lozano, A. Soong, and J. Zhang, "What will 5G be?" *IEEE J. Select. Areas Commun.*, vol. 32, no. 6, pp. 1065–1082, Jun. 2014. (Cited on page 4.)

[9] H. Anton and M. Dohler, *Machine-to-Machine (M2M) Communications: Architecture, Performance and Applications*. Woodhead Publishing, Jan 2015. (Cited on page 4.)

[10] J. B. Anderson, T. Aulin, and C.-E. W. Sundberg, *Digital Phase Modulation*. New York: Plenum Press, 1986. (Cited on pages 4, 6, 11, 15, 23, 24, 25, 50, 52 and 66.)

[11] A. Barbieri, D. Fertonani, and G. Colavolpe, "Spectrally-efficient continuous phase modulations," *IEEE Trans. Wireless Commun.*, vol. 8, pp. 1564–1572, Mar. 2009. (Cited on pages 4, 80, 84 and 96.)

[12] B. E. Rimoldi, "A decomposition approach to CPM," *IEEE Trans. Inform. Theory*, vol. 34, pp. 260–270, Mar. 1988. (Cited on pages 5, 18, 31 and 81.)

[13] G. D. Forney, Jr., "The Viterbi algorithm," *Proc. IEEE*, vol. 61, pp. 268–278, Mar. 1973. (Cited on pages 5, 9, 38 and 64.)

[14] H. Meyr, M. Oerder, and A. Polydoros, "On sampling rate, analog prefiltering, and sufficient statistics for digital receivers," *IEEE Trans. Commun.*, vol. 42, pp. 3208–3214, Dec. 1994. (Cited on page 8.)

[15] P. A. Murphy, G. E. Ford, and M. Golanbari, "MAP symbol detection of CPM bursts," in *in proc. 7th Virginia Tech. symp. on Wireless pers. comm*, 1997. (Cited on page 10.)

[16] L. R. Bahl, J. Cocke, F. Jelinek, and J. Raviv, "Optimal decoding of linear codes for minimizing symbol error rate," *IEEE Trans. Inform. Theory*, vol. 20, pp. 284–287, Mar. 1974. (Cited on pages 10, 22 and 64.)

[17] T. Aulin and C.-E. Sundberg, "Exact asymptotic behavior of digital FM spectra," *IEEE Trans. Commun.*, vol. 30, no. 11, pp. 2438–2449, Nov. 1982. (Cited on page 11.)

[18] ——, "Calculating digital FM spectra by means of autocorrelation," *IEEE Trans. Commun.*, vol. 30, no. 5, pp. 1199–1208, May 1982. (Cited on page 11.)

[19] E. T. S. Institute, "Radio transmission and reception," Jan. 1992, GSM Recommendations No. 05.05-DCS (version 3.0). (Cited on page 13.)

[20] "Specification of the Bluetooth System," Dec. 2010, Bluetooth Special Interest Group document. (Cited on pages 13, 42, 74 and 91.)

[21] ETSI EN 301 307 Digital Video Broadcasting (DVB); V1.1.2 (2006-06), Second generation framing structure, channel coding and modulation systems for Broadcasting, Interactive Services, News Gathering and other Broadband satellite applications, 2006, Available on ETSI web site (http://www.etsi.org). (Cited on page 13.)

[22] S. Benedetto and E. Biglieri, *Principles of Digital Transmission: With Wireless Applications*. (Cited on page 14.)

[23] G. Colavolpe, G. Montorsi, and A. Piemontese, "Spectral efficiency of linear and continuous phase modulations over nonlinear satellite channels," in *Proc. IEEE Intern. Conf. Commun.*, Jun. 2012, pp. 3345 – 3349. (Cited on page 18.)

[24] A. Goldsmith, *Wireless Communications*. Cambridge University Press, 2005. (Cited on page 18.)

[25] P. A. Laurent, "Exact and approximate construction of digital phase modulations by superposition of amplitude modulated pulses (AMP)," *IEEE Trans. Commun.*, vol. 34, pp. 150–160, Feb. 1986. (Cited on pages 19, 38, 60 and 61.)

[26] F. R. Kschischang, B. J. Frey, and H.-A. Loeliger, "Factor graphs and the sum-product algorithm," *IEEE Trans. Inform. Theory*, vol. 47, pp. 498–519, Feb. 2001. (Cited on pages 19, 60, 71, 72, 73 and 86.)

[27] D. M. Arnold, H.-A. Loeliger, P. O. Vontobel, A. Kavčić, and W. Zeng, "Simulation-based computation of information rates for channels with memory," *IEEE Trans. Inform. Theory*, vol. 52, no. 8, pp. 3498–3508, Aug. 2006. (Cited on pages 22 and 23.)

[28] T. M. Cover and J. A. Thomas, *Elements of Information Theory*, 2nd ed. New York: John Wiley & Sons, 2006. (Cited on page 22.)

[29] P. Moqvist and T. M. Aulin, "Serially concatenated continuous phase modulation with iterative decoding," *IEEE Trans. Commun.*, vol. 49, pp. 1901–1915, Nov. 2001. (Cited on pages 23, 32 and 80.)

[30] A. Graell i Amat, C. A. Nour, and C. Douillard, "Serially concatenated continuous phase modulation for satellite communications," *IEEE Trans. Wireless Commun.*, vol. 8, pp. 3260–3269, Jun. 2009. (Cited on page 23.)

[31] E. Perrins and M. Rice, "Reduced-complexity approach to iterative detection of coded SOQPSK," *IEEE Trans. Commun.*, vol. 55, no. 7, pp. 1354–1362, Jul. 2007. (Cited on page 24.)

[32] M. Messai, G. Colavolpe, K. Amis, and F. Guilloud, "Binary continuous phase modulations with constrained phase state," submitted to *IEEE Trans. Commun.*, Feb. 2015. (Cited on page 24.)

[33] E. Perrins and M. Rice, "A new performance bound for PAM-based CPM detectors," *IEEE Trans. Commun.*, vol. 53, no. 10, pp. 1688 – 1696, Oct. 2005. (Cited on pages 30 and 66.)

[34] C. Berrou, A. Glavieux, and P. Thitmajshima, "Near Shannon limit error-correcting coding and decoding: turbo-codes," in *Proc. IEEE Intern. Conf. Commun.*, Geneva, Switzerland, May 1993, pp. 1064–1070. (Cited on pages 30 and 31.)

[35] C. Shannon, "A mathematical theory of communication," *Bell System Tech. J.*, pp. 379–423, Jul. 1948. (Cited on page 30.)

[36] S. Benedetto and G. Montorsi, "Role of recursive convolutional codes in turbo codes," *IEE Electronics Letters*, vol. 31, no. 11, pp. 858–859, May 1995. (Cited on page 31.)

[37] F. Daneshgaran, M. Laddomada, and M. Mondin, "Interleaver design for serially concatenated convolutional codes: theory and application," *Information Theory, IEEE Transactions on*, vol. 50, no. 6, pp. 1177–1188, Jun. 2004. (Cited on page 31.)

[38] J. Yu, M.-L. Boucheret, and R. Vallet, "Design of turbo codes interleaver by loop distributions," in *Information Theory, 2002. Proceedings. 2002 IEEE International Symposium on*, 2002, pp. 54–. (Cited on page 31.)

[39] C. Brutel and J. Boutros, "Serial concatenation of interleaved convolutional codes and M-ary continuous phase modulations," *Annals of Telecommun.*, vol. 54, pp. 235–242, Apr. 1999. (Cited on page 32.)

[40] S. ten Brink, "Convergence behavior of iteratively decoded parallel concatenated codes," *IEEE Trans. Commun.*, vol. 49, no. 10, pp. 1727–1737, Oct. 2001. (Cited on pages 32 and 55.)

[41] R. Gallager, *Information Theory and Reliable Communication.* John Wiley & Sons, 1968. (Cited on page 34.)

[42] N. Wiberg, H.-A. Loeliger, and R. Kötter, "Codes and iterative decoding on general graphs," in *Proc. IEEE International Symposium on Information Theory*, 1995, p. 468. (Cited on page 34.)

[43] S. Simmons and P. Wittke, "Low complexity decoders for constant envelope digital modulations," *IEEE Trans. Commun.*, vol. 30, pp. 1273–1280, Dec. 1983. (Cited on page 38.)

[44] A. Svensson, "Reduced state sequence detection of partial response continuous phase modulation," *Communications, Speech and Vision, IEE Proceedings I*, vol. 138, no. 4, pp. 256–268, 1991. (Cited on page 38.)

[45] A. Svensson, C.-E. Sundberg, and T. Aulin, "A class of reduced-complexity Viterbi detectors for partial response continuous phase modulation," *IEEE Trans. Commun.*, vol. 32, no. 10, pp. 1079–1087, 1984. (Cited on pages 38, 44, 45, 46 and 47.)

[46] J. Huber and W. Liu, "An alternative approach to reduced-complexity CPM-receivers," *IEEE J. Select. Areas Commun.*, vol. 7, pp. 1437–1449, Dec. 1989. (Cited on page 38.)

[47] M. Costa, "A practical demodulator for continuous phase modulation," in *Information Theory, 1994. Proceedings., 1994 IEEE International Symposium on*, 1994, pp. 88–. (Cited on page 38.)

[48] S. Simmons, "Simplified coherent detection of CPM," *IEEE Trans. Commun.*, vol. 43, no. 234, pp. 726–728, 1995. (Cited on page 38.)

[49] W. Tang and E. Shwedyk, "A quasi-optimum receiver for continuous phase modulation," *IEEE Trans. Commun.*, vol. 48, no. 7, pp. 1087–1090, 2000. (Cited on page 38.)

[50] G. K. Kaleh, "Simple coherent receivers for partial response continuous phase modulation," *IEEE J. Select. Areas Commun.*, vol. 7, pp. 1427–1436, Dec. 1989. (Cited on page 38.)

[51] U. Mengali and M. Morelli, "Decomposition of M-ary CPM signals into PAM waveforms," *IEEE Trans. Inform. Theory*, vol. 41, pp. 1265–1275, Sep. 1995. (Cited on pages 38, 42 and 43.)

[52] G. Colavolpe and R. Raheli, "Non-coherent sequence detection of M-ary PSK," in *Proc. IEEE Intern. Conf. Commun.*, vol. 1, Montreal, Canada, 1997, pp. 21–25. (Cited on page 38.)

[53] E. Perrins and M. Rice, "Optimal and reduced complexity receivers for M-ary multi-h CPM," in *Proc. IEEE Wireless Commun. and Network. Conf.*, Mar. 2004, pp. 1165–1170. (Cited on page 39.)

[54] R. Raheli, A. Polydoros, and C. Tzou, "Per-survivor processing: A general approach to MLSE in uncertain environments," *IEEE Trans. Commun.*, vol. 43, pp. 354–364, February-April 1995. (Cited on page 39.)

[55] H.-K. Lee, D. Divsalar, and C. Weber, "Multiple symbol trellis coding of CPFSK," *IEEE Trans. Commun.*, vol. 44, no. 5, pp. 566–574, May 1996. (Cited on page 42.)

[56] L. Lampe, R. Schober, and M. Jain, "Noncoherent sequence detection receiver for Bluetooth systems," *IEEE J. Select. Areas Commun.*, vol. 23, no. 9, Sep. 2005. (Cited on pages 42, 61, 76 and 92.)

[57] G. Colavolpe and R. Raheli, "Reduced-complexity detection and phase synchronization of CPM signals," *IEEE Trans. Commun.*, vol. 45, pp. 1070–1079, Sep. 1997. (Cited on pages 42, 43, 61 and 65.)

[58] M. Figuera and J. Krogmeier, "Optimum and suboptimum receivers for M-ary CPM signals based upon the Laurent representation," in *Vehicular Technology Conference, 2002. Proceedings. VTC 2002-Fall. 2002 IEEE 56th*, vol. 4, 2002, pp. 2268–2272. (Cited on pages 45, 46 and 47.)

[59] M. K. Simon and C. C. Wang, "Differential detection of gaussian MSK in a mobile radio environment," *Vehicular Technology, IEEE Transactions on*, vol. 33, no. 4, pp. 307–320, Nov. 1984. (Cited on page 60.)

[60] S. Shin and P. Mathiopoulos, "Differentially Detected GMSK Signals in CCI Channels for Mobile Cellular Telecommunication Systems," *Vehicular Technology, IEEE Transactions on*, vol. 42, no. 3, pp. 289–293, Aug. 1993. (Cited on page 60.)

[61] A. Abrardo and G. Benelli, "Multiple-Symbols Differential Detection of GMSK," *IEE Electronics Letters*, vol. 29, no. 25, pp. 2167–2168, Dec. 1993. (Cited on page 60.)

[62] A. Abrardo, G. Benelli, and G. Cau, "Multiple-symbol differential detection of GMSK for mobile communications," *Vehicular Technology, IEEE Transactions on*, vol. 44, no. 3, pp. 379–389, Aug. 1995. (Cited on page 60.)

[63] M. K. Simon and C. Wang, "Differential versus limiter–discriminator detection of narrow-band FM," *Communications, IEEE Transactions on*, vol. 31, no. 11, pp. 1227–1234, Nov. 1983. (Cited on page 60.)

[64] M. Hirono, T. Miki, and K. Murota, "Multilevel decision method for band-limited digital FM with limiter-discriminator detection," *Selected Areas in Communications, IEEE Journal on*, vol. 2, no. 4, pp. 498–506, Jul. 1984. (Cited on page 61.)

[65] G. Kaleh, "Differential detection via the Viterbi algorithm for offset modulation and MSK-type signals," *IEEE Trans. Veh. Tech.*, vol. 41, no. 4, pp. 401–406, Nov. 1992. (Cited on page 61.)

[66] G. Colavolpe and R. Raheli, "Noncoherent sequence detection of continuous phase modulations," *IEEE Trans. Commun.*, vol. 47, pp. 1303–1307, Sep. 1999. (Cited on page 61.)

[67] D. Xu and Y. Zhang, "Estimation of the modulation index of CPM signals based on Laurent's decomposition," *IEEE Trans. Wireless Commun.*, vol. 12, no. 12, pp. 6268–6280, Dec. 2013. (Cited on pages 61, 62 and 89.)

[68] E. Perrins and M. Rice, "PAM decomposition of ternary CPM," *IEEE Trans. Commun.*, vol. 56, no. 12, pp. 2020–2024, Dec. 2008. (Cited on pages 61, 62, 66 and 82.)

[69] A. Barbieri and G. Colavolpe, "Simplified soft-output detection of CPM signals over coherent and phase noise channels," *IEEE Trans. Wireless Commun.*, vol. 6, no. 7, pp. 2486–2496, Jul. 2007. (Cited on pages 61, 65, 74 and 76.)

[70] N. Bouny, J. LeMaitre, and J.-P. Millerioux, "Results of measurement campaign for characterisation of ais transmitters," in *Advanced Satellite Multimedia Systems Conference (ASMS) and 12th Signal Processing for Space Communications Workshop (SPSC), 2012 6th*, Sep. 2012, pp. 258–265. (Cited on pages 62 and 74.)

[71] A. Papoulis and S. Pillai, *Probability, Random Variables, and Stochastic Processes*, ser. McGraw-Hill series in electrical engineering: Communications and signal processing. Tata McGraw-Hill, 2002. (Cited on page 66.)

[72] D. Bonacci, J.-P. Millerioux, R. Prevost, J. Lemaitre, M. Coulon, and J.-Y. Tourneret, "Advanced concepts for satellite reception of AIS messages (Toulouse Space Show, Toulouse, 25/06/2012-28/06/2012)," 2012. (Cited on pages 74 and 91.)

[73] S. Zarei, W. Gerstacker, G. Kilian, and W. Koch, "An iterative detection algorithm for coded CPFSK signals with irrational modulation index," in *Proc. European Signal Processing Conf.*, Aug. 2012, pp. 2541–2545. (Cited on pages 76 and 77.)

[74] A. Piemontese and G. Colavolpe, "A novel graph-based suboptimal multiuser detector for FDM-CPM transmissions," *IEEE Trans. Wireless Commun.*, vol. 9, pp. 2812–2819, Sep. 2010. (Cited on pages 80, 86, 88, 89, 91 and 96.)

[75] P. Murphy, M. Golanbari, G. Ford, and M. Ready, "Optimum and reduced complexity multiuser detectors for asynchronous cpm signaling," *Wireless Communications, IEEE Transactions on*, vol. 5, no. 8, pp. 1959–1965, Aug. 2006. (Cited on page 80.)

[76] P. Moqvist, "Multiuser serially concatenated continuous phase modulation," Ph.D. dissertation, Chalmers University of Technology, Goteborg, Sweden, 2002. (Cited on page 80.)

[77] A. Perotti, S. Benedetto, and P. Remlein, "Spectrally efficient multiuser continuous-phase modulation systems," in *Communications (ICC), 2010 IEEE International Conference on*, May 2010, pp. 1–5. (Cited on page 80.)

[78] L. Bing, T. Aulin, and B. Bai, "Spectrally-efficient FDMA-CPM systems," in *Communications (ICC), 2014 IEEE International Conference on*, Jun. 2014, pp. 5215–5220. (Cited on page 80.)

[79] ——, "A simplified detector for FDMA-CPM systems," in *Wireless Communications and Networking Conference (WCNC), 2014 IEEE*, Apr. 2014, pp. 606–611. (Cited on page 80.)

[80] N. Mazzali, G. Colavolpe, and S. Buzzi, "CPM-based spread spectrum systems for multi-user communications," in *Proc. IEEE Intern. Conf. Commun.*, Ottawa, Canada, Jun. 2012, pp. 2335–2339. (Cited on page 80.)

[81] N. Noels and M. Moeneclaey, "Iterative multiuser detection of spectrally efficient FDMA CPM," *IEEE Trans. Signal Processing*, vol. 60, no. 10, pp. 5254–5267, Oct. 2012. (Cited on page 81.)

[82] G. Colavolpe and G. Germi, "On the application of factor graphs and the sum-product algorithm to ISI channels," *IEEE Trans. Commun.*, vol. 53, pp. 818–825, May 2005. (Cited on page 88.)

[83] M. Messai, G. Colavolpe, K. Amis, and F. Guilloud, "Robust detection of binary CPMs with unknown modulation index," *IEEE Commun. Letters*, vol. 19, no. 3, pp. 339–342, March 2015. (Cited on page 89.)

CPM signal for Machine to Machine Communications

Abstract:

The analysis of communication evolution predicts an increase in the number of connected machines. This thesis aims to determine a multi-user communication system adapted to the material limitation of the machines and to the applications constraints. Power and cost efficient digital modulation is required for both economical and environmental reasons, the power consumption on the link should be as low as possible. Constant envelope modulation offers the possibility to use non-linear cost-effective and power efficient amplifiers. Continuous phase modulation (CPM) exhibits constant envelope and the continuous phase makes the power frequency spectrum well confined with the possibility to achieve small spectral sidelobes. The advantages of CPM are balanced with the primary disadvantages, which are the complexity at the receiver side, a lack of robustness to the parameters mismatch around their nominal values, and its lower spectral efficiency compared to linear modulation.

In this PHD, we focused on these issues. First, considering an AWGN transmission of a CPM with perfectly estimated modulation index, a reduced complexity per survivor processing (PSP) based CPM demodulation was derived for both mono-h and multi-h CPM signals. Second, the robustness issue is addressed on the receiver side and on the transmitter side. On the receiver side, a robust detector was designed based on the factor graph (FG) and the sum product algorithm (SPA) to deal with unknown modulation index error. Simulations were performed assuming a multiuser binary CPM transmission in the presence of phase noise. At the transmitter side, the robustness to the modulation index mismatch is also solved by the design of an appropriate precoder which limits the accumulation of phase errors. Third, a high spectral efficiency CPM scheme was derived based on an appropriate. design of the precoder. In a multiusers scheme, the overall spectral efficiency is increased by using a new AMI-based precoder, where a robust multi-user detection for synchronous binary CPMs signals based on phase separation is performed.

Keywords:

continuous phase modulation, EXIT charts, minimum Euclidean distance, per survivor processing, iterative decoding, CPM-FDM, frequency spacing, spectral efficiency, modulation index mismatch, phase noise, factor graph, sum product, iterative detection and decoding, multi-user detection.

Résumé

L'analyse de l'évolution des télécommunications prévoit une augmentation du nombre de machines connectées. Cette thèse vise à déterminer un système de communication multi-utilisateur adapté à la limitation matérielle des machines et aux spécificités des applications de collecte d'informations à grande échelle. Pour des raisons économiques et environnementales, il est nécessaire de réduire la puissance et le coût des systèmes de communications numériques. Il est également nécessaire de réduire la consommation d'énergie afin d'augmenter la durée de vie des batteries utilisées. La modulation à enveloppe constante permet d'utiliser des amplificateurs non linéaires qui ont un rendement énergétique plus importants que leurs homologues linéaires. Les modulations à phase continue (CPM) mettent en œuvre des signaux à enveloppe constante. De plus, la continuité de phase confine la densité spectrale depuissance tout en diminuant le niveau des lobes secondaires. Les principaux inconvénients de la CPM sont la complexité mise en œuvre pour une réception optimale, la sensibilité aux dispersions des paramètres d'émission, et la diminution de son efficacité spectrale par rapport à la modulation linéaire. Dans cette thèse, nous proposons des solutions pour ces trois aspects.

Tout d'abord, un démodulateur CPM d'une complexité réduite basé sur la technique per survivor processing (PSP) a été développé pour une transmission sur un canal Gaussien d'un signal CPM dont l'indice de modulation est parfaitement estimé. Deuxièmement, nous abordons le problème de la robustesse du côté récepteur puis du côté de l'émetteur vis-à-vis de l'indice de modulation ; il s'agit ici de compenser un écart entre l'indice de modulation nominal et l'indice de modulation réel et inconnu. Du côté récepteur, un détecteur robuste a été conçu en appliquant un algorithme de type somme-produit sur un graphe biparti afin de compenser l'erreur présente sur la connaissance de l'indice de modulation. Les simulations ont été réalisées en considérant un système multi-utilisateur des signaux CPM binaire en présence de bruit de phase. Du côté émetteur, la robustesse est obtenue par la conception d'un pré-codeur approprié conçu pour limiter l'accumulation de l'erreur de phase. Troisièmement, une amélioration de l'efficacité spectrale d'un signal CPM binaire est obtenue grâce à la conception d'un pré-codeur. Dans un système multi-utilisateur synchrone, l'efficacité spectrale est augmentée en associant chaque émetteur CPM binaire à un pré-codeur de type Alternate Mark Inversion suivie d'une séparation de phase ; une détection multi-utilisateur est effectuée au récepteur.

Mots-clés : Modulation à phase continue, Diagrammes EXIT, Distance euclidienne minimale, Per survivor processing, Décodage et détection itératifs, CPM-FDM, Efficacité spectrale, Erreurs d'indice de modulation, Bruit de phase, Graphes bipartis, Algorithme somme-produit, Détection multi-utilisateurs.

Abstract

The analysis of communication evolution predicts an increase in the number of connected machines. This thesis aims to determine a multi-user communication system adapted to the material limitation of the machines and to the applications constraints. Power and cost efficient digital modulation is required for both economical and environmental reasons, the power consumption on the link should be as low as possible. Constant envelope modulation offers the possibility to use non-linear cost-effective and power efficient amplifiers. Continuous phase modulation (CPM) exhibits constant envelope and the continuous phase makes the power frequency spectrum well confined with the possibility to achieve small spectral slidelobes. The advantages of CPM are balanced with the primary disadvantages, which are the complexity at the receiver side, a lack of robustness to the parameters mismatch around their nominal values, and its lower spectral efficiency compared to linear modulation.
In this PHD, we focused on these issues. First, considering an AWGN transmission of a CPM with perfectly estimated modulation index, a reduced complexity per survivor processing (PSP) based CPM demodulation was derived for both mono-h and multi-h CPM signals. Second, the robustness issue is addressed on the receiver side and on the transmitter side. On the receiver side, a robust detector was de- signed based on the factor graph (FG) and the sum product algorithm (SPA) to deal with unknown modulation index error. Simulations were performed assuming a multiuser binary CPM transmission in the presence of phase noise. At the transmitter side, the robustness to the modulation index mismatch is also solved by the design of an appropriate precoder which limits the accumulation of phase errors. Third, a high spectral efficiency CPM scheme was derived based on an appropriate design of the precoder. In a multiusers scheme, the overall spectral efficiency is increased by using a new AMI-based precoder, where a robust multi-user detection for synchronous binary CPMs signals based on phase separation is performed.

Keywords : Continuous phase modulation, EXIT charts, Minimum Euclidean distance, Per survivor processing, Iterative decoding, CPM-FDM, frequency spacing, Spectral efficiency, Modulation index mismatch, Phase noise, Factor graph, Sum product, Iterative detection and decoding, Multi-user detection.

TELECOM Bretagne

n° d'ordre : 2015telb0367
Télécom Bretagne
Technopôle Brest-Iroise - CS 83818 - 29238 Brest Cedex 3
Tél : + 33(0) 29 00 11 11 - Fax : + 33(0) 29 00 10 00